beyond
the obvious

Techno-economic assessment of the process for recovery of indium, germanium and tin from alloys obtained as byproducts of zinc production

Iris Winberg

VTT TECHNOLOGY 345

VTT TECHNOLOGY 345

Techno-economic assessment of the process for recovery of indium, germanium and tin from alloys obtained as byproducts of zinc production

Iris Winberg

VTT

ISBN 978-951-38-8678-3 (Soft back ed.)
ISBN 978-951-38-8677-6 (URL: http://www.vttresearch.com/impact/publications)

VTT Technology 345

ISSN-L 2242-1211
ISSN 2242-1211 (Print)
ISSN 2242-122X (Online)
http://urn.fi/URN:ISBN:978-951-38-8677-6
https://doi.org/

JULKAISIJA – UTGIVARE – PUBLISHER

Teknologian tutkimuskeskus VTT Oy
PL 1000 (Tekniikantie 4 A, Espoo)
02044 VTT
Puh. 020 722 111, faksi 020 722 7001

Teknologiska forskningscentralen VTT Ab
PB 1000 (Teknikvägen 4 A, Esbo)
FI-02044 VTT
Tfn +358 20 722 111, telefax +358 20 722 7001

VTT Technical Research Centre of Finland Ltd
P.O. Box 1000 (Tekniikantie 4 A, Espoo)
FI-02044 VTT, Finland
Tel. +358 20 722 111, fax +358 20 722 7001

Cover image: Instytut Metali Nieżelaznych (IMN), 2018

Juvenes Print, Tampere 2018

Executive Summary

This thesis consists of a techno-economic assessment of a process for recovery of indium, germanium and tin from lead-bearing alloys produced as side-streams of zinc production, and a literature review on the indium, germanium and tin markets.

Market review

Most of the primary applications of indium, germanium and tin are in advanced technology. The leading end-use for indium is flat panel displays. Finding a suitable substitute for this application is challenging. The most popular end-use for germanium is fiber optics, and for tin it is solders for electronics. Substitution challenges for tin and germanium are moderate.

Indium and germanium do not occur in concentrations high enough to economically justify specifically mining them. Both metals are commonly recovered as by-products in zinc production and germanium is additionally recovered from fly ash. In 2017, the world refinery production of indium was 720 metric tons (Anderson, 2018a) and germanium 130 metric tons (Thomas, 2018b). End-of-life recycling of both metals is close to nonexistent, but the metals are extensively recycled from manufacturing waste. In the process of manufacturing indium and germanium products, a high share of the metals end up in waste streams.

Around 350,000 metric tons of refined tin was produced in 2016 (Brown et al., 2018). World secondary production accounted for 7% of the total tin production in 2015 (Anderson, 2017a). Most of the secondary tin was produced in the United States and Belgium. China is the leading producer of all three metals. China accounts for more than half of the smelter production of tin and most of the rest is accounted for by countries in Southeast Asia and South America (Anderson, 2018b). Most of the indium production is accounted for by China (43%), South Korea, Canada and Japan (Anderson, 2018a). Germanium is produced in China (65%), Russia, Belgium, Canada and Ukraine (Brown et al., 2018).

Of the studied metals, germanium is the most valuable, with an average price of 1,400 USD/kg in 2017 (Thomas, 2018b). The average indium price for the same year was 210 USD/kg (Anderson, 2018a) and the average tin price for April 2018 was 21 USD/kg (Anderson, 2018c). Growth in demand is expected for all the metals, but a higher growth is expected for germanium compared to the others.

The European Commission has prepared a list of critical raw materials, based on the importance of the raw materials to the economy of the European Union and on the supply risk of the raw materials (European Commission, 2017). Indium and germanium are included in the list and tin is not, because of a lower supply risk. The current tin reserves are estimated to be 16 times higher than the mine production of 2017 (Anderson, 2018b). In the long term, alternative sources of tin will become increasingly important to ensure the availability of tin.

Techno-economic assessment

The proposed process concept involves the use of both pyro- and hydrometallurgical methods to recover the metals from two lead-bearing alloys, which are obtained as byproducts in zinc production. Lead-tin alloy, germanium concentrate and two different indium concentrates are obtained as main products in the process.

The flow-sheet simulation module (SIM) of the software HSC Chemistry 9 was used for calculation of the mass and energy balances of the process. As input data in the simulation, chemical reactions and mass distribution of elements to the products were used. The chemical reactions were determined on theoretical grounds or based on experimental data from similar processes described in the references. The mass distribution of elements was calculated based on the concentrations of elements in the products obtained in pilot-scale experiments, performed by the research institute, IMN (2018). Using the mass balances obtained from the simulation, the main equipment required for treatment of 280 tons of alloy per year was dimensioned. Production was assumed to be ongoing 16 hours a day and 250 days in a year.

The cost of the main equipment was estimated by adjusting the costs specified in references with material factor and cost index. Remaining capital costs were estimated as ratios of the costs of the main equipment as suggested by Towler and Sinnott (2013). The variable operating costs were estimated for the amount of chemicals, utilities, energy and waste that was obtained from the mass and energy balances. Labor costs were estimated for five employees and other fixed operating expenses based on the capital costs as suggested by Towler and Sinnott (2013).

The net present value of the investment was calculated with a discount rate of 10% for a period of 20 years. It was assumed that the construction of the plant takes one year and that the first year of production would be at 75% of the capacity. The net present value was calculated for five different cases where the value of the products varies between 50% and 90% of the pure metal value. Interest, taxes, depreciation or amortization were not taken into account. A sensitivity analysis was performed by varying the estimation of metal prices and selected costs by 25% and studying its impact on the net present value.

With a capacity of 280 t/a alloy, 0.56 t/a indium, 1.65 t/a germanium and 5.7 t/a tin can be recovered from the alloys per year. In pure metal, the products have a combined value of about 2.2 million EUR. Production of the metals on such a scale would increase European production of indium by an estimated 1% and production

of germanium outside China by 4%. The contribution of tin would be insignificant to both the global and European production.

The variable operating costs for processing 280 t/a alloy were estimated at 175,000 EUR and the fixed operating costs were estimated at 450,000 EUR/a. The cost of the main equipment was estimated at half a million EUR and the total capital investment at 3.2 million EUR. The net present value of the investment for 70% of the pure metal value, is 3.5 million EUR. The payback time for the same case is seven years.

The net present value is the most sensitive to variation in the germanium price. With a 25% increase in the market price of germanium, the net present value is almost 7 million EUR, while with a 25% decrease in the market price of germanium it is only one million EUR. A capacity increase of 25% gives a net present value of 5.7 million euros. This indicates that the recycling of byproducts, as proposed for the process but not included in process simulation, could significantly increase the profitability of the process. The byproducts that would be recycled contain 0.41 t/a indium, 0.42 t/a germanium and 8.0 t/a tin. Since recirculation does not necessarily imply an equal increase in both the revenue and in the size of the major equipment, this is uncertain.

The results show that an investment in the process, especially for a plant with a somewhat higher capacity, has potential to be profitable. Mainly due to the uncertainty of the germanium concentrate value, no definitive conclusion can be drawn regarding the feasibility process at the capacity that was studied.

Preface

This study is a thesis for the Master's Program in Chemical Engineering at Åbo Akademi University. The thesis work was performed at VTT in Otaniemi, Espoo. This activity has received funding from the European Institute of Innovation and Technology (EIT). This body of the European Union receives support from the European Union's Horizon 2020 research and innovation program.

First and foremost, I would like to thank D.Sc. Petteri Kangas at VTT, for taking the time to be a dedicated supervisor and giving thorough guidance and valuable advice.

I would like to thank Professor Anders Brink at Åbo Akademi University, for helping me to find this project and for giving constructive feedback on the thesis work.

Additionally, I extend my gratitude to the project partners at IMN, Gliwice, for providing detailed information about the process that was studied and for giving a prompt answer to every question I had about the process.

I would also like to thank my fellow thesis workers at VTT for the peer support and my team members at VTT for their genuine interest in my thesis and for including me in the team. Finally, I would like to express gratitude to my partner, friends and family for the encouragement and generous support they have given me throughout my thesis work.

Iris Winberg

Espoo, November 2018

Contents

List of symbols

a	annum
CS	carbon steel
FRP	fiber-reinforced plastic
EUR	euro
GJ	gigajoule
g/l	gram per liter
ISBL	inside battery limits
kg	kilogram
l/s	liters per second
mm	millimeter
m^2	square meter
m^3	cubic meter
MW	megawatt
MWh	megawatt hour
Nm^3/h	normal cubic meters per hour
OSBL	outside battery limits
ppm	parts per million
t	metric ton
USD	United States dollar
wt-%	weight percent
°C	degrees Celsius
ΔH	enthalpy difference

1. Introduction

Modern technology relies on a growing number of raw materials, of which some are irreplaceable in their applications. There is a growing concern regarding reliable access to certain raw materials both within the European Union and globally. The European Commission has prepared a list of critical raw materials, based on the importance of the raw materials to the economy of the European Union and on the supply risk of the raw materials (European Commission, 2017). Among others, indium and germanium are included on the list. On the other hand, the mineral resources of certain metals, such as tin, are diminishing, and in the long term alternative sources of these metals will become increasingly important to ensure their availability.

The aim of this thesis is to make a techno-economic assessment for a process for recovery of indium, germanium and tin. The proposed process involves the use of both pyro- and hydrometallurgical methods to recover the metals from two lead-bearing alloys, which are obtained as byproducts in zinc production. Lead-tin alloy, germanium concentrate and two different indium concentrates are obtained as main products in the process.

Additionally, a literature study on the markets of indium, germanium and tin is conducted with the aim to investigate the risks and opportunities of an investment, the profitability of which relies on the market price of the metals. The aim is also to clarify whether production of the metals, at the scale for which the process is studied (a total of 280 t/a alloy), could contribute significantly to the supply in Europe and globally. The properties and applications of the metals are studied and their substitutes are investigated for the market review. Additionally, the market price, future demand, supply risk and the size and geographical distribution of both primary and secondary production is studied.

For the technical assessment of the process, the flow-sheet simulation module (SIM) of the software HSC Chemistry 9 was used. The aim was to calculate the mass and energy balances of the process. As input data in the simulation, chemical reactions and mass distribution of elements to the products are used. The mass distributions of elements are calculated from the results of pilot-scale experiments, performed by the research institute IMN (2018). Using the mass balances obtained from the simulation, the main equipment required to treat 280 metric tons of alloy per year is dimensioned.

For the economic assessment, the capital cost, the operating costs and the revenue for the process are estimated. Using these, the net present value of the investment is calculated. A sensitivity analysis is conducted by varying the estimation of metal prices and selected costs and studying its impact on the net present value.

Indium, germanium and tin markets are reviewed in chapters 2–4. The technical assessment based on process simulation is described in chapter 5, including also the sizing of main process equipment. The economic feasibility of the process is evaluated in chapter 6. The final discussion and conclusions are given in chapter 7.

2. Indium market review

Indium is a soft and silvery-white post-transition metal, discovered in 1863 by Ferdinand Reich and Theodor Richter. It was discovered by spectroscopic methods and was named indium because of the indigo blue line in its spectrum. Indium is not particularly scarce, but mining for it alone is not economically feasible, as it does not occur in high enough concentrations. It is most commonly recovered as a by-product of zinc production. Most indium ends up in flat panel displays as indium tin oxide, but it also has other important applications. Due to its status as a byproduct, the challenges in its substitution and the geographical concentration of its production, there are concerns about the future indium supply.

2.1 Properties

Elemental indium is very soft and it has a bright luster. It has a low melting point (156°C) and a high boiling point (2080°C) (Chagnon, 2010). Indium has a plastic nature, which is probably its most noted feature. It does not work-harden, it can endure considerable deformation through compression and it cold-welds easily (Chagnon, 2010). Even at cryogenic temperatures, it is ductile and malleable (Shanks et al., 2017).

Indium, with the atomic number 49 and the symbol In, is placed in the boron group in the periodic table. It has similar chemical properties as its group neighbors, i.e. gallium and thallium (Alfantazi and Moskalyk, 2003). Most commonly, it occurs in +3 valence state (Shanks et al., 2017). Air does not oxidize indium at ordinary temperatures, but upon heating, it burns to form a trioxide (In_2O_3) and can also react with metalloids, halogens, sulfur and phosphorus (Chagnon, 2010). Inorganic acids dissolve indium and it amalgamates with mercury, but alkali, boiling water and most organic acids have minimal effect on it (Chagnon, 2010).

2.2 Applications

Since its discovery, indium has found a wide variety of applications. The leading end-use for indium is production of indium tin oxide, which is used in a variety of flat-panel devices. Other end-uses include solders and alloys, photovoltaic cells and semiconductor devices. Indium is also used a substitute for mercury in alkaline batteries, to prevent corrosion of the zinc anode (European Commission, 2017). The share of indium used for each of the applications, is illustrated in Figure 1.

Production of indium tin oxide (ITO) accounts for the majority of indium consumption (Anderson, 2018a). It is a gray-yellow powder made either by blending indium oxide and tin oxide powders or by coprecipitation of a solution containing indium and tin (Chagnon, 2010). Typically, ITO consists of 90% indium(III) oxide (In_2O_3) and 10% tin(IV) oxide (SnO_2) (European Commission, 2017). It is primarily used as a transparent electrode in a variety of flat-panel displays, such as liquid crystal dis-

plays (LCD), plasma display panels and OLED displays (organic light emitting diodes). ITO is deposited, by sputtering, as a thin-film coating to the display, where it transforms electrical data into an optical form. Flat panel displays are manufactured exclusively in Japan, South Korea and China (European Commission, 2017).

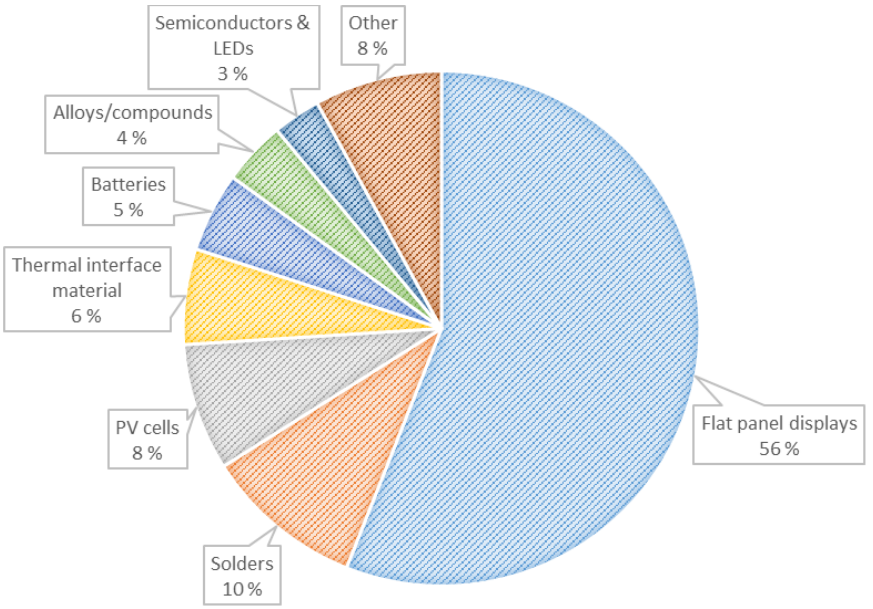

Figure 1. Global end-uses of indium in 2013. Data from Indium Corporation cited in ETF.COM (Vulcan, 2013).

ITO is also deposited as thin coatings on car and aircraft windshields for defogging and deicing (European Commission, 2017). It functions as an electrically conductive coating, which heats the glass when an electric current is applied. A similar type of indium oxide coating has an infrared-reflecting function, which has great potential for savings on heating and cooling energy when deposited on structural glass (Chagnon, 2010). In thin-film photovoltaic cells, ITO works as a top transparent electrode, maximizing light transmission to the light absorbing materials (European Commission, 2014a).

Apart from being used in the form of ITO as a top transparent electrode in all thin-film solar cells, indium is used in thin film copper-indium-gallium-selenide (CIGS) and copper-indium-selenide (CIS) photovoltaic cells in the light absorbing material. Compared to the conventional crystalline silicon-based cells, thin films require less functional material, as the layer is only a few micrometers deep (European Commission, 2017). Another advantage relative to crystalline silicon is that thin films can be manufactured in continuous rolls and that they can be deposited on flexible

substrates (Chu, 2011). The thin film technology has shown promise of high conversion efficiency and short energy payback time.

The module production of CIS and CIGS thin films has tripled during the years 2010–2016, but there has not been any increase in their market share, as there has been a strong growth in the whole photovoltaics market (Fraunhofer Institute for Solar Energy Systems, 2018). There has actually been a slight decrease in the market share of CIS and CIGS, which was 1.5% in 2016, and a more substantial decrease from 15% in 2010 to 6% in 2016 for the market share of all thin films (Fraunhofer Institute for Solar Energy Systems, 2018). In 2011, the silicon prices dropped sharply, making crystalline silicon PV cells much more cost competitive with thin-film cells (Chu, 2011). The crystalline silicon-based cells account for more than 90% of the global photovoltaics market (Fraunhofer Institute for Solar Energy Systems, 2018).

Indium is usually also used in multi-junction photovoltaic cells employed in concentrator photovoltaics (CPV) and satellites (Wiesenfarth et al., 2017). The CPV technology involves mirrors and lenses focusing the sunlight onto the multi-junction solar cells, which have multiple ultrathin layers capturing different light wavelengths. Indium is present in the semiconducting layers, most commonly as gallium indium phosphide (GaInP) and/or gallium indium arsenide (GaInAs) (Wiesenfarth et al., 2017).

Indium is easily combined with nonmetallic elements and metalloids, and is used combined with such in semiconductor substrate compounds, such as indium antimonide (InSb), indium arsenide (InAs) and indium phosphide (InP) (Chagnon, 2010). Several indium-containing compounds can also be used as semiconductor substrate coating, such as indium gallium arsenide (InGaAs) (Shanks et al., 2017). Indium-based semiconductors are used for light emitting diodes (LEDs) and laser diodes. Indium-based LEDs are used mainly for optical data transmission and, to a lesser extent, in LED displays (Shanks et al., 2017).

Solders and alloys constitute together the second most popular end-use of indium (Shanks et al., 2017). Indium-containing solders show improved resistance to thermal fatigue and lower crack propagation compared to tin-lead solders (Shanks et al., 2017). They are useful for circuit board manufacturing, as indium lowers the melting range and thereby makes soldering without damaging the electronic components possible (Chagnon, 2010).

An important use for indium, both as a metal and as an alloy, is in thermal interface materials (European Commission, 2017). Thermal interface materials are placed between two components to enhance their thermal coupling. Usually this means transferring heat generated by semiconductors to a heat sink and thereby preventing devices from overheating. Indium is suitable for this application due to its thermal conductivity and malleability, which allows it to fill microscopic gaps (European Commission, 2017).

Indium brings certain benefits to alloys, such as strength and corrosion resistance. Indium is used for corrosion resistive purposes in coatings for high-performance engines, where it also improves abrasion resistance and helps to retain an oil film on the surface (Chagnon, 2010). When added to aluminum and zinc alloys

for use in sacrificial anodes, indium increases the anode efficiency as well as the potential (Chagnon, 2010). Indium is also used as an additive in nuclear reactor control rod alloys, dental alloys and alloys for sealing applications (Chagnon, 2010).

2.3 Substitutes

On a scale where 0 stands for highly substitutable and 100 stands for completely irreplaceable, indium has been rated 60, suggesting that replacing indium in its end-uses, especially without a loss in functionality or performance, would pose some technical challenges (Graedel et al., 2013). Harper et al. (2015) give indium the score 55 on a similar 0-to-100 scale. Many alternatives for ITO, the most common end-use of indium, has been developed and explored, but none of them is used on a larger scale.

As an alternative to ITO, antimony tin oxide coatings have been developed and successfully annealed to LCD glass (Anderson, 2018a). Also the cheaper aluminum doped zinc oxide and fluorine doped tin oxide could replace ITO, but not without loss in performance (Jackson, 2012). Carbon nanotube coatings could substitute ITO in flexible displays, solar cells and touch screens, but they are expensive to manufacture in high purity and there are separation problems as manufacturing produces both metallic and semiconducting nanotubes (Jackson, 2012). Other ITO alternatives include graphene quantum dots (Chu, 2011), silver nanowires (Cambrios, 2018) and PEDOT [poly(3,4-ethylene dioxythiophene)] (Anderson, 2018a). LCD manufacturers are reluctant to substitute ITO, as a switch would disrupt established manufacturing lines (Jackson, 2012). As the cost impact of ITO in liquid crystal displays is only about 1% of the total cost, an increase in indium prices would not work as much of an incentive (Jackson, 2012).

As for other indium compounds, gallium arsenide can replace indium phosphide in semiconductor applications and hafnium works as a substitute for indium in nuclear control rod alloys (Anderson, 2018a). Bismuth can replace indium in tin alloys for low-temperature bonding and soldering applications and lead-based alloys could work as a substitute for indium-tin alloys for sealing at cryogenic temperatures (European Commission, 2017). Of the above-listed materials, antimony, gallium, hafnium and bismuth are, like indium, listed as critical raw materials by the European Commission (2017).

2.4 Occurrence

The abundance of indium in the upper continental crust is about 0.066 ppm (Hu and Gao, 2008). It is widely dispersed and it does not occur in concentrations high enough to economically justify mining it alone. Thus, it is referred to as a minor metal. The most important indium-containing deposit types are volcanic- and sediment-hosted base-metal sulfide deposits (European Commission, 2017). Other deposit types containing recoverable amounts of indium include polymetallic vein-type

deposits, vein-stockwork deposits of tin and tungsten and epithermal deposits (Schwarz-Schampera, 2014 cited in European Commission, 2017).

Minerals containing indium as a major element, such as roquesite ($CuInS_2$), are found as inclusions inside more common minerals, including chalcopyrite, cassiterite, stannite and sphalerite, allowing indium to be recovered as a byproduct during the refining process of other base-metal ores and concentrates (Werner, Mudd and Jowitt, 2017). Most commonly, indium is recovered from the zinc-sulfide sphalerite, as a byproduct of zinc production. Indium can be easily incorporated into the crystal lattice of sphalerite by coupled substitution with copper ($2Zn^{2+} \leftrightarrow Cu^{+} + In^{3+}$) (Cook et al., 2012). The indium content of the minerals it is recovered from typically range from 20 ppm to 350 ppm (Frenzel et al., 2017; Werner, Mudd and Jowitt, 2017).

2.5 Processing

Indium recovery follows different techniques depending on its source material, i.e. fumes, dusts, slags, residues and alloys from other mining and refining operations. Hydrometallurgical stages and electrolytic refining are usually preferred. Generally, the recovery process includes leaching of the source material with sulfuric or hydrochloric acid to dissolve indium, solvent extraction to increase the indium concentration in the solution, cementation to remove indium from the solution and electrolytic refining to desired purity (Alfantazi and Moskalyk, 2003). The normal purity of commercial-grade indium is 99.99%, but higher purities are required in the electronics industry (Chagnon, 2010). Indium is typically formed to ingots, but also to wire, ribbon and foil, which are used for soldering (Shanks et al., 2017).

2.6 Primary production

The estimated total world refinery production of indium in 2017 was 720 metric tons, with China, South Korea, Canada and Japan dominating the market (Figure 2) (Anderson, 2018a). A large share of the world indium resources is estimated to be located in these countries, but a considerable amount also is located in Bolivia, Portugal and Australia, which are not currently producing indium (Werner, Mudd and Jowitt, 2017). Bolivia (Tolcin, 2017a) and Australia (Werner et al., 2018) *produce* indium-bearing concentrates, but export it for processing elsewhere.

In Europe, there are significant refining operations in Belgium and France. Umicore's precious metals refinery at Hoboken in Belgium produced approximately 20 metric tons of indium in 2017 (Anderson, 2018a) and has the capacity to recover 50 metric tons of indium-containing product per year (Umicore, 2018b). In Auby, France, Nyrstar's indium production plant shut down in November 2015 due to a fire, but resumed indium production in 2017 after a plant extension increasing its capacity to 70 metric tons per year (European Commission, 2017). 30 metric tons of indium metal was produced there in 2017 (Nyrstar, 2018).

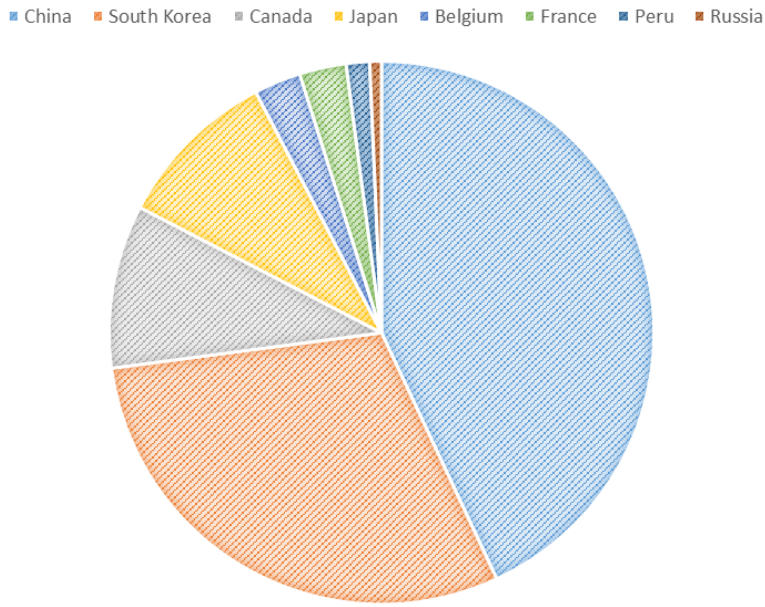

Figure 2. Estimated world primary production of indium 2017, by country. Based on data from U.S. Geological Survey's Mineral Commodity Summary 2017 (Anderson, 2018a).

China is the leading producer of indium, currently accounting for about 43% of the world production. From 2014 to 2016, the annual Chinese indium production decreased 35% (Figure 3), due to the collapse of the Fanya Metal Exchange in China and the concurrent drop in indium prices. Indium was the most affected metal, as 3,600 metric tons of indium was held at Fanya's warehouses in November 2015, when its web site was shut down (Tolcin, 2016). Indium prices and Chinese indium production continued decreasing in 2016 due to the oversupply, but China's net exports of indium increased by 30% (Tolcin, 2017b). The production of indium in other countries continued more or less on the same level. As of November 2017, the 3,600 metric tons of indium was still held at Fanya's warehouses and no information was available as to when it would be released to the market (Anderson, 2018a). According to Fu, Polli and Olivetti (2018) an anonymous industry expert claims that it might take more than 10 years for the inventory to be sold.

2.7 Secondary production

Secondary production of indium became significant for the first time in 1996 (Brown, 1996) and by 2007, it accounted for a greater share of indium production than primary production (Chu, 2011). Secondary production of indium is mostly accounted

for by recycling of ITO manufacturing waste. In 2016, the Indium Corporation estimated that 1,200 metric tons of indium can be reclaimed from ITO manufacturing waste (Tolcin, 2017a). A large extent of the ITO waste recycling can be explained by the fact that only about 30% of the ITO target material is successfully deposited on the substrate and thereby 70% is conceivably available for recovery and reuse (Chagnon, 2010). In 2010, it was estimated that 60–65% of this could be recovered and it was reported that research was underway to improve this rate further (Chagnon, 2010). In a global substance flow analysis by Licht, Peiró and Villalba (2015b), a lower yield for the ITO deposition process and a higher yield for the recycling process was used. According to their estimations, 76% of indium used for ITO production in 2011 could be recovered from manufacturing waste, whereas only 3% ended up in final products and the rest was lost. ITO recycling has grown in parallel with the ITO-producing countries Japan, China and South Korea. As they represent together about 90% of global ITO capacity (Tolcin, 2017a), these countries are dominant in secondary production of indium as well. Also, Belgium is a notable producer of secondary indium (Lokanc et al., 2015).

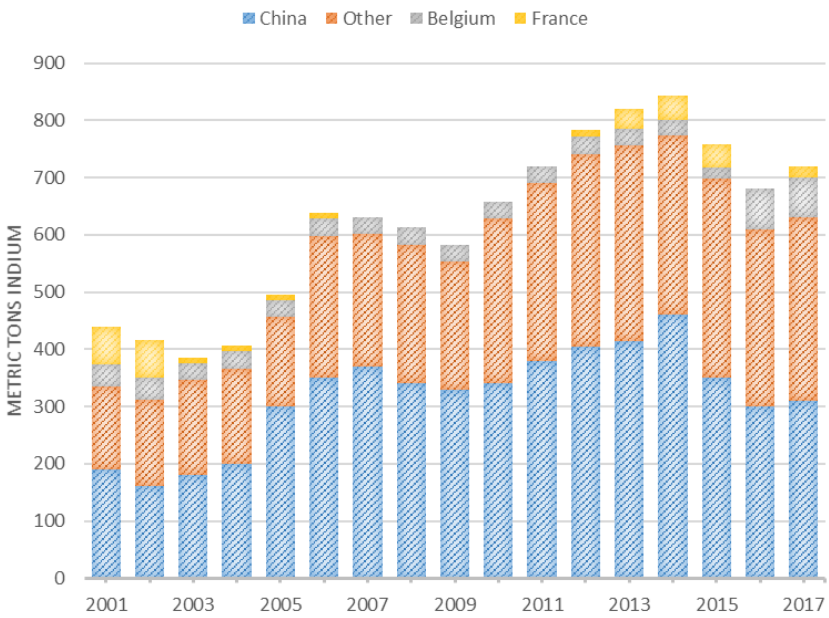

Figure 3. Estimated world primary production of indium 2001–2017. Based on data from U.S. Geological Survey's Mineral Yearbooks 2005 (Callaghan and Carlin, 2007), 2010 (Tolcin, 2012) and 2015 (Tolcin, 2017a) and Mineral Commodity Summaries 2016 (Tolcin, 2017b) and 2017 (Anderson, 2018a).

There is a significant amount of indium that has accumulated in tailings, i.e. the uneconomic fraction of ore that is discarded during mineral processing, and in slags,

i.e. a byproduct of smelting (Werner, Mudd and Jowitt, 2017). Recovery of indium from tailings has taken place at least in China (Phipps, Mikolajczak and Guckes, 2008) and Japan (Chu, 2011). Phipps, Mikolajczak and Guckes (2008) reported that some slags and tailings are economical to treat due to higher indium prices and improving recovery process technology. This is not necessarily the case anymore, since the indium prices were significantly higher in 2008 than current prices. Frenzel et al. (2017), however, claim that recovery from most waste sources depends on the value of the contained main products, e.g. copper or zinc, rather than the value of the byproduct, in this case indium. Thereby, indium from slags and tailings could only contribute significantly to the supply if they contribute significantly to the main-product supply, which is unlikely for most industrial metals.

The Roast-Leach-Electrowinning (RLE) process, which is the most common process for zinc production, produces jarosite residues that are classified as hazardous waste and have traditionally been disposed in waste facilities, or in on-site residue areas or tailings dams (Creedy et al., 2013). Environmental concerns and legislation now force companies to find environmentally viable solutions for jarosite residues. Kangas et al. (2017) propose a hydrometallurgical process for treatment of jarosite residues, including recovery of indium and germanium. Other alternatives for treatment of jarosite residues are stabilization for use as a landfill and pyrometallurgical smelting, which produces an inert slag and recovers some of the metal content (Kangas et al., 2017).

Licht, Peiró and Villalba (2015) argue that manufacturing processes do not offer a significant opportunity for increasing indium recovery much further and that the greatest efforts should be aimed toward increased end-of-life recycling in order to meet increasing indium demand in the future. The end-of-life recycling rate was less than 1% for indium in 2011 (UNEP, 2011) and no information indicating a significant increase since could be found.

Waste electric and electronic equipment (WEEE) could be a future source of secondary indium, as LCD and other flat panels consume most of world indium production. The collection and separation of indium from waste is among the main problems with end-of-life recycling. Only about one-third of the amount of electrical and electronic equipment that was put on the market in the EU in 2015 was collected in the same year (Eurostat, 2017). Because of minor indium concentrations in the products, indium recovery from end-of-life waste requires sorting, preprocessing with manual dismantling as well as increased selective extraction (Ylä-Mella and Pongrácz, 2016). Considering critical materials recycling, current policies put too much focus on maximizing recycling rates and too little on high product qualities (Velis and Brunner, 2013). Also, the wide variety of goods with versatile product design and the requirements of high purity in ITO production challenges the development of economically viable indium recycling processes (Ylä-Mella and Pongrácz, 2016). In addition, there is uncertainty if end-of-life recycling could result in net environmental benefits (Ciacci et al., 2018).

Recycling of indium contained in end-of-life solders and alloys shares one of the problems with recycling from WEEE. Indium contained in solders and alloys could potentially be recycled, but it would require selective separation from other alloys

and recycling by alloy type (Ciacci et al., 2018). Still, the recovery routes of alloy recycling are built around the recovery of major carrier metals, such as iron, aluminum, zinc and copper (Reck and Graedel, 2012).

2.8 Market price

Annual average prices for indium are illustrated in Figure 4. The U.S. producer price for indium in 1995 was 380 USD/kg. In 1996, when the secondary production first became significant, the price dropped to around 300 USD/kg and was stable until 2000, when low-priced indium from China forced world prices further down, even though there was a strong increase in indium demand for LCD production (Brown, 2001). Indium prices hit bottom in 2002, when U.S. producer price was 100 USD/kg. The annual average price increased almost tenfold to 2005, due to increased demand for ITO and closure of Chinese smelters, which created the perception that Chinese indium production would decrease (George, 2005b).

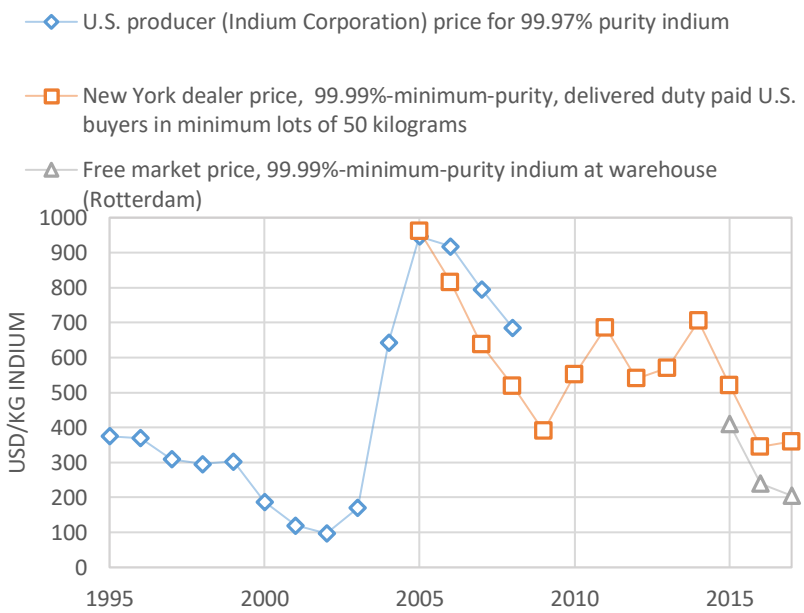

Figure 4. Annual average indium prices 1995–2017. Indium corporation's price data from U.S. Geological Survey's Mineral Commodity Summaries 2009 (Tolcin, 2010), 2005 (Carlin, 2006) and 2000 (Brown, 2001). New York dealer price data from Mineral Commodity Summaries 2010 (Tolcin, 2011), 2015 (Tolcin, 2016) and 2018 (Anderson, 2018a). Free market price data from Mineral Commodity Summaries 2018 (Anderson, 2018a).

The New York dealer price for indium steadily decreased from 960 USD/kg in 2005 to 390 USD/kg in 2009. Secondary production of indium increased and accounted for more than half of the total production in 2007, but because of the continued increase in ITO demand, the market remained in supply deficit (Tolcin, 2008). Due to the collapse of the Fanya Metal Exchange in China, the New York dealer price decreased from 710 USD/kg in 2014 to 350 USD/kg in 2016. The estimated average free market price of indium in 2017 is 210 USD/kg.

2.9 Future demand

Indium consumption is expected to increase especially with the growing demand for small- and medium-sized LCD panels for e-books, smartphones and tablets, while growth rates for large-sized panels are estimated to be more moderate (Ylä-Mella and Pongrácz, 2016). IGZO (Indium Gallium Zinc Oxide) technology, which provides displays with high resolution, low power consumption and a fine touch sensitivity, has a growing market and can contribute to a growing indium demand (European Commission, 2017). Pavel et al. (2016) estimated that the demand for indium for displays and LED technology, which was about 300 metric tons in 2016, will increase 30–50% by 2020. Erdmann (2009) predicts that indium demand in 2030 will be 3.3 times higher than the world production in 2009.

The photovoltaics market is growing fast, but given the decreasing market share of thin-films, this is not likely to contribute substantially to an increased indium demand, at least not in the short term. CPV installations could increase in the future, but the amount of indium required for typical multi-junction cells is very small and an expansion of the indium supply chain is not expected to be needed to achieve gigawatt annual production volumes (Wiesenfarth et al., 2017). However, the use of indium in cryogenic metallurgy, automotive alloys and low-melting alloys for security purposes, which is limited today, could increase in the future (Ciacci et al., 2018).

2.10 Supply risk

The European Commission (2017) and the U.S. Department of Energy (Chu, 2011) have, among others, classified indium as a critical material, due to concerns about future supply. On a 0 to 100 scale, Harper et al. (2015), gave indium the score of 97 for supply risk. According to Werner, Mudd and Jowitt (2017) a minimum of 76,000 metric tons of indium has been reported to be contained and 263,000 metric tons is inferred to be contained in known mineral deposits. They conclude that geological scarcity will not be an issue in the short to medium term. The sheer resource quantities of indium are not the key issue, but the dependency on mining of its carrier metal, zinc.

The supply of indium largely follows the supply of zinc and an unsuspected increase in indium demand, for instance due to a new application, could result in a serious supply deficit. Sprecher et al. (2017) investigated a scenario where graphene partly replaces zinc in galvanic applications, resulting in a 33% decrease in

zinc demand by 2040. They conclude that the scenario would result in a 30–50% shortage in indium supply by 2050. For a scenario without any disruption in zinc production, Sprecher et al. (2017) estimate that there will be a slight to moderate indium supply deficit.

Since the early 1970's, exponential growth of indium demand has been met with limited shortages, owing to improvements in the efficiency of production (Werner, Mudd and Jowitt, 2017). How long the faster growth of indium production compared to zinc will be sustainable, is a major question in the assessment of supply risk. Frenzel et al. (2017) use the percentage of extractable indium that was actually recovered in 1994–2014, to estimate that in 20 years, growth of indium extraction relative to zinc production may no longer be possible without increases in indium prices. Since the estimation does not consider additional sources of indium that might be available in the future, sources such as end-of-life recycling or historic smelter residues could increase the time estimate.

In the scenario where indium prices start limiting further growth of indium extraction compared to zinc production, the elasticity of the supply and demand of indium will dictate the magnitude of the increase in indium prices. An elastic regime would permit large increases in supply or decreases in demand with only a moderate increase in price. According to Frenzel et al. (2017), 76% of all the indium contained in sulfidic zinc concentrates is already extractable at current price levels, indicating limited elasticity in supply. Due to the cost impact of indium being minor in its primary applications, also the demand for indium is inelastic (O'Neill, 2010). This implies that when the production of indium reaches its potential, the increase in indium prices will be substantial and a supply deficit will be probable.

About 80% of the primary production of indium is in China, South Korea and Japan. Such a geographical concentration of production is typical for critical materials and increases the risk of supply disruptions and volatility of prices due to political and/or economic reasons. Chu (2011) considers the indium producer diversity and expansion possibilities for minor indium producers to be sufficient and states that no significant political, regulatory or social factors are likely to affect future indium production. Werner, Mudd and Jowitt (2017) suggest that restrictions of exports in major indium producing countries, like China, could be counteracted by countries currently not producing, but who are well positioned to enter the market, like Bolivia and Australia.

3. Germanium market review

Germanium is a hard and brittle metalloid with a grayish-white color. It has the symbol Ge and the atomic number 32. In 1871, before its discovery, Dmitri Mendeleev predicted the properties of germanium and called it ekasilicon (beyond silicon) due to its position in the periodic table (Shanks et al., 2017). The chemist Clemens Winkler, who was the first to isolate germanium in 1886, named it after his native country, Germany (Shanks et al., 2017). The first use of germanium was established during World War II, when it was used in the first radar devices in the United Kingdom (Thomas, Mahmood and Lindhal, 2011). Today, the most common end-use of germanium is optical fibers, for which the demand is expected to increase. Germanium is produced as a byproduct of zinc production or from coal fly ash, and to some extent it is mined as a main product from germanium-rich coal mines. The production of germanium is far from reaching its supply potential, but germanium is one of the metals with the greatest concern regarding supply disruptions resulting from non-geological factors.

3.1 Properties

Germanium is a hard and brittle metalloid with a characteristic cubic face-centered crystal structure. Germanium is between silicon and tin in the carbon group and due to similar properties, it is commonly also used as a substitute for them (Shanks et al., 2017). Like silicon, germanium can form glass in a randomly ordered tetrahedral arrangement with oxygen (Shanks et al., 2017). Germanium is an intrinsic semiconductor, which together with the high refractive index and low chromatic dispersion, makes a unique combination of properties (Shanks et al., 2017). These properties make germanium hard to replace in many of its applications.

Germanium metal is stable in air up to 400°C and resists concentrated hydrochloric acid, concentrated hydrofluoric acid and sodium hydroxide solutions (Thomas, Mahmood and Lindhal, 2011). It reacts slowly with hot sulfuric acid and more readily with nitric acid, especially in a mixture with hydrofluoric acid (Thomas, Mahmood and Lindhal, 2011). Most commonly, germanium has the valence state +4 or +2, with the divalent compounds tending to be less stable than the tetravalent ones (Thomas, Mahmood and Lindhal, 2011). It forms bromides, chlorides, fluorides, iodides, hydrides, oxides and sulfides (Thomas, Mahmood and Lindhal, 2011). In aluminum and magnesium alloys, germanium improves the physical strength and hardness (Moskalyk, 2004).

3.2 Applications

Major applications of germanium are optical fibers, semiconductor devices, photovoltaic cells, infrared optics and polymerization catalysis. Other uses include gamma-ray detectors, organic chemistry, phosphors, metallurgy and chemotherapy (European Commission, 2017). Relatively little germanium is used for alloys, but it

has proven useful in solder for gold jewelry, in dental alloys and in very small amounts as a hardener of metals (Butterman and Jorgenson, 2005). The most common end-use of germanium is optical fibers (Figure 5).

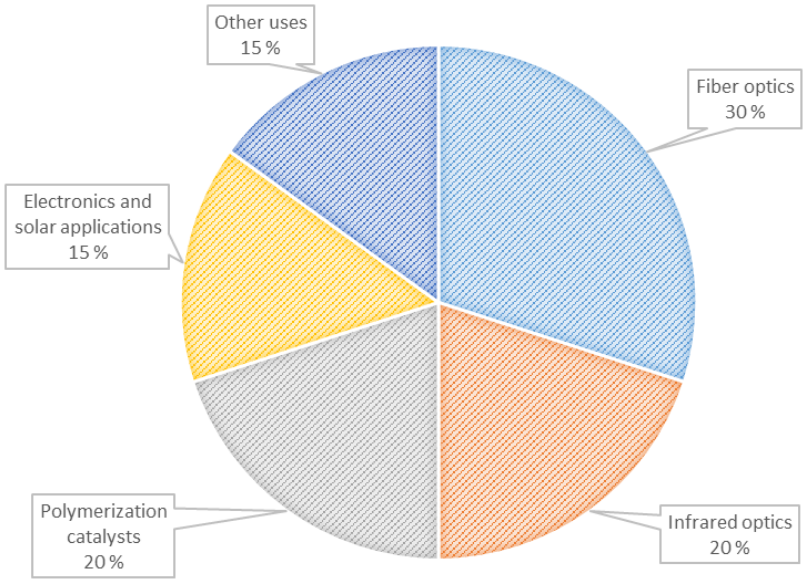

Figure 5. Estimated share of global end-uses of germanium. Based on estimations in U.S. Geological Survey's Mineral Commodity Summaries 2015 (Guberman, 2016b).

Glass optical fibers are used to transport data across long distances and germanium oxide (GeO_2) is used in their core as a dopant. The core of optical fibers contain about 4% germanium (Brunot et al., 2013). The addition of germanium to the pure silica glass core increases the refractive index and minimizes signal loss over long distances (Shanks et al., 2017). In recent years, there has been substantial growth in the telecommunications sector and an increasing demand for more bandwidth (European Commission, 2017).

Another important application for germanium is infrared optical systems, in which germanium is used in lenses and windows. The transparency to a part of the infrared spectrum and the high refractive index of germanium are making it ideal for this application. The lenses and windows are a part of thermal imaging systems that detect infrared radiation, convert it into an electronic signal, process the signal and display it on a screen (Thomas, Mahmood and Lindhal, 2011). Germanium is also incorporated in infrared detection sensors (Tercero, 2018). About half of all infrared-optical systems have germanium crystal lenses and about 80% are used in military applications (Thomas, Mahmood and Lindhal, 2011).

Germanium oxide (GeO_2) works as a catalyst in the polymerization reaction of polyethylene terephthalate (PET). PET is used for plastic bottles, plastic film and synthetic textile fibers. Estimates have indicated a decreasing consumption of germanium for PET since 2011 (Guberman and Thomas, 2017). The majority of germanium consumption for PET production has taken place in Japan, where producers reacted to germanium price increases by substitution with lower-cost antimony- and titanium-based products (Guberman and Thomas, 2017).

Germanium was used in the first transistor, developed by Bell Laboratories (Thomas, Mahmood and Lindhal, 2011). A growing germanium market was provided by its use in power transistors and telephonic applications in the 1950's and 1960's, until it was to a large extent substituted by silicon semiconductors, due to the abundance of silicon and its ease of processing (Thomas, Mahmood and Lindhal, 2011). The use of germanium in semiconductor devices is now minimal, but not completely phased out.

Germanium-based semiconductors are used in light-emitting diodes (LEDs) for general lightning purposes as well as in displays for cameras and smartphones, but are expected to lose their relevance in lighting purposes over the next ten years, as they are already widely substituted by gallium-based semiconductors (Pavel et al., 2016). Silicon-germanium alloy is used in high-frequency diodes and transistors (Velte, 2015). Silicon-germanium transistors have greater speeds and require less power than the traditional silicon components (Thomas, Mahmood and Lindhal, 2011). Germanium also works as a semiconductor in photovoltaic cells.

In the photovoltaics industry, germanium is mainly used in multi-junction solar cells. Multi-junction solar cells have multiple ultrathin layers that are deposited on a germanium substrate and capture different light wavelengths (Shanks et al., 2017). They are the highest-efficiency photovoltaic cells available, with a record laboratory efficiency of 46%, using the concentrator photovoltaic (CPV) technology (Fraunhofer Institute for Solar Energy Systems, 2018). The CPV technology involves mirrors and lenses focusing the sunlight onto the solar cells. Although the CPV installations have decreased in recent years, the market is only beginning to be established and is a potential growth area for germanium use (Wiesenfarth et al., 2017). Due to high manufacturing costs, the use of multi-junction solar cells is restricted to CPV power plants and space-based solar applications. The majority of satellites are powered by germanium-containing solar cells (Thomas, Mahmood and Lindhal, 2011).

3.3 Substitutes

On a scale from 0 to 100, where 0 indicates that there are excellent substitutes available for all major uses and 100 indicates that there is no existing substitute with even adequate performance, germanium was given the value 44 (Graedel et al., 2013). Harper et al. (2015) give germanium the score 35 for substitutability, also on a 0-to-100 scale. Substitutes for germanium exist for all of its major applications, but in many cases loss of performance or functionality is involved.

Silicon can be a less-expensive substitute for germanium in certain electronic applications. Silicon is the natural substitute for silicon-germanium alloy in high-frequency diodes and transistors, but it is, as mentioned above, inferior in performance. Germanium in LEDs is already largely substituted by gallium. A possible substitute for multi-junction solar cells with germanium is inverted metamorphic (IMM) solar cells. Instead of germanium, gallium arsenide is used as substrate in IMM multi-junction solar cells, and it is peeled off at the end of the manufacturing process (Pickerel, 2017).

Phosphorus pentoxide (P_2O_5) and alumina (Al_2O_3) can be used in the core of optical fibers for the same purpose as germanium, i.e. to increase the refractive index (Paschotta, 2008). Harper et al. (2015) named alumina as the primary substitute for germanium in optical fibers and considered its substitute performance as good. According to the European Commission (2017), referring to communication with an industrial player in October 2016, substitutes of germanium in optical fibers are not really used because of performance losses, but fluorine and phosphorus can be mentioned, with a low probability of industrial use. Graphene-core optical fibers (Das and Sahoo, 2016) or ZBLAN glass (ZrF_4-BaF_2-LaF_3-AlF_3-NaF) (Butterman and Jorgenson, 2005) could theoretically exhibit better properties for telecommunication optical fibers than standard silica fibers. Photonic crystal fibers (PCF), with air holes surrounding the core and lowering the refractive index, are commercially available as substitutes for standard silica fibers (Tercero, 2018).

Zinc selenide (ZnSe), zinc sulfide (ZnS) and chalcogenide glass are substitutes for germanium in infrared optical systems. Umicore (2018a) offers infrared optics made from germanium, ZnSe, ZnS and chalcogenide glass (GASIR®) and claims that their chalcogenide glass product is ideal for both high-performance infrared imaging systems and high-volume commercial applications. It has a wider spectral range than germanium and much better athermalization possibilities (Umicore, 2018a). According to Pleşa et al. (2015), chalcogenide materials offer approximately the same image quality like germanium and are future prospective materials that would provide less expensive technical devices in the field of night vision electro-optics. The chalcogenide investigated by Pleşa et al. (2015) contains germanium ($Ge_{30}As_{13}Se_{32}Te_{25}$), which could also be the case for GASIR®, as the composition of the chalcogenide is not available in the reference. Zinc selenide and zinc sulfide usually substitutes germanium at the expense of performance (Thomas, 2018b).

Of all major germanium applications, Harper et al. (2015) report PET catalysis as the only one with less than good substitute performance. Despite of this, its substitutes are often used, due to germanium being considered too expensive (East, 2006). Antimony trioxide is a commonly used PET catalyst, but it has raised environmental and health concerns, as the catalyst is present in the final product. Although the Swedish Chemicals Agency (2008) reports that there is profound leaching of antimony from PET bottles to water, they conclude that regarding the health of consumers, there is no need for risk reduction measures beyond those already being applied. Antimony trioxide has a susceptibility to reduction to metallic antimony, which can lead to an undesirable gray color in the final product and other

PET catalysts, like titanium alkoxides or alkyl-tin catalysts cause yellowing of the product (East, 2006).

3.4 Occurrence

The abundance of germanium in the upper continental crust is about 1.3 ppm (Hu and Gao, 2008). Germanium is dispersed and does not occur as a native metal in nature (Butterman and Jorgenson, 2005). 30 minerals containing germanium can be found in the Mineralogy Database (Barthelmy, 2012), but only rarely can any of these be found in commercial quantities. An example of a deposit containing significant amounts of germanium mineral is the Kushib Springs deposit in the Otavi Mountain Land, Namibia. The central and lower parts of its orebody contain up to 200 ppm germanium, mostly in the form of colusite ($Cu_{26}V_2(As,Ge)_6S_{32}$), but also as germanite ($Cu_{13}Ge_2Fe_2S_{16}$) (Melcher, Oberthür and Rammlmair, 2006).

Germanium is present as a trace element in some common minerals, most frequently in zinc-sulfide sphalerite, which contains some tens of ppm germanium on average (Frenzel, Ketris and Gutzmer, 2014). Sulfidic lead-zinc deposits and lignite deposits with high germanium content are the most important known germanium deposits, as current germanium production is mostly from zinc-smelter residues and coal ashes. Coal contains on average about 2 ppm germanium (Ketris and Yudovich, 2009), but there are some coal deposits with a germanium content above 100 ppm, especially in Eastern Asia (Du et al., 2009). The Wulantuga coal deposit in the Schengli coalfield, northeastern China, shows an average germanium concentration of 298 ppm in its most germanium-rich coal seam (Du et al., 2009). Frenzel, Ketris and Gutzmer (2014) estimate that a minimum amount of 120,000 metric tons of easily recoverable germanium is present in highly concentrated coal and zinc deposits and that more than 400,000 metric tons is hosted by low-concentration coal and zinc deposits.

3.5 Processing

The preliminary processing methods of germanium raw materials depend on the origin of the source material. Drzazga (2018) gives a general description of the extraction process as follows. The source material can be treated with pyro- or hydrometallurgical methods, or both. The pyrometallurgical treatment results in dusts and fumes, with germanium in oxide (GeO_2) or sulfide (GeS_2) form. In most cases, the leaching is done with sulfuric acid. Germanium is precipitated as sulfide, metal germanate, germanium cement or germanium tannin complex. Before purification, the germanium concentrate is oxidized. The tannin method is often applied for precipitation, particularly for germanium from zinc residues, when the germanium content of the solution is less than 1 g/l. The resulting germanium tannin complex is roasted into germanium oxide concentrate.

Regardless of the source material, the purification process is similar for all germanium concentrates. The extent of purification does however depend on the end-

use of germanium, as shown in Figure 6. The purification process is described by Butterman and Jorgenson (2005) as follows. First, the germanium concentrate is dissolved in concentrated hydrochloric acid, producing germanium tetrachloride ($GeCl_4$). The $GeCl_4$ is purified by fractional distillation and hydrolyzed with deionized water to yield GeO_2. The GeO_2 is reduced with hydrogen at 760°C to form germanium metal powder, which is melted and cast into bars. Finally, the bars are zone refined and, for electronic and some optical uses, melted and grown to single crystal ingots.

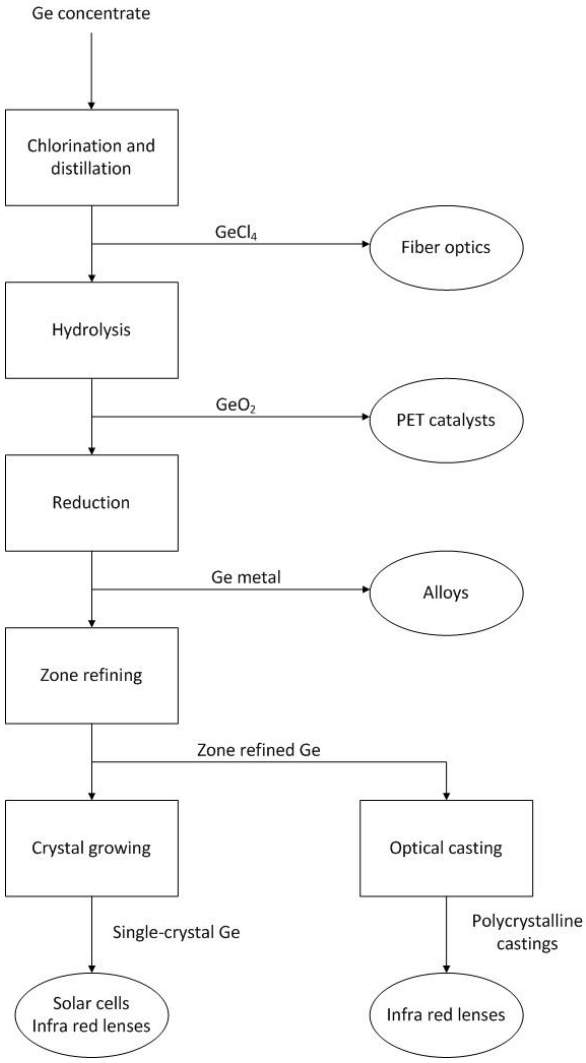

Figure 6. Purification process and applications of germanium. Figure reproduced from Melcher and Buchholz (2012).

3.6 Production and prices

The United States Geological Survey (USGS) estimates that the world refinery production of germanium, including recycled germanium but excluding United States production, was 130 metric tons in 2017 (Thomas, 2018b). Brown et al. (2018) estimate that 2 metric tons of germanium was produced in the United States in 2016, which indicates that exclusion of United States production does not result in substantial errors in world refinery estimates. China accounted for about 65% of the world refinery production in 2017 (Thomas, 2018b). Other germanium-producing countries are Russia, Belgium, Canada and Ukraine (Brown et al., 2018).

A share of the Chinese germanium production and all of the Russian germanium production come from fly ash. Germanium is the main product for some germanium-rich coals mined in these countries (Frenzel, Tolosana-Delgado and Gutzmer, 2015). Both Thomas (2018) and Brown et al. (2018) estimate that the annual production of germanium in Russia has been around 5 metric tons in recent years, but capacity for higher production volumes have been reported. Germanium and Applications Ltd. reported that coal production from their mine in the Russian Far East could yield about 20 metric tons of germanium per year, and JSC Germanium reported that as much germanium could be produced at their refinery in Krasnoyarsk, Russia (Thomas, 2018a).

Teck, the company producing germanium in Canada, has not released production data since 2007, when they produced about 40 metric tons of germanium (Thomas, 2018a). Canada exported an estimated 20 metric tons of germanium contained in dioxide in 2016 (Thomas, 2018a). At its refinery and recycling plant in Olen, Belgium, Umicore produces germanium metal, germanium tetrachloride, germanium substrates and germanium optical products (Thomas, 2018a). Not much information about germanium production in Ukraine is available, but the recovery is likely to be from fly ash, as germanium concentrations of 780 ppm in Ukrainian fly ash has been reported (Licht, Peiró and Villalba, 2015b).

The estimated annual world refinery production of germanium since 2000 is illustrated in Figure 7. In the early 2000's there was a decline in germanium production, due to a downturn in the general economy and the fiber optics market (Jorgenson, 2004). The world output was reduced with the closure of a major smelter in France and several scale-backs and closures of mine sources of germanium (Jorgenson, 2004). The year-end price of germanium metal (Figure 8) decreased from 1300 USD/kg in 2000 to 380 USD/kg in 2003.

The demand for germanium started increasing in 2004, creating a supply deficit that lasted through 2008 (Guberman, 2009). During this period, the fiber optics market recovered and it was reported in 2007 that the fiber optic demand was growing about 15% per year (Smith, 2008). In 2004, a new zinc mine in the United States began producing germanium-rich ore, which was sent to Canada for processing (George, 2005a). Canada and China produced approximately equal amounts of germanium that year and accounted together for more than half of the global production (Gabby, 2006). The price of germanium metal began increasing in 2004 and the annual average price peaked in 2008 at 1500 USD/kg.

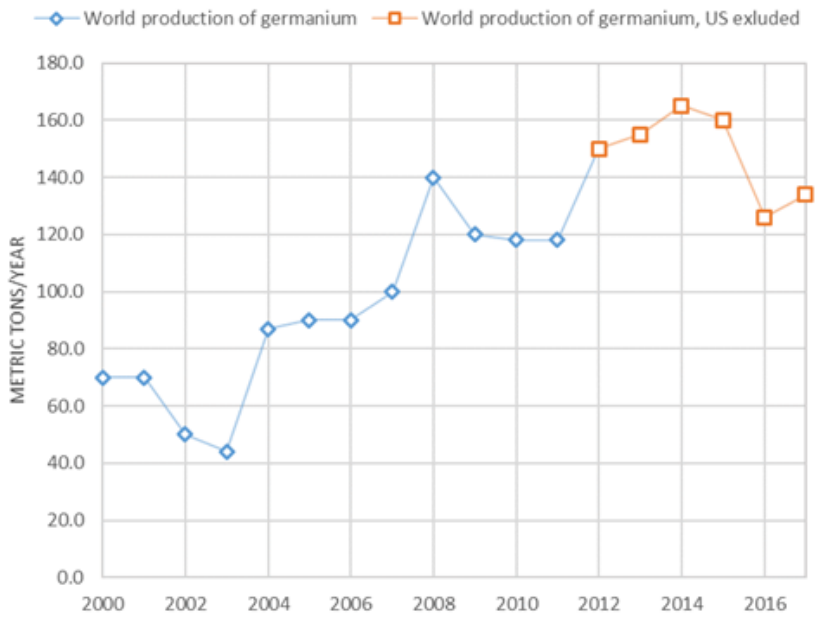

Figure 7. Estimated world refinery production of germanium 2000–2017. Based on data from U.S. Geological Survey's Historical Statistics for germanium (U.S. Geological Survey, 2015a) and Mineral Commodity Summaries 2017 (Thomas, 2018b).

The overall downturn in the global economy caused steep declines in demand for germanium in 2009. During the first nine months of 2009, the market price of germanium metal (99.99%) decreased 30% (Guberman, 2010). Instead of selling at reduced prices, some Chinese suppliers held excess supply as the market declined (Guberman, 2010). The stocks held by producers elevated in 2010 (Guberman, 2011) before the germanium prices started increasing again in 2011.

While the increase in the annual average price from 2010 to 2011 was more moderate for germanium metal, it increased by more than 100% for germanium oxide. The price increase was possibly due to a Chinese export tax on germanium oxide introduced in 2010 and the shutdown of a Chinese germanium oxide plant in early 2011 (Guberman, 2012). There was also a 46% increase in Japanese imports of germanium oxide in 2011, compared to 2010 (Guberman, 2013). Three additional Chinese germanium oxide plants were shut down in 2012, due to environmental concerns (Guberman, 2013). The germanium metal prices peaked in 2014, when the annual average price of germanium metal (99.99%) was 1900 USD/kg. The price increase is attributed to Chinese stockpiling activities (Guberman, 2015). China was responsible for most of the increase in germanium production, as the annual Chinese production increased from about 80 metric tons in 2011 (Guberman, 2013) to about 120 metric tons in 2014 (Guberman, 2016b). From 2010

to 2015, germanium was also produced in Finland. The annual production of germanium was around 15 metric tons (Brown et al., 2018).

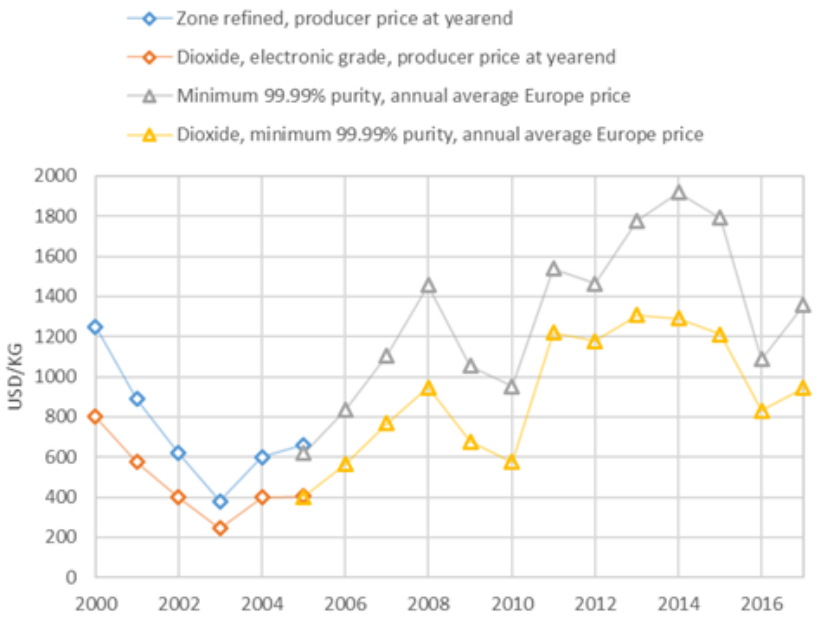

Figure 8. Estimated germanium prices 2000–2017. Based on data from U.S. Geological Survey's Mineral Commodity Summaries 2004 (George, 2005a), 2017 (Thomas, 2018b) and Mineral Yearbook 2014 (Guberman, 2016a).

Germanium dioxide and germanium metal prices were decreasing from the middle of 2015 through the end of October 2016 (Guberman, 2017). During 2015, the State Reserve Bureau in China ended its stockpiling and the buildup of germanium in the Fanya Metal Exchange warehouses ceased (Guberman, 2016b). At this time, 30 metric tons of germanium was held by the State Reserve Bureau, more than 90 metric tons was held by the Fanya Metal Exchange warehouses and 20 to 40 metric tons was held by producers in China (Guberman, 2016b). The germanium market started showing signs of recovery in 2017. In March, the germanium prices started trending upward and production of germanium in 2017 was estimated to have increased from the previous year (Thomas, 2018b).

3.7 Secondary production

According to a global substance flow analysis of germanium (Licht, Peiró and Villalba, 2015a), around 60% of the total amount refined germanium in 2011 entered

waste streams in the manufacturing processes of germanium-containing products. About 20% ended up in products considered available for future recycling and most of the remaining amount was incorporated in PET plastic (Licht, Peiró and Villalba, 2015a). Products considered available for future recycling are fiber optics, IR optics and semiconductor devices. About 30% of the refined germanium consumed in 2011 could be recovered through recycling of waste from manufacturing of germanium-containing products. Also in 2017, recycled germanium accounted for about 30% of refined germanium produced globally (Thomas, 2018b). About 60% of the germanium recovered through recycling came from fiber optics manufacturing in 2011, which is also the least efficient process, as 85% of the germanium used in the process entered waste streams (Licht, Peiró and Villalba, 2015b).

According to the United Nations Environment Programme (UNEP, 2011) the end-of-life recycling rate for germanium is less than one percent and according to the European Commission (2017) the end-of-life recycling input rate of germanium is 2%. The low recycling rate is, according to the European Commission (2017), due to a low collection rate of germanium-containing products and the technical and economic difficulties that come with low concentrations of germanium in the products. In addition, most of the installed fiber optic cables has not yet been taken out of use. Corning (2016) claims the fiber optic cables installed in the 1980's are commonly still in operation, with updated transmission equipment for higher data rates, and that there is no general evidence suggesting that they will not continue to perform for many years.

In the United States, the recovered amount of germanium from end-of-life infrared optics in the year 2000 was 10–15% of the contained germanium sold the same year (Jorgenson, 2006). In 2015, a program to recover germanium scrap from end-of-life U.S. Army components was initiated by the United States Defense Logistics Agency and by the end of September 2017, 1,843 kg of germanium scrap was recovered (Thomas, 2018b). End-of-life recycling of germanium has increased during the past decade, and is expected to continue increasing over the next two decades (Thomas, 2018a).

Limited information about recovery of germanium from slags and tailings is available, but Jorgenson (2003) reported that there were intentions of recovering germanium from slag dumps at the old Tsumeb mine in Namibia and the Big Hill slag pile in the Democratic Republic of Congo. ZincOx Resources plc acquired a 51% controlling interest in the Tsumeb slag dumps, which total about 2.9 million metric tons of slag, containing 260 ppm germanium (ZincOx Resources plc, 2002). The recovery of germanium was expected to approach 94% and the concentrate was assumed to be sold for further refining (Jorgenson, 2003). The germanium-enriched material from the Big Hill slag pile was planned for processing at a refinery in Kokkola, Finland, owned by OM Group, Inc. (Jorgenson, 2003). Germanium concentrate from Congo was processed in Finland in 2000–2015, but information is not available on whether the concentrate was from the Big Hill slag pile.

3.8 Future demand

Melcher and Buchholz (2012) expect an increasing demand for germanium, that would reach 300 metric tons in 2030. Erdmann (2009) has a similar prediction for the same year, estimating that the demand will be 2.4 times the world production of germanium in 2009. Increasing demand is predicted for all major germanium applications, except for the use of germanium as PET catalyst, for which the trend is decreasing (Melcher and Buchholz, 2012). The estimation by Melcher and Buchholz (2012) is mainly based on the fiber optics demand, which they are expecting will grow 5–7% per year. Also Thomas (2018a) expects increasing global demand for fiber-optic cable, led by emerging Asian economies and Brazil. Infrared optics are expected to continue being used by military and law enforcement agencies and new commercial applications for infrared optics represent a significant potential for consumption growth, but increased specialty glass substitution for germanium may continue (Thomas, 2018a).

3.9 Supply risk

Evaluating the supply risk is often a central part of criticality assessments of raw materials. The European Commission (2017) lists germanium as a critical raw material, based on its economic importance and its supply risk. Supply risk is also one of three indicators of criticality considered by Harper et al. (2015), investigating germanium and other elements in the geological zinc, tin and lead family. The byproduct status together with social, regulatory and geopolitical considerations point to a higher supply risk of germanium, but because of a long depletion time, germanium was given the score 50, on a 0 to 100 scale (Harper et al., 2015).

On a supply risk list, published by British Geological Survey, only rare earth elements, antimony and bismuth have a higher supply risk index than germanium (National Enviromental Research Council, 2015). Neither supply potential nor depletion time was considered in the assessment of supply risk, but instead non-geological factors. Non-geological factors resulting in supply restrictions could be geopolitics, resource nationalism, labor strikes, accidents or infrastructure availability.

The production of germanium is far from reaching its supply potential. Fu, Polli and Olivetti (2018) estimate that the supply potential of germanium from zinc is five times that of current germanium production, and that supply potential from coal is double that of germanium from zinc. Frenzel, Tolosana-Delgado and Gutzmer (2015) assess the supply potential for germanium from Mississippi Valley-type (MVT) deposits, which they estimate supplied about 40% of the germanium produced in 2013. Their calculations result in a supply potential seven times higher than the actual production of germanium from MVT deposits. Frenzel et al. (2017) estimate that it will take 85 years before the production of germanium will be equal to the current supply potential.

Both the supply and demand of germanium has, however, been found to be inelastic (Tadjfar, 2017). This implies both that the supply will respond poorly to increasing demand and that the demand will respond poorly to the resulting in price increases. The result is a supply deficit and extreme prices increases. The lack of responsiveness to market prices is thought to be caused by national strategic stockpiling (Fu, Polli and Olivetti, 2018). Sprecher et al. (2017) investigate a scenario where zinc demand decreases by 33% to 2040. The scenario would result in a germanium supply deficit of around 30%. The supply deficit is smaller relative to indium in the same scenario, owing to the fact that germanium can also be sourced from coal. A moderate supply deficit is expected for a scenario with undisrupted zinc demand.

4. Tin market review

Tin is a post-transition metal with the chemical symbol Sn (from Latin: stannum) and atomic number 50. Tin does not occur naturally as a metal, but is most commonly obtained from the mineral cassiterite (SnO_2). Tin was one of the earliest metals known to humanity and together with lead the first metal to be smelted (Kamili, Kimball and Carlin, 2017). Evidence points to tin being used in bronze implements as early as 3500–3200 BCE (Britton, 2013). In some of its applications, tin still serves the same purpose as in the Bronze Age, i.e. to strengthen and harden alloys, but it has also found other important applications in the chemicals, soldering and canning industries. Both in terms of mining and smelting, most tin production takes place in Southeast Asia, where about half of current tin reserves are held. Tin reserves and resources are sufficient to satisfy global demand long into the future, but higher tin prices or more efficient extraction technologies are needed in the medium-to-long term.

4.1 Properties

Pure tin metal has a silvery-white color. It is soft and pliable, but imparts hardness and strength to alloys with other metals (Britton, 2013). It has a relatively low melting point (232°C), considering that its boiling point (2625°) is higher than that of most metals (Britton, 2013). Tin has two allotropic forms, of which white tin (β) is most familiar. Gray tin (α), which is formed when high-purity tin is exposed to temperatures below 13.2°C, is brittle and has no metallic properties (Kamili, Kimball and Carlin, 2017). The presence of impurities in commercial tin usually lowers the transition temperature to below 0°C and the spontaneous transformation can be entirely prevented by addition of antimony or bismuth (Kamili, Kimball and Carlin, 2017).

Possible oxidation states for tin are +2 and +4. Tin reacts with both strong acids and strong bases, whereas it is rather resistant to neutral solutions (Britton, 2013). Distilled water has no effect on tin, but oxygen accelerates corrosion in aqueous solutions. A thin protective oxide layer appears on tin metal, preventing further oxidation. Tin resists nitrogen, hydrogen, carbon dioxide or gaseous ammonia, but reacts with moist sulfur dioxide and halogens (Britton, 2013). Nonaqueous organic solvents have little effect, but oxidizing salt solutions dissolve tin (Britton, 2013).

4.2 Applications

The use of refined tin in various industry sectors is illustrated in Figure 9. The leading industry sector in terms of tin use is consumer electronics, where tin is used in solder alloys. As shown in Figure 10, solders account for almost half of the use of refined tin in 2014. Tin plate, which is extensively used in the packaging sector, together with chemicals and various alloys account for most of the remaining tin use. Apart from the packaging and consumer electronics sector, tin is used in the construction, transportation and industrial sectors.

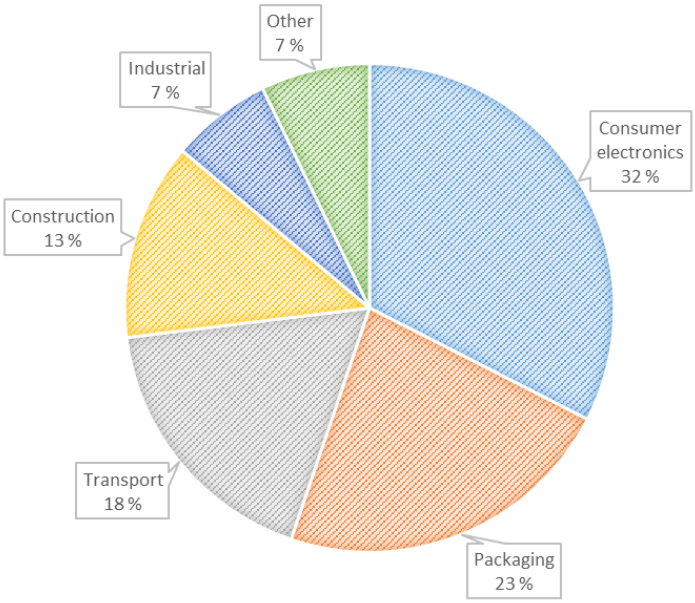

Figure 9. Use of refined tin by industry sector in 2014. Based on data from Roskill (2015).

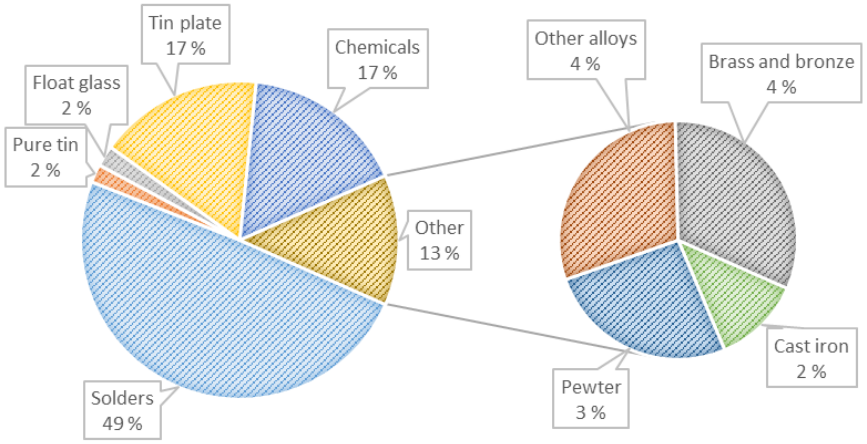

Figure 10. Use of refined tin by application in 2014. Based on data from Roskill (2015).

4.2.1 Solders

The low melting point of tin and its ability to wet and adhere to many metals makes it useful in soldering. Tin and lead, combined in various ratios, form a group of alloys called soft solders (Britton, 2013). Soft solders are favored in most applications, because of the low price of lead. For solders requiring high strength, nontoxicity or special corrosion resistance, tin is instead combined with antimony, silver, gold, zinc or indium (Britton, 2013). Most of the refined tin used for solders in 2014, was used in electronic applications (Roskill, 2015). Other applications include plumbing and sheet-metal work.

4.2.2 Tin plate

Tin plate, consisting of steel with a tin coating, is mostly used for metal cans for preserving foods. Tin plate is an inexpensive material with the strength of steel and corrosion resistance of tin. The tin coating prevents iron from dissolving into the product, which would affect the flavor and the appearance of the product (Britton, 2013). Tin is also nontoxic. In addition to food and beverage cans, tinplate can be used for aerosol containers for products including cosmetics, paint and polishes.

Tin plate can be manufactured by electroplating or by passing steel sheets through a bath of molten tin. The electrolytic process is flexible, it can be run continuously and coatings of different thickness can be applied to each side of the plate (Britton, 2013). It is also the most popular method in the United States, as less than 1% of tin plate produced there comes from hot-tinning machines (Britton, 2013). In contrast to the hot-tinned coating, which is bright, electrodeposited coatings are normally dull, but may be brightened by heating momentarily to the melting point (Britton, 2013).

4.2.3 Chemicals

Organotin accounts for about two thirds of the use of tin chemicals. Organotin is most commonly used as a stabilizer in polyvinyl chloride (PVC) production or as catalyst for polyurethane foams and silicones, but it is also used in some biocides (Hoch, 2001). Organotin prevents the decomposition of PVC plastic that would otherwise occur upon heating and prolonged exposure to light (Hoch, 2001). Organic tin is toxic and represents a risk to aquatic and terrestrial ecosystems (Hoch, 2001). Industrially used inorganic compounds include tin(II) chloride, tin(II) oxide and tin(II) fluoride. The most important use of tin chloride and oxide are as industrial reducing agents, while tin fluoride is primarily used as an ingredient in toothpaste (Howe, Wood and Watts, 2005). Although used in small amounts, tin(IV) oxide is a critical component in indium tin oxide (ITO), which is used in flat-panel displays.

4.2.4 Alloys

Among alloys, soldering is the most important end-use of tin and most of the remaining use of tin for alloys is accounted for by bronze, brass, pewter and cast iron. Tin is used in alloy with other metals, including lead, zinc and nickel, for various coating applications and many babbitt alloys, used for the bearing surface in a plain bearing, have a tin content higher than 80% (Britton, 2013). In addition, alloys of tin with rarer metals, such as niobium, titanium and zirconium have been developed (Britton, 2013).

Bronze is a general name for copper-tin alloys which usually also contain modifying elements, most commonly zinc or phosphorus (Britton, 2013). Bronzes have varying compositions, but most of them contain 5–20% tin. Bronze is used for marine and railway engineering pumps, valves, pipefittings, bearings, bushings, gears, springs and ship propellers (Britton, 2013). Brass consists mainly of copper and zinc, but some types of brass contain a few percent tin, improving corrosion resistance.

Pewter is an alloy, containing 90–95% tin and usually some antimony and copper, acting as hardeners (Britton, 2013). It is easily cast and can be compressed, bent, spun and formed into any shape (Britton, 2013). During the 17th and 18th century many daily items, such as cups, plates, spoons and buttons, were made of pewter, but today it is used only as architectural and ornamental metal and in specialty items (The Pewter Society, 2014).

Cast iron is a group of iron-carbon alloys, with less than 2% carbon. An addition of as little as 0.1% tin to cast iron is needed for a pearlite structure, reduced amount of free carbon and increased strength and hardness (Messina, 1975). Addition of tin also improves the retention of shape with heating (Britton, 2013). Cast iron with tin is used for engine blocks, transmissions and automotive parts (Britton, 2013).

4.3 Substitutes

On a scale where 0 stands for highly substitutable and 100 stands for completely irreplaceable, tin has been rated 36, suggesting that replacing tin in its end-uses would be possible with limited technical challenges and result in limited loss in functionality or performance (Graedel et al., 2013). Also on a scale from 0 to 100, Harper et al. (2015) gives tin the score 46 for substitutability.

Electrically conductive adhesives (ECA) could replace tin solder in electronics. ECA's consist of electrically conductive particles, like silver, nickel, copper or aluminum, dispersed in adhesives, like epoxy, silicone, polyamide or polyurethane (Sancaktar and Bai, 2011). They offer multiple advantages compared to traditional soldering technology, but also some major disadvantages, like lower conductivity and sensitivity to type and quality of the surface material (Sancaktar and Bai, 2011).

Tinplate can be easily substituted by aluminum, which according to Harper et al. (2015) has excellent substitute performance. Glass, paper, plastic and tin-free steel are mentioned as other substitutes for tinplate cans (Anderson, 2018b). Aluminum

alloys, alternative copper-based alloys and plastics could substitute for bronze, and some tin chemicals could be substituted by sodium and lead compounds (Anderson, 2018b).

4.4 Occurrence and reserves

The abundance of tin in the upper continental crust is about 2.2 ppm (Hu and Gao, 2008). The tin mineral cassiterite (SnO_2), is the primary source of tin, but small amounts of tin are also recovered from sulfide minerals such as stannite (Anderson, 2017b). Tin deposits are generally smaller than commercially viable copper, lead or zinc deposits and they often contain 0.1–1% tin (Kamili, Kimball and Carlin, 2017). Minor quantities of tin are recovered as byproducts of the mining of tungsten, tantalum and lead, as cassiterite is sometimes found in association with these metals (Kamili, Kimball and Carlin, 2017).

Global tin reserves are at about 4.8 million metric tons (Anderson, 2018b). About half of this is in the belt of placer deposits in Southeast Asia, stretching from China, through Thailand, Burma and Malaysia, to Indonesia (Figure 11). The rest of the tin reserves are in South America, Australia, Africa and Russia. The Cornwall mine in England and the Western Ore Mountains on the border between southern Germany and the Czech Republic have historically been sources of tin ore, but are now largely exhausted (ITRI, 2016). Current mine production of tin in Europe mainly comes from the massive sulfide deposits of the Neves Corvo mine in Portugal. There, tin is produced as a byproduct from recovery processes (Kamili, Kimball and Carlin, 2017).

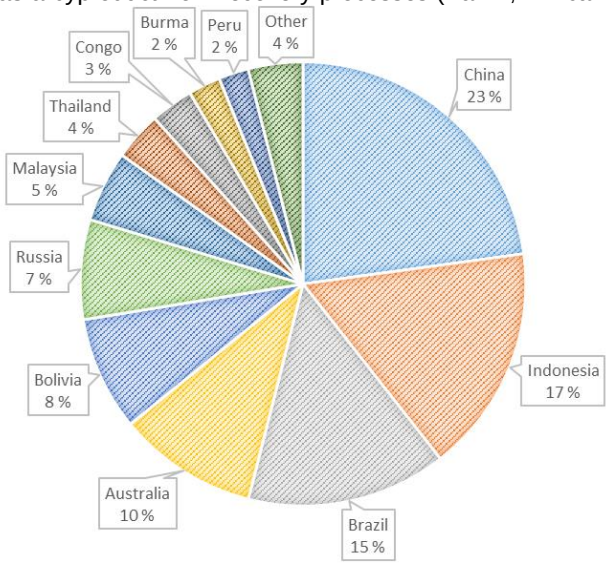

Figure 11. Distribution of global tin reserves by country. Based on data from U.S. Geological Survey's Mineral Commodity Summaries 2017 (Anderson, 2018b).

4.5 Processing

The initial treatment of tin ore usually takes place in close proximity to the mining location and includes flotation, gravity concentration and magnetic processes, producing a cassiterite concentrate containing 70–77% tin (Anderson, 2017b). The concentrate is sent to a smelter, operating at 1200–1300°C with carbon present as a reducing agent (Anderson, 2017b). Smelting and refining of tin is described by Britton (2013) as follows. Primary smelting is carried out in a reverberatory, rotary or electric furnace. During smelting, reduced iron forms high-melting compounds with tin, called the hard head of the tin smelter. Tin and iron also react with silica to form stannous and ferrous silicates, which fuse with added fluxes to form a liquid slag. Since both the hard head and the slag hold a considerable amount of tin, the primary smelting is followed by a second stage to process the slag and hard head together with dross from the refining stage. Pyrite (FeS_2) is added to the slag, producing tin sulfide (SnS), which vaporizes. The tin sulfide then oxidizes to SnO_2 and is collected and recycled.

Refining of crude tin from the smelter is carried out by heat treatment or by electrolytic processing. Conventional refining by heat treatment includes liquidation and boiling. Liquidation implies heating up the crude tin to the melting point of tin and removing solids, called dross. Boiling involves agitating the molten tin with steam or compressed air, which results in the remaining impurities forming a scum that can be removed and recycled to the smelting stage. This results in a minimum purity of 99.8%. Electrolytic processing is carried out by placing electrodes in the tin concentrate and heating to the tin melting point with electricity (Anderson, 2017b). Electrolytic processing is more expensive than heat treatment, but also provides tin of a higher purity (Anderson, 2017b).

4.6 Production and prices

In 2017, total mine production of tin was 290,000 metric tons (Anderson, 2018b), of which more than 70% was produced in Southeast Asia (Figure 12). China, accounting for 35% of global mine production of tin, is the leading producer, followed by Burma and Indonesia. Brazil, Bolivia and Peru together account for 21% of the production. Mine production in Peru and China has decreased in recent years, but production in Burma has increased substantially. In Russia, where mine production of tin is currently about 1,000 metric tons, there are plans to develop two tin deposits, which are, according to predictions made by the Russian Ministry of Energy, to improve the production of tin in Russia tenfold (Anderson, 2018b).

Smelter production, including secondary production, was 350,000 metric tons in 2016 (Brown et al., 2018). Especially concerning the major tin-mining countries, smelter production tends to occur in the same country where the ore has was mined. The exception is Burma, exporting its ore concentrate to China for smelting (Anderson, 2018b). Consequently, China accounts for more than half of the smelter

production of tin. Metallo Chimique in Belgium, specialized in recycling of non-ferrous materials, is a major producer of secondary tin and accounts for 2% of the total smelter production.

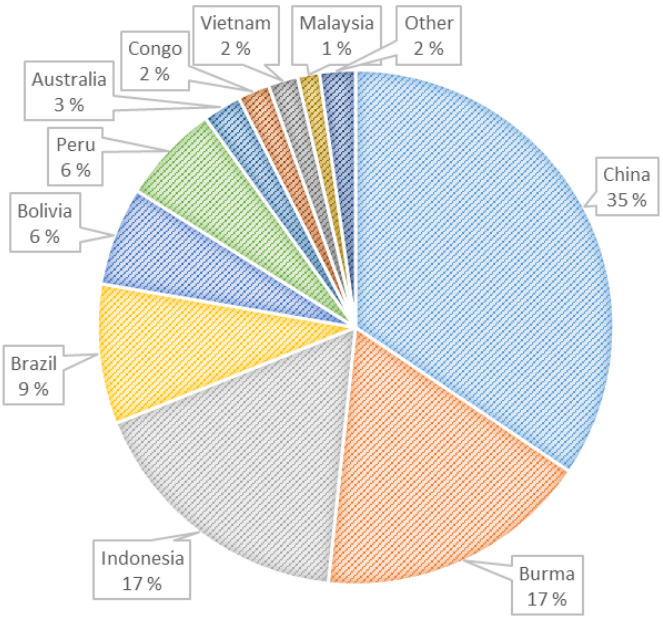

Figure 12. Mine production of tin by country in 2017. Data from U.S. Geological Survey's Mineral Commodity Summaries 2017 (Anderson, 2018b).

Mine production and prices of tin for 2000–2017 are presented in Figure 13. For the most part of the period, mine production of tin has been between 250,000 and 300,000, not showing any signs of either an upward or a downward trend. Annual average tin prices, however, have increased from 5.4 USD/kg in 2000 to 20 USD/kg in 2017.

Tin prices have declined in the beginning of the 2000's, due to an oversupply and an economic slowdown in many countries (Carlin, 2003). Mine production also declined, but had recovered by 2004. Despite this, the world tin market was thought to be in a supply deficit (Carlin, 2005), which triggered price increases. There was a trend in major tin-consuming countries to move to lead-free solder, which tends to contain greater amounts of tin (Carlin, 2008). Due to decreased demand owing to the global economic slowdown, there was a sharp decline in tin prices in 2009 (Carlin, 2010).

The prices increased again the two following years, reaching 26 USD/kg. The price increases are attributed to lower production in key producing countries, moderately higher world tin consumption, and to investment fund buying and selling (Carlin, 2012b). The prices were relatively stable at around 20 USD/kg between

2012 and 2014, before decreasing to 16 USD/kg in 2015. Investments in tin mines by companies from China, resulted in a near doubling of production in Burma since 2013, and reduced demand in China for imported tin metal (Anderson, 2016). Since 2016, tin prices have been increasing. The price of tin in April 2018 was 21 USD/kg (Anderson, 2018c).

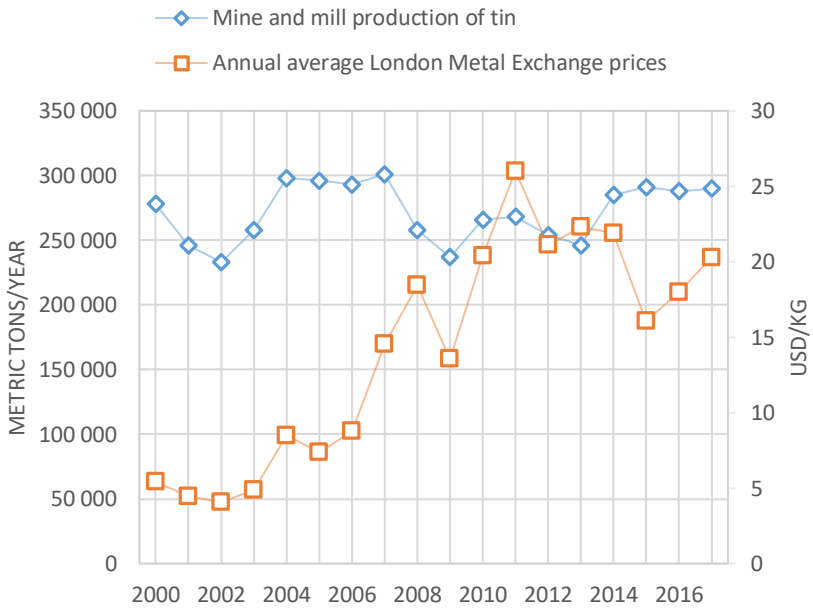

Figure 13. Production and prices of tin 2000–2017. Production data from U.S. Geological Survey's Historical Statistics for Mineral and Material Commodities in the United States (U.S. Geological Survey, 2015b). Price data from U.S. Geological Survey's Mineral Yearbooks 2015 (Anderson, 2017a), 2010 (Carlin, 2012a), 2005 (Carlin, 2007) and 2000 (Carlin, 2002) and Mineral Commodity Summaries 2017 (Anderson, 2018b).

4.7 Secondary production

World secondary production of tin was 23,000 metric tons in 2015, accounting for 7% of the total tin production (Anderson, 2017a). Belgium and the United States are the largest producers of secondary tin. Metallo Chimique in Beerse, Belgium, produced around 12,000 metric tons and the United States produced around 10,000 metric tons of secondary tin in 2015 (Anderson, 2017a). In 2017, the United States produced approximately 10,000 metric tons of tin by end-of-life recycling and 2,000 metric tons of tin from new scrap, originating from a fabrication or manufacturing

process (Anderson, 2018b). Australia, Brazil and Russia were the only other countries producing secondary tin in quantities exceeding 50 metric tons per year (Anderson, 2017a).

The production volume of secondary tin has varied through the years, but it has since 2011 stayed above 20,000 metric tons per year (Anderson, 2017a). Whether the secondary tin production will increase or decrease depends on the balance of future improvements in tin recycling technology and economics, versus the falling concentrations of tin found in end-of-life products as a result of economization (ITRI, 2016).

As most of the tin solder is used for electronics, it should be collected and recycled with WEEE. No information is available on how much, if any, tin is recovered from WEEE. Yang et al. (2017) summarize the various technologies available for the recovery of tin from printed circuit boards, which contain on average 4% tin. Tin constitutes 15% of the economic value of materials present in printed circuit boards (Yang et al., 2017).

Tin in alloy form is not reprocessed to its elemental form, because of the thermodynamic behavior that makes separation of the alloying elements either very energy-intensive or essentially impossible (Reck and Graedel, 2012). Tin alloy scrap is re-melted and impurities are removed before returning it to the market as binary or ternary alloy (Britton, 2013). From clean tinplate, however, high-purity tin can be recovered (Britton, 2013). Tin plate is also extensively recycled. According to Metal Packaging Europe (2018), 75% of metal packaging in Europe is recycled.

4.8 Future demand

Asia accounts for about 70% of world tin consumption, but the advanced economies are still believed to account for the majority of tin consumption in terms of contained tin in end-use products (Roskill, 2015). Because of the tendency for an increasing intensity of tin use by GDP per capita, there is a strong potential for growth in demand for tin in emerging markets, particularly in Latin America and Asia (Roskill, 2015). Growth is expected in demand for tin-containing products, but the demand for tin is expected to lag behind, because of miniaturization, 3D-printing, substitution and process efficiency gains (Roskill, 2015). The strongest growth of tin demand in the medium-to-long term is predicted to come from the chemical industry, where intensity of use has declined less.

4.9 Supply risk

The current tin reserves are 16 times higher than the current mine production, both reported by Anderson (2018b). This implies that with current prices, production volume and technology, the tin reserves would run out in 16 years. When the reserves run out, either an increase in prices or improvement in extraction technologies will be necessary for tin resources to be economically viable to mine. Anderson (2018b) does not provide an estimate for tin resources, but ITRI (2016) estimated that they

were 11.7 million metric tons, with reserves included, in 2015. These tin resources should satisfy global demand long into the future.

Harper et al. (2015), give tin the score 40 for supply risk on a criticality score scale going from 0 to 100. On the risk list published by British Geological Survey (National Environmental Research Council, 2015), tin has the value 6.6 on a 0–10 scale. Also, the European Commission (2014b) considers the supply risk of tin to be moderate, as the score given to tin for supply risk is close to, but under the limit for being considered a critical raw material.

5. Technical assessment

For the technical assessment, the process of indium, germanium and tin recovery from two alloys was simulated with the aim to provide mass and heat balances for each stage of the process. Using the mass balances obtained in the simulation, the major equipment for the process was dimensioned.

The two alloys, from which the metals are recovered, are obtained as byproducts from refining of crude zinc, produced in the imperial smelting process. The recovery process can be divided into five subprocesses according to Figure 14. Both raw material alloys are first treated pyrometallurgically, with the aim to concentrate indium and germanium in an oxide dross. The remaining alloy from the pyrometallurgical treatment is directed to tin recovery, resulting in a tin-lead alloy, whereas the oxide dross is further treated hydrometallurgically to produce indium and germanium concentrate.

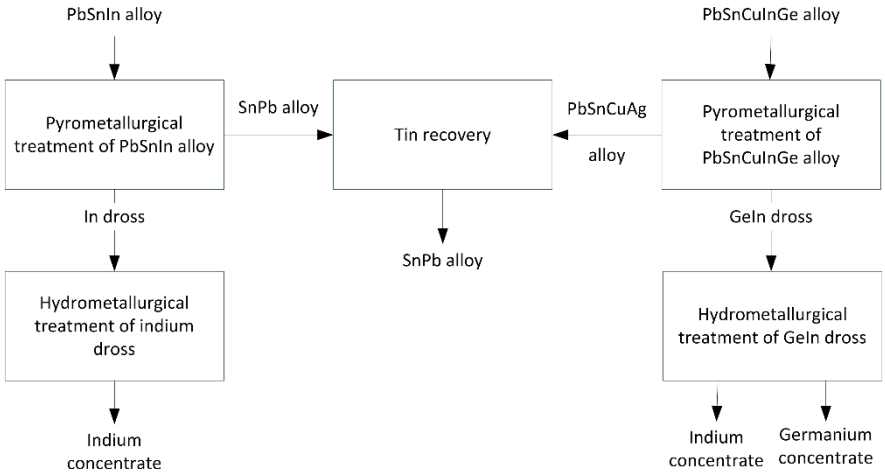

Figure 14. The process of recovering indium, germanium and tin, divided into subprocesses.

5.1 Method

The process simulation module of HSC Chemistry 9 was used for modeling and simulation of the recovery process. HSC Chemistry is a software toolkit, developed by Outotec, for process research, development and design (Outotec, 2018). The process simulation module of HSC Chemistry consists of a graphical flowsheet and spreadsheet-type process unit models. The units were modeled using two different approaches available in the software. The pyrometallurgical stages of the process were modeled using distribution units, where element distributions to output streams and compounds are defined by the user, and the hydrometallurgical stages of the

process were modeled as reaction-based units, where chemical reactions and distribution of compounds to phases and output streams are defined by the user.

The process was simulated as a continuous process, but selection and sizing of equipment was based on batch processing. The model was created based on results from pilot-scale experiments performed by the research institute IMN (2018). The experiments provided mass fractions and concentrations of the main elements in the products, based on which elemental yields were calculated and used in the simulation model. The elemental yields were used directly as input data in the pyrometallurgical units and the chemical compounds of the output streams were determined using chemical reactions. In the hydrometallurgical units, the elemental yields were used for the progress of chemical reactions, where 100% of the product containing the element was distributed to the output stream for which the elemental yield applies.

The chemical reactions in the simulation were either determined on theoretical grounds or based on experimental data from similar processes described in the literature. The reactions used in the simulation have not been experimentally confirmed for this process. For the heat balance, the net reaction heat is presented together with the thermal enthalpy difference and the heat flow. The thermal enthalpy difference refers to the heat difference between the input material and the product. Since the reaction heat is given as a negative value for exothermic reactions, the sum of the thermal enthalpy difference and the reaction heat equals the heat flow, i.e. the amount of heating or cooling required in the process.

The input temperature was set to 25°C for the raw materials, chemicals and water. The steam was as assumed to have a temperature of 145°C. The input temperature of the intermediates was set to equal the output temperature from the previous unit, with a few exceptions noted in the results below. Heat losses in the physical separation units were assumed to result in a temperature of 25°C for all streams exiting a physical separation unit.

In the hydrometallurgical subprocesses, where direct heating with steam was applied, the amount of steam was calculated in accordance with the heat balance, assuming that all of the steam condenses. The water amount was adjusted in order for the H_2O amount to correspond to the amount used in the experiments. Unless noted in the results below, all other raw materials and chemicals were used in the same ratio in the model as in the experiments. Unknown elements as well as elements constituting a minor part of the raw material were handled as inert material with the thermodynamic behavior of silica. The inert material was distributed to the products in accordance with the distribution of total mass in the experiments. Liquid-solid and gas-solid separation units were assumed to be ideal and consequently the output stream of solids from filtration have zero moisture content. Material losses were not taken into account in the simulation model.

A description of each of the subprocesses, as they were conducted in the pilot-scale experiments (IMN, 2018), is presented below. The yields of the key elements and the composition of the raw materials, intermediates and products are provided as well as the chemical reactions assumed to occur during each stage of the process. The results for the simulation are presented in the form of mass and heat

balances. The imperial smelting process, wastewater treatment, steam production or any other process not described below, was not included in the simulation. Presentation of the method and results for sizing of the major equipment are presented in section 5.8.

5.2 Pyrometallurgical treatment of the PbSnIn alloy

The PbSnIn alloy mainly consists of lead, tin and zinc and has an indium content of 0.23% (Table 1). The pyrometallurgical treatment of the PbSnIn alloy consists of zinc removal, oxidation and screening. The aim is to produce an oxide dross enriched in indium, to be directed to hydrometallurgical treatment, and a tin-containing alloy, to be directed to tin recovery. Additionally, a zinc dross is obtained as a side product during zinc removal. The zinc dross can be redirected to the imperial smelting process, where zinc and lead are recovered. Any indium incorporated in the zinc dross will be concentrated to the PbSnIn and PbSnCuInGe alloys in the zinc refining process.

Table 1. The chemical composition of the PbSnIn alloy.

ELEMENT	In	Sn	Pb	Zn	Sb	Ge	As	Bi
MASS FRACTION (%)	0.23	2.62	93.3	2.23	0.076	0.012	<0.02	0.3

The pilot-scale experiments of the pyrometallurgical treatment of the PbSnIn alloy were performed as follows (IMN, 2018). Both zinc removal and oxidation was conducted in a refining kettle holding one metric ton. The zinc removal took between three and seven hours and the temperature in the experiments was 430–580°C. Sodium hydroxide was added to the molten alloy in multiple stages and in the final stage, also sodium nitrate was added. Oxidation was conducted immediately after zinc removal in the presence of free atmospheric air. The oxidation stage took between seven and twelve hours and was performed at a temperature of 600–680°C.

In the experiments, the oxides formed a dross, also containing metal drops, on the surface of the molten alloy. The dross was removed multiple times during the production of one batch. In order to separate the metal drops from the oxides, the dross was screened and the particles exceeding 0.32 mm in size, were redirected to oxidation. The oversized fraction of the last dross removed from the melt was directed to the next batch. The undersized particles constitute the oxide indium dross ready for hydrometallurgical treatment.

In the simulation model, indium, tin, lead and zinc were considered as the only reactive components of the PbSnIn alloy and other elements, adding up to 1.62%, were regarded as inert material. The temperature for the zinc removal stage was set to 560°C. Reactions presented by Guo et al. (2015) for a sodium hydroxide and

sodium nitrate fusion process for recovery of metals from waste printed circuit boards were used. The reactions can be described as follows.

$$2\ NaNO_3 \rightarrow Na_2O + N_2 + 5\ O \quad (1)$$

$$Zn + 2\ NaOH + O \rightarrow Na_2ZnO_2 + H_2O \quad (2)$$

$$Sn + 2\ NaOH + 2\ O \rightarrow Na_2SnO_3 + H_2O \quad (3)$$

$$Pb + 2\ NaOH + O \rightarrow Na_2PbO_2 + H_2O \quad (4)$$

The conversion of both sodium hydroxide and sodium nitrate was set to 100%. Additionally, all the components in the zinc dross were assumed to be in oxide form. Air was added in the simulation model in order to oxidize additional zinc, tin and lead as well as a small amount of indium, according to the reactions described for the oxidation stage below.

The temperature was set to 670°C for the oxidation stage. Considering the elements present in the melt, the remaining zinc will oxidize first and indium second, according to Ellingham diagrams by Howard (2006). It was, however, assumed that all the components of the undersized indium dross are in oxide form. Since also tin and lead were present in the final indium dross obtained in the experiments, the following oxidation reactions were used in the model.

$$2\ Zn + O_2 \rightarrow 2\ ZnO \quad (5)$$

$$4\ In + 3\ O_2 \rightarrow 2\ In_2O_3 \quad (6)$$

$$Sn + O_2 \rightarrow SnO_2 \quad (7)$$

$$2\ Pb + O_2 \rightarrow 2\ PbO \quad (8)$$

The yield of oxide compounds to the indium dross was assumed to be 100% and the metal drops in the indium dross assumed to consist of elemental tin and lead. In the screening unit, all of the metal drops and 2% of the oxides were set to constitute the oversized indium dross, which is redirected to the oxidation stage.

Table 2 presents the yields of the main elements of from the PbSnIn alloy to the output streams, as calculated from the results of pilot-scale experiments (IMN, 2018) without consideration of material losses. The yield of indium from the PbSnIn alloy to the undersized dross is 90%. Table 2 also presents the mass fraction of the main elements in the output streams, as a result of the simulation. The mass fractions and yields presented for the oversized dross apply to the stream that circulates in the process in a steady-state situation. Since this stream is not considered an input stream in the calculation of yields, and the yields to this stream thereby imply a total yield higher than 100%; the yields are presented in parentheses.

The heat balance is presented in Table 3. In Figure 15, the mass flow of each of the components of the PbSnIn alloy and the output streams is presented. Table 4

presents the mass balance for each stage of the process in the form of mass flows of the raw materials, intermediates, chemicals and products.

Table 2. Yields and mass fractions of the main elements to and in the products of the pyrometallurgical treatment of the PbSnIn alloy.

UNIT			**Zn removal**	**Oxidation**	**Screening**	
STREAM			Zn dross	PbSn	In dross > 0.3 mm	In dross < 0.3 mm
ELEMENT	In	wt-%	0.15	0.02	0.27	1.12
		Yield[a] (%)	3.6	6.8	(1.8)	89.6
	Sn	wt-%	5.03	1.55	2.67	6
		Yield[a] (%)	10.8	47	(1.6)	42.2
	Pb	wt-%	16.6	98.4	93.7	77.6
		Yield[a] (%)	1	83.7	(1.6)	15.3
	Zn	wt-%	35.3	-	0.28	1.36
		Yield[a] (%)	88.8	0	(0.2)	11.2
[a](IMN, 2018)						

Table 3. Heat balance for the hydrometallurgical treatment of the indium dross.

	Zn removal 560°C	**Oxidation 670°C**	**Screening 25°C**
$\Delta H_{THERMAL}$ (GJ/a)	31.8	15.8	-9.7
$\Delta H_{REACTION}$ (GJ/a)	-24.9	-56.6	0
$\Delta H_{HEAT\ FLOW}$ (GJ/a)	6.9	-40.8	-9.7

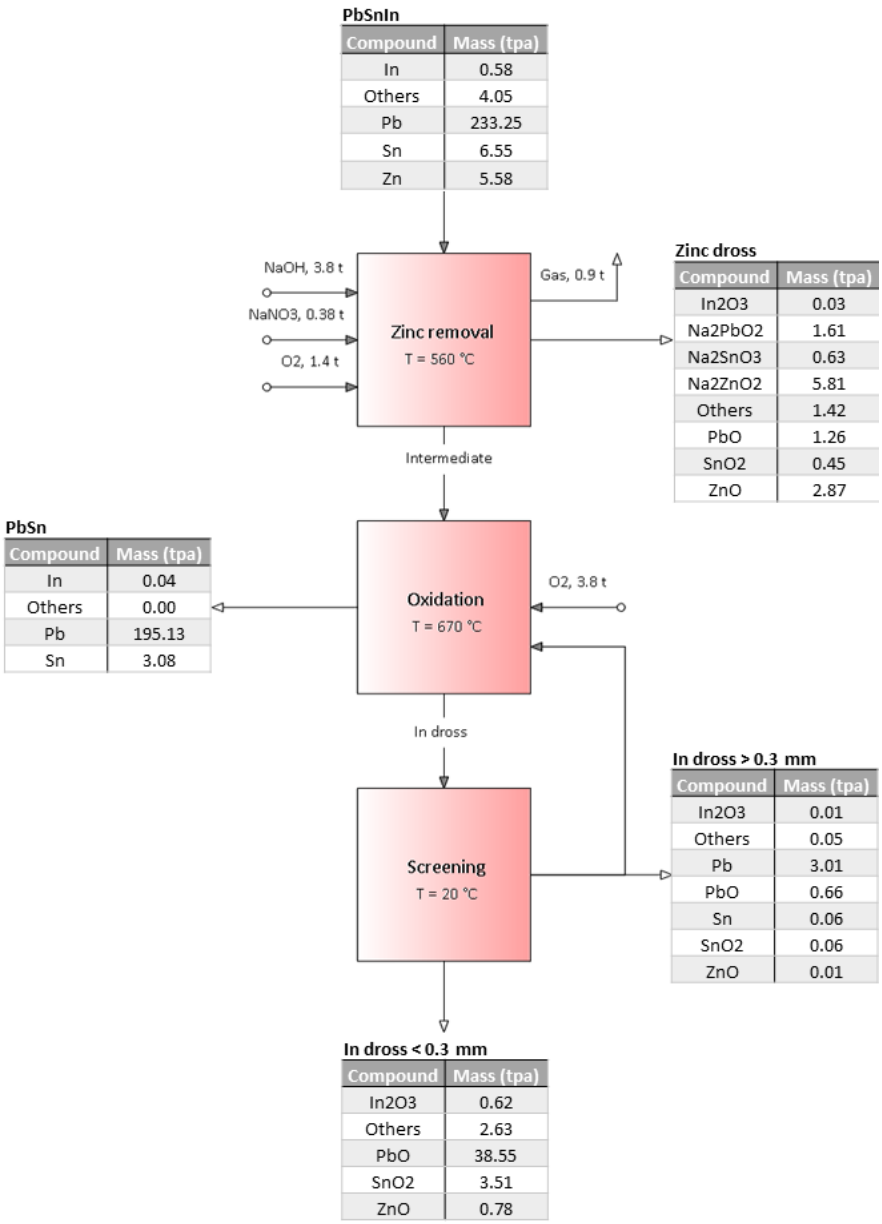

Figure 15. Mass flow of each of the components in the PbSnIn alloy and in the output streams of the pyrometallurgical treatment of the PbSnIn alloy, calculated with HSC Chemistry 9.

Table 3. Mass balance for each stage of the pyrometallurgical treatment of the PbSnIn alloy.

UNIT	Zn removal		Oxidation		Screening	
	Stream	Mass flow (t/a)	Stream	Mass flow (t/a)	Stream	Mass flow (t/a)
INPUT	PbSnIn alloy	250	Intermediate	241	In dross	50.0
	NaOH	3.75	In dross > 0.3 mm	3.87		
	$NaNO_3$	0.38	O_2 (air)	3.77		
	O_2 (air)	1.4				
OUTPUT	Zn dross	14.1	PbSn	198	In dross > 0.3 mm	3.87
	N_2	0.063	In dross	50.0	In dross < 0.3 mm	46.1
	H_2O	0.84				
	Intermediate	241				

5.3 Hydrometallurgical treatment of indium dross

The oxide dross obtained in the pyrometallurgical stage is further treated with hydrometallurgical methods, with the aim to produce indium concentrate. The hydrometallurgical treatment includes leaching of the oxide dross and neutralization of the leaching solution to precipitate indium. Additionally, the indium precipitate is pulped. In addition to the indium concentrate, lead concentrate and wastewater is produced in the process. The wastewater is directed to industrial wastewater treatment, while the lead concentrate could be returned to the imperial smelting process after dehalogenation. Neither wastewater treatment nor dehalogenation and recycling of the lead concentrate was included in the simulation model.

Pilot-scale experiments were conducted in the following manner (IMN, 2018). A leaching tank with a volume of one cubic meter was used in all stages of the process. The tank was equipped with a mixer and direct heating with steam was applied. Leaching of the oxide dross was conducted with an aqueous solution of hydrochloric acid at 75°C. The suspension was mixed for three hours, during which a lead concentrate was formed. The suspension was cooled to room temperature before filtering with a filter press.

The filtrate was again heated to 75°C for neutralization. Sodium hydroxide was added to the solution until the pH reached 5.0. The suspension was mixed for three hours, after which flocculant was added. Then the solids, constituting the indium concentrate, were allowed to sediment for one day. The clear solution was removed

and the sediment was pulped with water heated to 55°C and mixed for one hour. After sedimentation and filtering, the final indium concentrate was obtained.

In the process simulation model, the metal oxides were assumed to dissolve in the acid solution with a conversion corresponding to the yields obtained from the experiments. The lead oxide was assumed to react with the hydrochloric acid to form lead chloride, as described by the following reaction.

$$PbO + 2\,HCl \rightarrow PbCl_2 + H_2O \qquad (9)$$

Lead chloride is poorly soluble and constitutes most of the solid lead concentrate. The remaining part of the lead concentrate in the simulation model is undissolved metal oxides.

A heat exchanger was modelled for the cooling stage, with the input temperature of the cooling water set to 10°C and the output temperature of the solution set to 25°C, resulting in a mass flow of about 400 t/a cooling water.

In accordance with the results from the experiments, indium and tin were set to precipitate completely, during the neutralization, while most of the zinc and remaining lead were set to stay in the solution. The addition of flocculant was not included in the model. All the indium in the solution was assumed to precipitate as indium hydroxide and all the tin as stannic oxide, in accordance with the following reactions.

$$In^{+3} + 3\,OH^- \rightarrow In(OH)_3 \qquad (10)$$

$$Sn^{+4} + 4\,OH^- \rightarrow SnO_2 + 2\,H_2O \qquad (11)$$

Additionally, a small amount of lead was set to form lead chloride as in (9) and zinc was set to form zinc hydroxide in accordance with the following reaction.

$$Zn^{+2} + 2\,OH^- \rightarrow Zn(OH)_2 \qquad (12)$$

Since separation stages were modelled as ideal, the pulping stage is included in the model only to indicate the utilization of water and steam, as well as for the heat balance. The indium concentrate output from the neutralization stage is therefore identical to the indium concentrate output from the pulping stage.

Table 5 presents the yields of the main elements of from the undersized indium dross to the output streams, as calculated from the results of pilot-scale experiments (IMN, 2018) without consideration of material losses. The yield of indium from the indium dross to the indium concentrate is 55%, which makes the total yield of indium from the PbSnIn alloy to the concentrate 49%. Table 5 also presents the mass fraction of the main elements in the output streams, as a result of the simulation.

Table 6 presents the mass balance for each stage of the process in the form of mass flows of the raw materials, intermediates, chemicals and products. In Figure 16, the mass flow of each of the components of the undersized indium dross and the output streams is presented. The heat balance is presented in Table 7.

Table 4. Yields and mass fractions of the main elements to and in the products of the hydrometallurgical treatment of the indium dross.

UNIT			**Leaching**	**Neutralization & Pulping**	
STREAM			Pb concentrate	Waste solution	SnIn concen-trate
ELEMENT	In	wt-%	0.46		15.4
		Yield[a] (%)	45	0.2	54.8
	Sn	wt-%	3.78		45.8
		Yield[a] (%)	69.5	0.2	30.4
	Pb	wt-%	69.9		1.12
		Yield[a] (%)	99	1	0.06
	Zn	wt-%	0.01		0.64
		Yield[a] (%)	0.9	97.2	1.9
[a] (IMN, 2018)					

Table 5. Mass balance for each stage of the hydrometallurgical treatment of the indium dross.

UNIT	**Leaching**		**Neutralization**		**Pulping**	
	Stream	Mass flow (t/a)	Stream	Mass flow (t/a)	Stream	Mass flow (t/a)
IN-PUT	In dross < 0.3 mm	46.1	Leaching solution	535	SnIn concentrate	1.84
	HCl	52	NaOH	32	Steam	2
	Steam	31	Flocculant	0.0038	Water	51
	Water	456	Steam	48		
			Water	131		
OUT-PUT	Pb concentrate	49.9	Waste solution	744	Waste solution	53
	Leaching solution	535	SnIn concentrate	1.84	SnIn concentrate	1.84

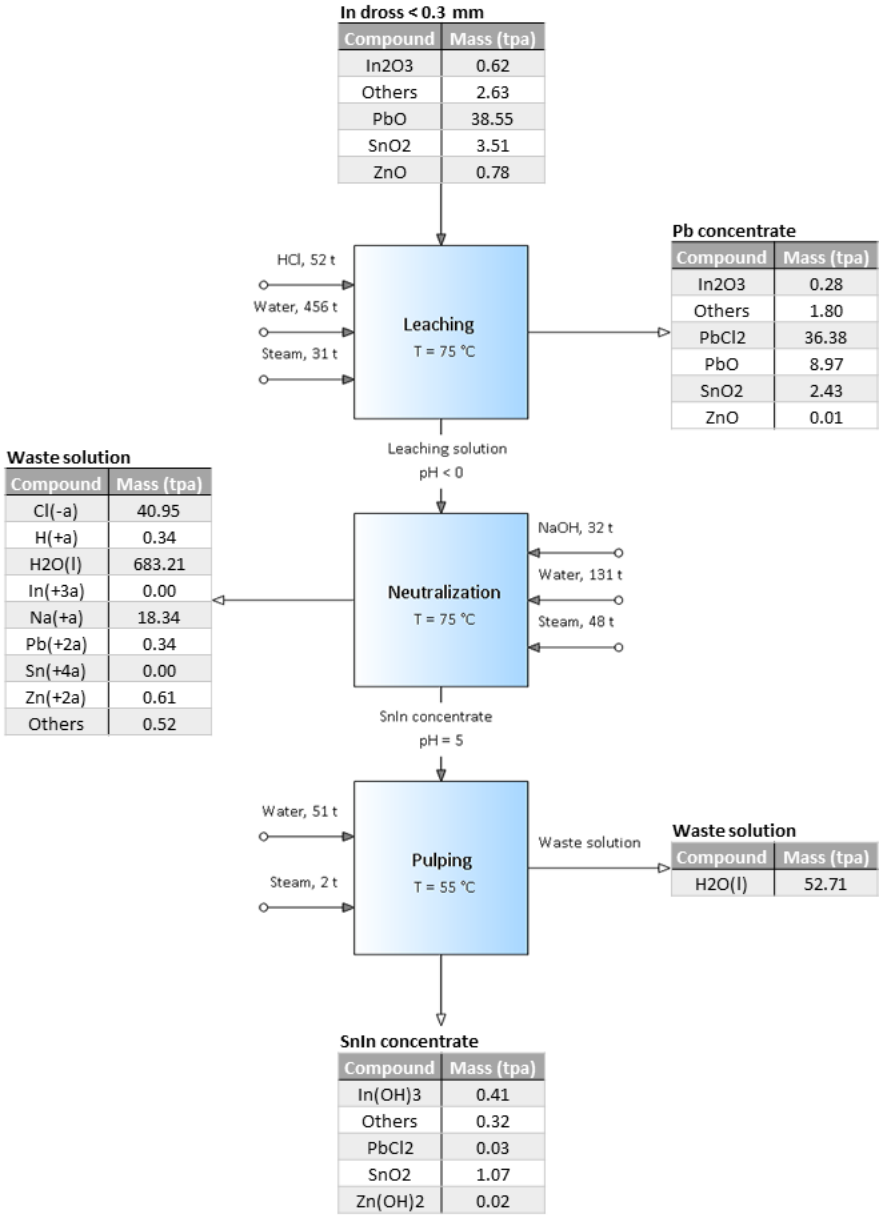

Figure 16. Mass flow of each of the components in the undersized indium dross and in the output streams of the hydrometallurgical treatment of the indium dross, calculated with HSC Chemistry 9.

Table 6. Heat balance for the hydrometallurgical treatment of the indium dross.

	Leaching 75°C	Neutralization 75°C	Pulping 55°C
$\Delta H_{THERMAL}$ (GJ/a)	93.7	125.8	5.4
$\Delta H_{REACTION}$ (GJ/a)	-13.5	-2.3	0
$\Delta H_{HEAT\ FLOW}$ (GJ/a)	80.2	123.5	5.4

The composition of the indium concentrate obtained in the simulations is presented in Table 8. Compared to the results from the experiments, the results show smaller amounts of tin, oxygen and chlorine. The lack of oxygen and chlorine in the indium concentrate in the simulation could be a result of the assumption that minor or unknown elements in the PbSnIn alloy will be inert in the process. The mass fraction of indium in the indium concentrate obtained from the simulation is slightly higher than that from the experiments. As the mass of the concentrate in the simulation is lower than reported in experiments, the yield obtained in the simulation is close to the one reported for the experiments.

Table 7. The composition of the indium concentrate

ELEMENT	In	Sn	Pb	Zn	O	Cl	Others
MASS FRACTION (%)	15.4	45.8	1.12	0.64	22.6	0.39	14.1

5.4 Pyrometallurgical treatment of PbSnCuInGe alloy

Compared to the PbSnIn alloy, the PbSnCuInGe alloy contains much less lead and instead higher concentrations of not only germanium, indium and tin, but also copper, zinc, silver and antimony (Table 9). In addition to indium and tin, also germanium is recovered from the alloy. The pyrometallurgical treatment of the PbSnCuInGe-alloy is similar to the treatment of the PbSnIn alloy, but instead of first removing the zinc from the alloy, the alloy is straight away oxidized and the oxide dross is screened. The alloy remaining after oxidation is directed to tin recovery, while the oxide dross awaits hydrometallurgical treatment.

The pilot-scale experiments were conducted as follows (IMN, 2018). The same one-ton kettle used for the treatment of the PbSnIn alloy was used. The temperature was between 650 and 700°C during the oxidation stage, which took 20–60 hours to execute. Sodium nitrate was added to the melt in multiple stages. An oxide dross, also containing metal drops, was formed and the dross was removed and screened,

redirecting the larger particles of the dross to the kettle. As in the pyrometallurgical treatment of the PbSnIn dross, the screening was performed with the aim to remove metal drops from the dross. The screening was conducted at room temperature with a 0.32 mm sieve.

Table 8. Elemental composition of PbSnCuInGe alloy.

ELEMENT	Ge	In	Sn	Pb	Cu	Zn	Ag	Sb
MASS FRACTION (%)	6.9	1.74	35.9	19.0	21.4	8.63	1.55	1.06

All elements in Table 11 were treated individually in the simulation of the process, except for antimony, arsenic and bismuth. They were, together with unknown elements, treated as an inert material, constituting 4.9% of the alloy. The temperature for the oxidation was set to 680°C. The sodium nitrate added in the oxidation stage was assumed to undergo thermal decomposition as described by Hoshino, Utsunomiya and Abe (1981).

$$2\ NaNO_3 \rightarrow 2NaNO_2 + O_2 \quad (13)$$

$$4\ NaNO_2 \rightarrow 2\ Na_2O + 4\ NO + O_2 \quad (14)$$

The conversion of sodium nitrate was set to 100% and the conversion of sodium nitrite to 96%. Zinc, indium, tin and lead were assumed to oxidize in accordance with (5–8). Germanium was set to oxidize in accordance with the following reaction.

$$Ge + O_2 \rightarrow GeO_2 \quad (15)$$

The conversion of germanium, indium and zinc to oxides was set to 100%. Around half of the tin and lead contained in the alloy was assumed to oxidize. All oxides were distributed to the dross, together with some of the elemental copper, silver, tin and lead, which together constitute the metal drops. In the screening stage, most of the oxides were distributed to the smaller particles. This resulted in the larger particles being constituted of mostly tin, lead and copper.

Table 10 presents the yields of the main elements of from the PbSnCuInGe alloy to the output streams, as calculated from the results of pilot-scale experiments (IMN, 2018) without consideration of material losses. The yield of indium and germanium to the undersized dross is 99.4% and 100%, respectively. Table 10 also presents the mass fraction of the main elements in the output streams, as a result of the simulation. The mass fractions and yields presented for the oversized dross apply to the stream that circulates in the process in a steady-state situation. Since this stream is not considered an input stream in the calculation of yields, and the yields

to this stream thereby imply a total yield higher than 100%, the yields are presented in parenthesis.

The heat balance is presented in Table 11. In Figure 17, the mass flow of each of the components of the PbSnCuInGe alloy and the output streams is presented. Table 12 presents the mass balance for each stage of the process in the form of mass flows of the raw materials, intermediates, chemicals and products

Table 9. Yields and mass fractions of the main elements to and in the products of the pyrometallurgical treatment of the PbSnCuInGe alloy.

UNIT			**Oxidation**	**Screening**	
STREAM			PbSnCuAg	GeIn dross > 0.3 mm	GeIn dross < 0.3 mm
ELEMENT	In	wt-%	0.03	2.17	2.19
		Yield[a] (%)	0.6	(3.6)	99.4
	Ge	wt-%	0	7.12	8.75
		Yield[a] (%)	0	(3.0)	100
	Sn	wt-%	45.6	29.3	25.8
		Yield[a] (%)	43.4	(2.4)	56.6
	Pb	wt-%	15.2	19.9	17.5
		Yield[a] (%)	27.4	(3.0)	72.6
	Cu	wt-%	32.6	18.7	13.1
		Yield[a] (%)	52.1	(2.5)	47.9
[a] (IMN, 2018)					

Table 10. Heat balance of the pyrometallurgical treatment of the PbSnCuInGe alloy.

	Oxidation 680°C	**Screening 25°C**
$\Delta H_{THERMAL}$ (GJ/a)	19.6	-8.0
$\Delta H_{REACTION}$ (GJ/a)	-58.9	-
$\Delta H_{HEAT\ FLOW}$ (GJ/a)	-39.3	-8.0

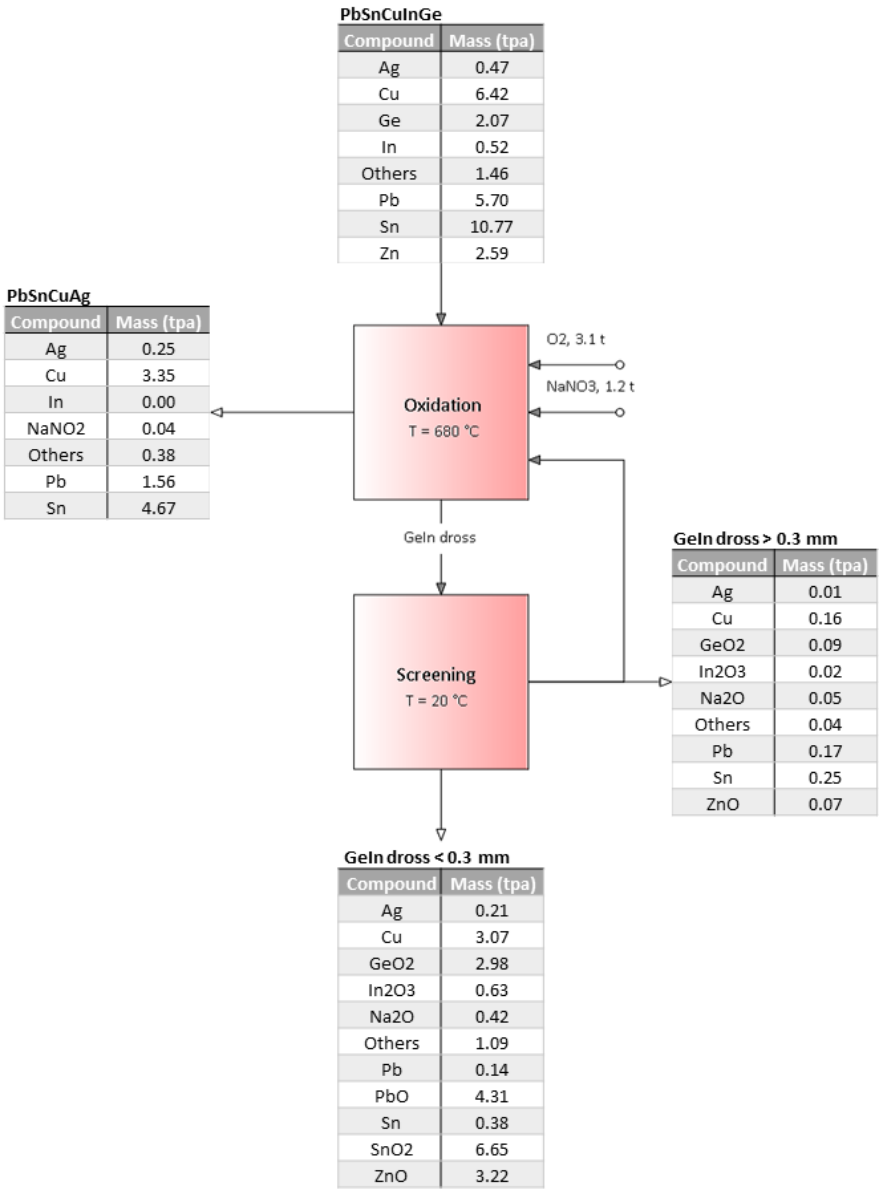

Figure 17. Mass flow of each of the components in the PbSnCuInGe alloy and in the output streams of the pyrometallurgical treatment of the PbSnCuInGe alloy, calculated with HSC Chemistry 9.

Table 11. Mass balance for each stage of the pyrometallurgical treatment of the PbSnCuInGe alloy.

UNIT	Oxidation		Screening	
	Stream	Mass flow (t/a)	Stream	Mass flow (t/a)
INPUT	PbSnCuInGe	30	GeIn dross	24.5
	GeIn dross > 0.3 mm	0.9		
	$NaNO_3$	1.2		
	O_2 (air)	3.1		
OUT-PUT	PbSnCuAg	10.3	GeIn dross > 0.3 mm	0.9
	NO	0.4	GeIn dross < 0.3 mm	23.6
	GeIn dross	24.5		

5.5 Hydrometallurgical treatment of GeIn dross

The oxide dross obtained in the pyrometallurgical stage is further treated with hydrometallurgical methods, including leaching, tin precipitation, germanium precipitation and indium precipitation. The aim of the hydrometallurgical treatment is to produce an indium concentrate and a germanium concentrate. Additionally, lead-tin-copper concentrate and wastewater is produced in the process. The concentrate may be recycled to previous stages of pyrometallurgical processing, while the wastewater is directed to industrial wastewater treatment. Neither recycling of the concentrate nor wastewater treatment were included in the simulation of the process.

Pilot-scale experiments were performed in the following manner (IMN, 2018). All stages of the process were performed in a leaching tank with a volume of one cubic meter. The tank was equipped with a mixer and direct heating with steam was applied. Leaching of the oxide dross was performed with an aqueous solution of sulfuric acid at 80°C. The suspension was mixed for two hours, during which the lead-tin-copper concentrate was formed. The suspension was filtered with a filter press.

For tin precipitation, hydrogen peroxide was added to the filtrate. The suspension was then heated to 70°C and mixed for one hour, in order to decompose any excess hydrogen peroxide. Flocculent was added and the suspension was left to sediment overnight. The clarified solution was directed to the next stage, while the tin suspension was redirected to the leaching stage, in order to improve both germanium and indium yields as well as precipitate filterability.

In the germanium precipitation stage, sodium hydroxide was first added to the solution to adjust the pH of the solution to 2.0. The solution was heated to 80°C and

technical tannic acid powder was added to the solution. The solution was mixed for two hours, during which a germanium-tannin concentrate precipitated. Afterwards, the suspension was filtered using a filter press. The concentrate was pulped with water at 70°C and filtration was repeated.

The filtrate from the previous stage was again heated to 60°C and sodium hydroxide was added for the pH to reach 5.0. During the neutralization, an indium concentrate precipitated. The suspension was mixed for two hours before filtering with a filter press. The indium concentrate was pulped with water at 70°C and filtration was repeated.

In the simulation model, most of the indium, germanium and zinc was set to dissolve in the sulfuric acid solution during leaching. All the sodium oxide, tin(II) oxide and elemental tin was assumed to dissolve and the opposite was assumed for the tin(IV) oxide, which is poorly soluble. All the elemental lead and lead oxide present in the dross was assumed to form lead sulfate in accordance with the following reactions.

$$Pb + 2\ H_2SO_4 \rightarrow PbSO_4 + SO_2 + H_2O \quad (16)$$

$$PbO + H2SO4 \rightarrow PbSO_4 + H_2O \quad (17)$$

Lead sulfate is poorly soluble and was assumed to precipitate completely. Together with the full amount of copper and silver present in the dross, the lead sulfate and the undissolved oxides constitute the lead-tin-copper concentrate.

In the tin precipitation unit, the hydrogen peroxide was set to oxidize the bivalent tin almost completely to the tetravalent insoluble form, as described in the following reaction.

$$Sn^{+2} + H_2O_2 \rightarrow SnO_2 + 2\ H^+ \quad (18)$$

In addition to the tin oxide, the tin precipitate from the experiments also contained some indium, germanium and a small amount of zinc. In the simulation model, indium and zinc were assumed to precipitate as hydroxides in accordance with (10) and (12). Since no suitable reaction for germanium precipitation was found in the literature, the germanium was assumed precipitate as germanium oxide. Neither in this stage nor in the indium precipitation stage was the use of flocculant taken into account.

The addition of tannic acid in the germanium precipitation stage was not included in the simulation model, due to limited data on tannic acid being available. Instead, germanium was assumed to precipitate as germanium oxide. Since the absence of tannin radically decreases the mass of the germanium concentrate, the mass fractions reported below were calculated with a total mass equal to the mass of the germanium concentrate obtained in the experiments. The same mass is reported in the mass balance. The mass added to the concentrate equals 96% of the input mass of tannic acid.

In addition to germanium, some indium, zinc and sodium was also present in the germanium concentrate obtained in the experiments. In the model, indium and zinc were assumed to precipitate as hydroxides, in accordance with (10) and (12). About 2% of the sodium ions in the solution was assumed to form sodium sulfate and precipitate.

In the indium precipitation stage, indium was set to precipitate as indium hydroxide in accordance with (10). The small amount of germanium left in the solution was assumed to precipitate as germanium oxide and a part of the zinc as zinc hydroxide, as described by (12). A minor amount of sodium sulfate was also set to form and precipitate. As the resulting mass of precipitate was less than half of what was reported in the experiments, some of the remaining tannic acid in the solution after germanium precipitation was assumed to precipitate in the indium precipitation stage. A mass equal to 3% of the input mass of tannic acid to germanium precipitation was added to the total mass of the indium precipitate and taken into account in the results below in the same way as in the case of the germanium precipitate.

As the full mass of the indium and germanium concentrates was not programmed into the simulation model and the water to concentrate mass ratio of the pulping stages was unknown, the pulping stages were not included in the model. Instead, the unit modelled for pulping of the indium concentrate produced in the hydrometallurgical treatment of the indium dross was used, with updated temperature and input mass, to obtain the amount of water and steam used. This resulted in 35 t/a water and 3 t/a steam for the indium concentrate. Due to the high mass of the germanium concentrate, the water to concentrate mass ratio was lowered to one for the germanium concentrate pulping, resulting in an input amount of 30 t/a water and 2 t/a steam. These results are not presented in the tables below, but are taken into account when calculating the total amount of water and steam used, and waste water produced, in the process.

Table 13 presents the yields of the main elements of the indium-germanium dross to the output streams, as calculated from the results of pilot-scale experiments (IMN, 2018) without consideration of material losses. The yield of indium from the dross to the indium concentrate is 54% and the yield of germanium to the germanium-tannin concentrate is 80%. These are also the final yields for the recovery of indium and germanium from the PbSnCuInGe alloy, as the yield of both elements to the dross in the pyrometallurgical stage was close to 100%. Table 13 also presents the mass fraction of the main elements in the output streams, as a result of the simulation. The mass fractions and yields presented for the tin concentrate apply to the stream that circulates in the process in a steady-state situation. Since this stream is not considered an input stream in the calculation of yields, and the yields to this stream thereby imply a total yield higher than 100%, the yields are presented in parentheses.

Table 14 presents the mass balance for each stage of the process in the form of mass flows of the raw materials, intermediates, chemicals and products. The heat balance is presented in Table 15. The reaction heat is not presented for the germanium precipitation, since tannin was excluded from the simulation. The absence of

tannin also affects the reaction heat of the indium precipitation and the thermal enthalpy difference both in the germanium and indium precipitation unit. In Figure 18, the mass flow of each of the components of the undersized indium-germanium dross and the output streams is presented.

Table 12. Yields and mass fractions of the main elements to and in the products of the hydrometallurgical treatment of the germanium-indium dross.

UNIT			**Leaching**	**Sn precipitation**	**Ge precipitation**	**In precipitation**	
STREAM			PbSnCu	Sn conc.	Ge-tannin conc.	Zn solution	In conc.
ELEMENT	In	wt-%	0.95	2.91	0.16		19.6
		Yield[a] (%)	29.1	(9.1)	11.1	5.44	54.4
	Ge	wt-%	2.15	15.3	5		0.25
		Yield[a] (%)	20.3	(11)	79.6	0	0.16
	Sn	wt-%	31.5	56.7	-		-
		Yield[a] (%)	99.8	(14)	0	0.25	0
	Pb	wt-%	21.4	-	-		-
		Yield[a] (%)	100	0	0	0	0
	Zn	wt-%	1.31	1.26	0.81		4.74
		Yield[a] (%)	8.9	(0.7)	10.5	78.2	2.44

[a] (IMN, 2018)

The composition of the concentrates is presented in Table 16 and Table 17. The mass fraction of germanium and indium in the germanium-tannin concentrate is the same as in the results from the experiments, while the mass fraction of zinc and sulfur is higher. The assumption that all sodium present in the concentrate is in the form of sodium sulfate explains the higher sulfur content in the simulation results. The indium content in the indium concentrate obtained in the simulation is significantly lower than the reported value from the experiments. This is due to adjustments that had to be made to the yields from the experiments to avoid inaccuracies in the mass balance of the process. Additionally, the zinc content of the indium concentrate is somewhat higher and the sulfur content is somewhat lower in the simulation compared to the experiments.

Table 13. Mass balance for each stage of the hydrometallurgical treatment of the germanium-indium dross.

UNIT	Leaching		Sn precipitation		Ge precipitation		In precipitation	
	Stream	Mass flow (t/a)	Stream	Mass flow (t/a)	Stream	Mass flow (t/a)	Stream	Mass flow (t/a)
INPUT	GeIn dross <0.3 mm	23.6	Leach. solution	264	Leach. solution	280	Leach. solution	327
	Sn conc.	1.49	H_2O_2	0.4	NaOH	6.5	NaOH	0.5
	H_2SO_4	27	Floccu-lant	0.45 kg/a	Tannic acid, 75%	32.5	Floccu-lant	1.1 kg/a
	Steam	17	Steam	16	Steam	21	Steam	16
	Water	215	Water	1.5	Water	20	Water	2.3
OUTPUT	PbSnCu conc.	19.3	Sn conc.	1.49	Ge conc.	32.8	Zn so-lution	345
	SO_2	0.3	O_2	0.09	Leach. solution	327	In conc.	1.31
	Leach. solution	264	Leach. solution	280				

Table 14. Heat balance of the hydrometallurgical treatment of the germanium-indium dross.

	Leaching 80°C	Tin precipitation 70°C	Germanium precipitation 80°C	Indium precipitation 60°C
$\Delta H_{THERMAL}$ (GJ/a)	49.1	43.1	53.6	42.8
$\Delta H_{REACTION}$ (GJ/a)	-7.1	-3.2	N/A[a]	-0.6
$\Delta H_{HEAT\ FLOW}$ (GJ/a)	42.0	39.9	53.6	42.2

[a] Not available, since the chemical reaction of germanium-tannin precipitation was excluded from the simulation.

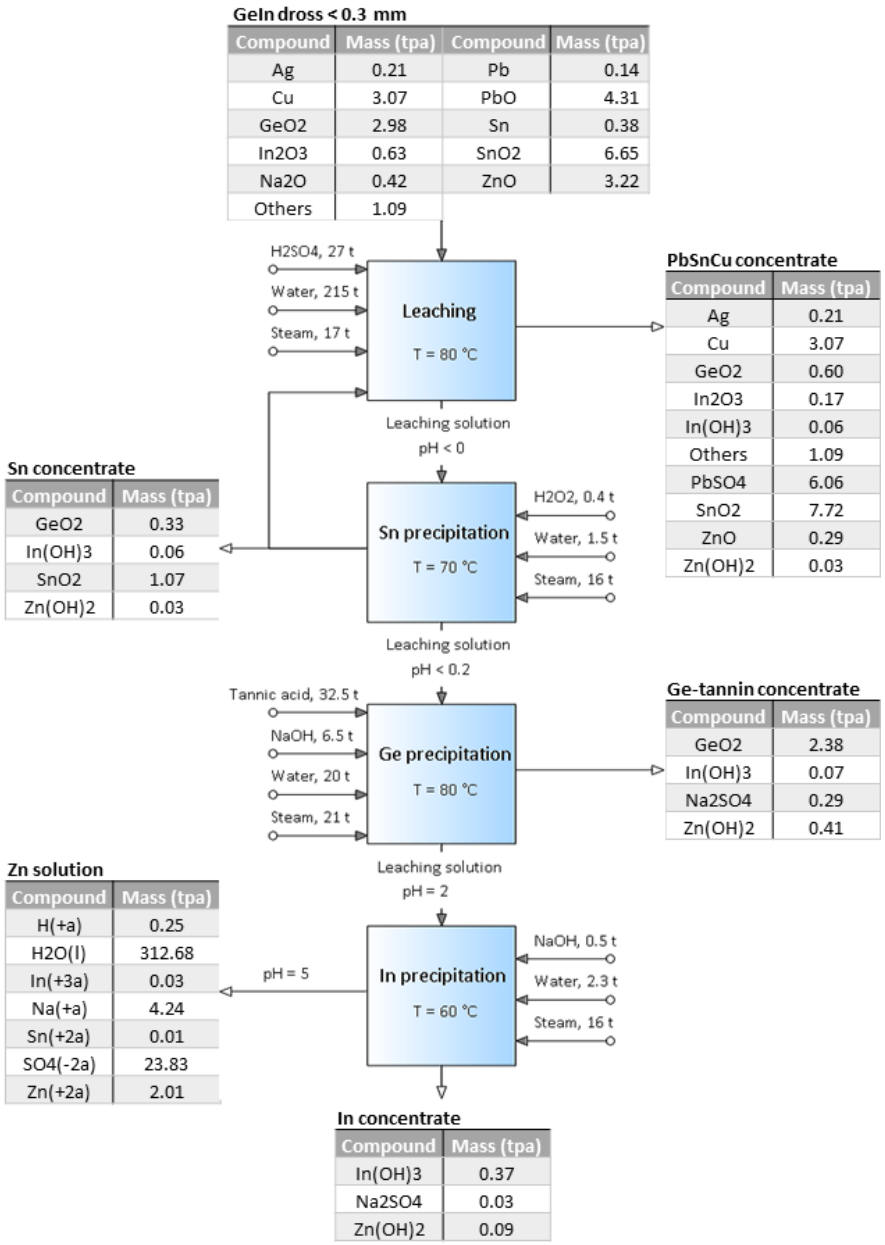

Figure 18. Mass flow of each of the components in the undersized indium-germanium dross and in the output streams of the hydrometallurgical treatment of the InGe dross, calculated with HSC Chemistry 9.

Table 15. The composition of the germanium-tannin concentrate.

ELEMENT	Ge	In	Zn	S	Na
MASS FRACTION (%)	5.0	0.16	0.81	2.1	3.0

Table 16. The composition of the indium concentrate.

ELEMENT	In	Ge	Zn	S	Na
MASS FRACTION (%)	19.6	0.25	4.73	0.53	0.76

5.6 Tin recovery

Tin is recovered from the remaining part of the PbSnIn and PbSnCuInGe alloys after pyrometallurgical treatment. The tin recovery includes copper removal, tin removal and tin smelting. In the process, tin is concentrated to a tin-lead alloy, which is obtained from the tin smelting stage together with soda slag and dust. Additionally, copper dross is produced in the copper removal stage and crude in the tin removal stage. The copper dross may be reductively smelted using the soda slag and dust as a flux, producing crude lead and copper matte. The crude lead may be directed to fire refining to produce quality grade lead. Neither smelting of the copper dross nor fire refining of the crude lead is included in the simulation model.

The pilot-scale experiments of tin recovery were conducted as follows. The same one-ton kettle that was used in the pyrometallurgical subprocesses described above was used for the copper and zinc removal stages. The copper removal took between two and five hours and was conducted in two steps. First, liquation drossing was conducted at 450–480°C, after which the temperature was allowed to decrease to 340–380°C and sulfur was added. The dross formed during copper removal was removed from the melt. Tin removal was conducted immediately after copper removal at a temperature of 540–600°C. The tin removal stage took between 20 and 32 hours. Sodium hydroxide and sodium nitrate was added to the melt in multiple stages and the tin dross formed was removed. The remaining melt constitutes the crude lead.

A short rotary furnace heated with natural gas was used for the tin smelting. The tin dross from the previous stage was reductively smelted with addition of coke in the furnace. The smelting time was four hours and the final temperature 1,230°C. The soda slag formed in the process was separated from the tin-lead alloy after solidification of the alloy. The dust was removed from the process gas using a bag filter.

In the simulation model, the temperature of the copper removal stage was set to 450°C. The temperature of the alloys coming from the oxidation units were assumed

to decrease to 25°C before tin recovery. All of the sulfur added to the alloys was assumed to bind copper in the form of copper sulfide, as follows.

$$2\ Cu + S \rightarrow Cu_2S \quad (19)$$

Most of the indium, some of the tin and a small part of the lead in the melt was assumed to oxidize in accordance with (6-8). The oxides and copper sulfide, together with elemental copper and silver, constitute the copper dross in the process simulation.

The temperature of tin removal stage was set to 580°C. The sodium hydroxide and sodium nitrate was assumed to react with tin and lead forming sodium stannate and sodium plumbite in accordance with (1) and (3–4). The conversion of both tin and lead was set to 95% for these reactions. The remaining amount of tin and lead was assumed to oxidize as described by (7–8). The rest of the sodium hydroxide, sodium nitrate and the sodium nitrite originating from the oxidation stage of the PbSnCuInGe alloy were assumed to decompose to sodium oxide. The input amount of sodium hydroxide and sodium nitrate was adjusted in order for 50% of the input amount to decompose, resulting in a 24% decrease from the amount used in the experiments. The oxides constitute the tin dross together with a small amount of elemental copper.

The coke used in the tin smelting was assumed to contain 85% carbon, 6.5% silica and 8.5% other components considered inert. The tin dross was assumed to cool down to 25°C before tin smelting, for which the temperature was set at 1,200°C. During the smelting, the tin components were set to react with carbon monoxide to form sodium carbonate, in accordance with reactions described by Liu et al. (2016). The lead components and the sodium oxide in the tin dross were assumed to react in the same way. The reactions are described as follows.

$$SnO_2 + 2\ CO \rightarrow Sn + 2\ CO_2 \quad (20)$$

$$Na_2SnO_3 + 2\ CO \rightarrow Sn + Na_2CO_3 + CO_2 \quad (21)$$

$$PbO + CO \rightarrow Pb + CO_2 \quad (22)$$

$$Na_2PbO_2 + CO \rightarrow Pb + Na_2CO_3 \quad (23)$$

$$Na2O + CO \rightarrow Na_2CO_3 \quad (24)$$

The elemental tin and lead formed in the reaction constitute the tin-lead alloy produced in the tin smelting stage. The sodium carbonate formed in the reactions is the main component of the soda slag. Additionally, the soda slag contains a small amount of tin silicate. According to Britton (2013), silica reacts with tin during smelting as follows.

$$SnO_2 + CO + SiO_2 \rightarrow SnSiO_3 + CO_2 \quad (25)$$

The dust was in the simulation set to contain only oxides. About half of the dust was sodium oxide and most of the rest was lead and tin oxide.

Table 18 presents the yields of the main elements of from PbSn and PbSnCuAg alloys to the output streams, as calculated from the results of pilot-scale experiments (IMN, 2018) without consideration of material losses. The mass fraction of tin in the tin-lead alloy is 58% and the yield of tin from the mixed alloy to the tin-lead alloy is 74%. This results in a tin yield of 33% from the PbSnIn and PbSnCuInGe alloys. Both the mass of the tin-lead alloy and its tin content is slightly higher in the simulation compared to the results from the experiments. Table 18 also presents the mass fraction of the main elements in the output streams, as a result of the simulation.

In Figure 19, the mass flow of each of the components of the PbSn and PbSnCuAg alloys and the output streams is presented. Table 19 presents the mass balance for each stage of the process in the form of mass flows of the raw materials, intermediates, chemicals and products. The heat balance is presented in Table 20. The input temperature of both the alloys in the copper removal stage and the tin dross in the tin smelting stage was set to 25°C.

Table 17. Yields and mass fractions of the main elements to and in the products of the tin recovery process.

UNIT			**Cu removal**	**Sn removal**	**Sn smelting**		
STREAM			Cu dross	Crude lead	Soda slag	Dust	SnPb
ELEMENT	Sn	wt-%	11.3	0.16	2.6	2.98	58
		Yield[a] (%)	18.6	3.87	3.35	0.54	73.7
	Pb	wt-%	54	99.5	0.22	31.6	41.5
		Yield[a] (%)	3.5	94.2	0.01	0.23	2.08
	Cu	wt-%	24.4	0.12	0.05	0.07	0.16
		Yield[a] (%)	92.8	6.6	0.15	0.03	0.48
	Na	wt-%	-	0	41.2	40.1	0
		Yield[a] (%)	-	0	88.2	11.8	0

[a] (IMN, 2018)

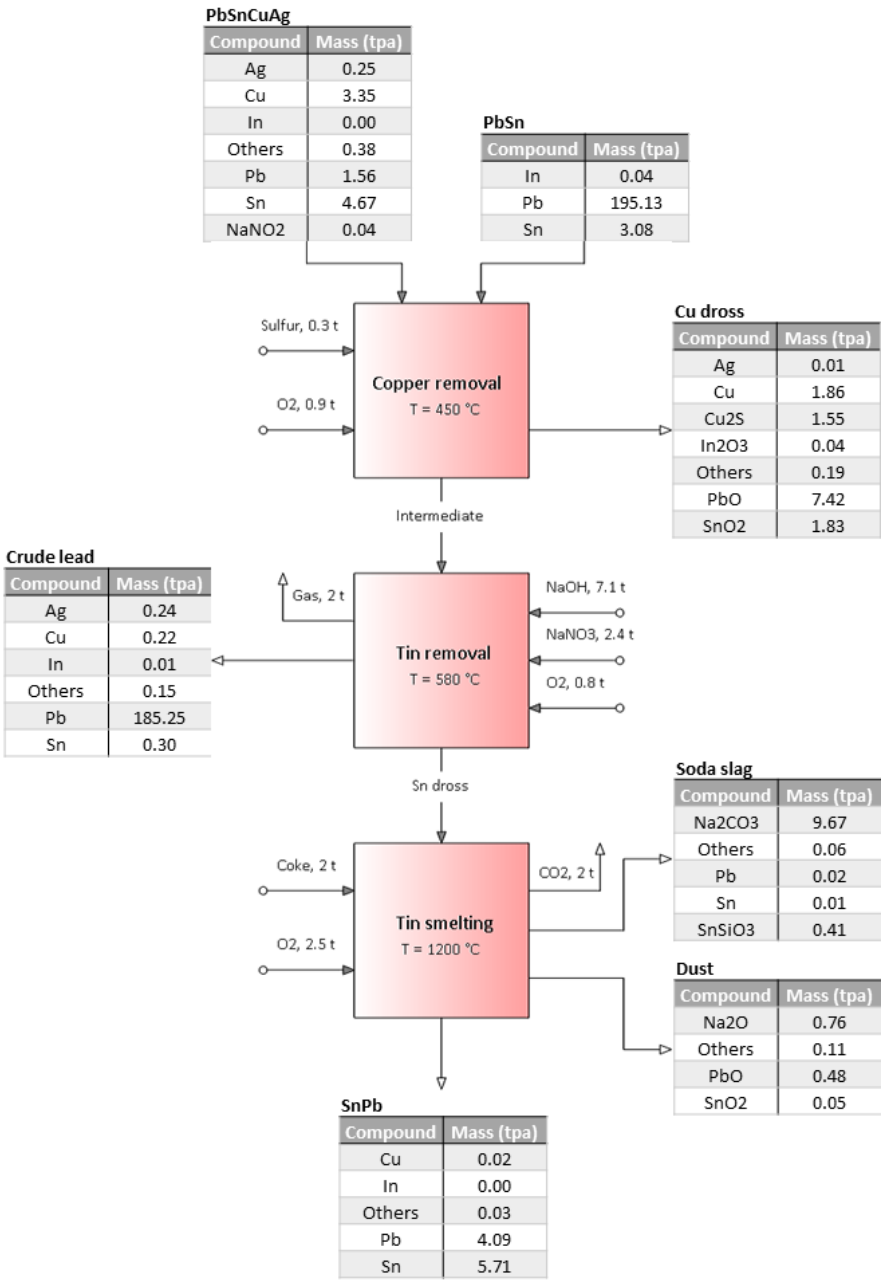

Figure 19. Mass flow of each of the components in PbSn and PbSnCuAg alloys and in the output streams of the tin recovery, calculated with HSC Chemistry 9.

Table 18. Mass balance for each stage of the tin recovery process.

UNIT	Cu removal		Sn removal		Sn smelting	
	Stream	Mass flow (t/a)	Stream	Mass flow (t/a)	Stream	Mass flow (t/a)
IN-PUT	PbSn	198	Intermediate	197	Sn dross	19.0
	PbSnCuAg	10.3	NaOH	7.1	Coke	2
	Sulfur	0.3	$NaNO_3$	2.4	O_2 (air)	2.5
	O_2 (air)	0.9	O_2 (air)	0.8		
OUT-PUT	Cu dross	12.9	Crude lead	186	Soda slag	10.2
	Intermediate	197	N_2	0.4	Dust	1.4
			H_2O	1.6	CO_2	2.1
			Sn dross	19.0	SnPb	9.84

Table 19. Heat balance of the tin recovery process.

	Cu removal 450°C	Sn removal 580°C	Sn smelting 1,200°C
$\Delta H_{THERMAL}$ (GJ/a)	20.3	17.4	36.9
$\Delta H_{REACTION}$ (GJ/a)	-15.3	-20.9	-39.9
$\Delta H_{HEAT\ FLOW}$ (GJ/a)	5.0	-3.5	-3.0

5.7 Overview of process simulation results

The results of the simulation show that 0.56 t/a indium, 1.65 t/a germanium and 5.7 t/a tin is recovered from the PbSnIn and PbSnCuInGe alloys. The amount of tin in the indium concentrate is so small relative to the value of tin, it is not considered as recovered tin in the calculations. Production of the metals on such a scale would increase European production of indium by an estimated 1% and production of germanium outside China by 4%. The contribution of tin would be insignificant to both the global and European production.

The mass flow of recovered indium, germanium and tin in the recovery process is illustrated in Figure 20. The same amount of indium is recovered from both the PbSnIn and the PbSnCuInGe alloy, with similar yields. Since the yields of indium and germanium to the oxide dross in both pyrometallurgical processes are high, the

highest losses occur in the hydrometallurgical processes. More than half of the tin contained in the input alloys is incorporated in the oxide dross and directed to hydrometallurgical treatment.

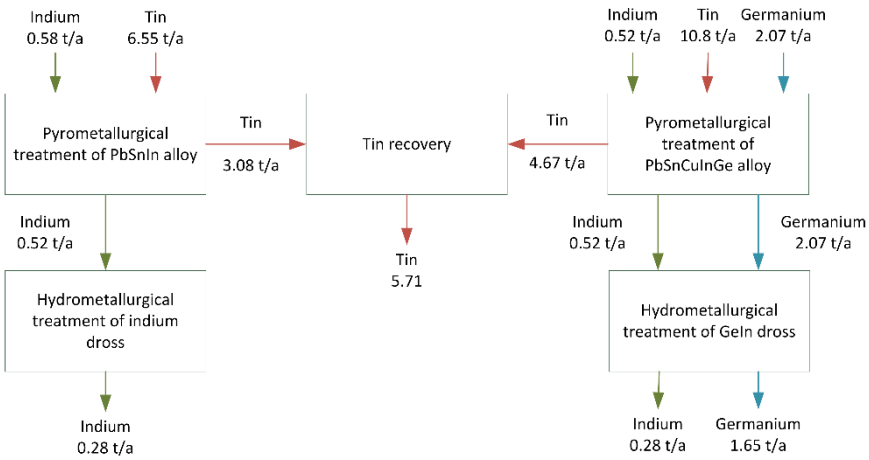

Figure 20. The mass flow of recovered indium, germanium and tin in each subprocess, measured in tons per year.

Redirection of the lead concentrate and the lead-tin-copper concentrate, both produced in the hydrometallurgical processes, back to the process has been proposed, but was not included in the simulation. Both concentrates combined contain 0.41 t/a indium, 0.42 t/a germanium and 8.0 t/a tin, which indicates that recirculation of the streams could significantly increase the yield of all three metals. It would, however, also increase the mass flow of most streams and thereby also size of the equipment. The mass flow of the lead-tin-copper concentrate is 19 t/a and the mass flow of the lead concentrate is 50 t/a. The lead concentrate is planned to be recirculated to the imperial smelting process, where lead is recovered. This will reduce the mass that is recirculated to the indium, germanium and tin recovery process.

Central figures for the economic feasibility assessment of the recovery process are presented in Table 21. The pure metal value of the recovered metals, calculated with a currency exchange rate of 1 USD equaling 0.86 EUR, is about 2.2 million EUR/a. Most of the value comes from germanium, which also has the highest yield of the three metals. The recovered tin and indium have pure metal values that are close to equal.

Table 20. Key figures of the recovery process.

	INDIUM	GERMANIUM	TIN
YIELD	51%	80%	33%
MASS FRACTION	15.4% (SnIn conc.) 19.6% (In conc.)	5.0%	58.0%
PURE METAL MASS	0.56 t/a	1.65 t/a	5.7 t/a
PURE METAL PRICE	210 USD/kg	1400 USD/kg	21 USD/kg
PURE METAL VALUE	102,000 EUR/a	1,982,000 EUR/a	103,000 EUR/a

5.8 Sizing of major equipment

To enable estimation of capital costs, the major equipment required for the process and their key dimensions were determined. No major equipment was assumed to be available for the process at the site for which it is planned. Equipment required for steam production, wastewater treatment or any other process not included in the simulation of the process, was not taken into account. Capacity to process 250 t/a of the PbSnIn alloy and 30 t/a of the PbSnCuInGe alloy was considered. The process was designed as a batch process, with one set of equipment for all pyrometallurgical processing and one set of equipment for all hydrometallurgical processing. Production was assumed to be ongoing, 16 hours a day and 250 days in a year.

5.8.1 Equipment for pyrometallurgical treatment

The pyrometallurgical equipment, illustrated in Figure 21, includes one kettle (AA-101), one rotary furnace (AB-101), one screen (CA-101), one bag filter (CB-101), one fan (DB-101) and two silos (FA-101, FA-102). The kettle is used for all stages of the pyrometallurgical treatment of the alloys, as well as in the copper removal and the tin removal stage of tin recovery. Tin smelting is conducted in the rotary furnace. In the oxidation stages of the pyrometallurgical treatment of the alloys, the dross is screened and the dust is collected with the bag filter. The bag filter also collects the dust from tin smelting. The indium dross from both the screen and the bag filter is collected in one of the silos, and the germanium-indium dross in the other.

The pyrometallurgical treatment of the PbSnIn alloy, the pyrometallurgical treatment of the PbSnCuInGe alloy and the tin recovery, excluding tin smelting, were

each assumed to be possible to perform in one day. The oxidation of the PbSnCuInGe alloy and the tin recovery would consequently have to be performed in a significantly shorter time than in the experiments. Since the bag filter is used both during oxidation and tin smelting, the tin smelting cannot be performed simultaneously with pyrometallurgical treatment of either alloy. However, assuming than the pyrometallurgical treatment of the PbSnIn alloy is conducted in the same time as the fastest experiment, there is sufficient time for tin smelting the same day. With this schedule, a batch size of about 2 t for the kettle and 170 kg for the rotary furnace is obtained.

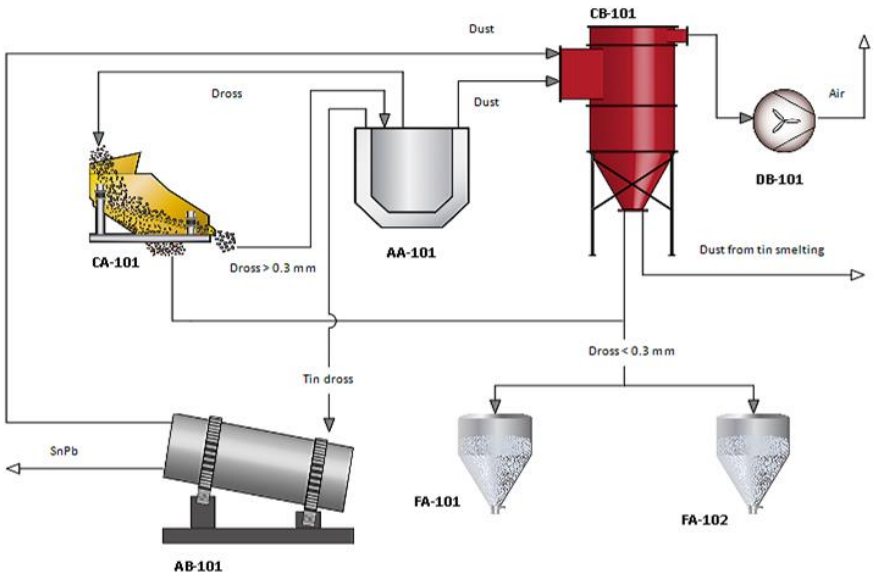

Figure 21. Major equipment used for tin recovery and pyrometallurgical treatment of the PbSnIn and PbSnCuInGe alloy.

The volume of the kettle was calculated for the processing stage with the highest volume. According to the simulation, from which the volume was obtained for standard temperature and pressure, the volume of the input material to the oxidation of the PbSnCuInGe alloy, was the highest. For the volume of the silos, the density of the dross was calculated using a weighted average of the bulk densities of the components present in the dross. The silos were dimensioned to hold the amount of dross required for one batch of hydrometallurgical treatment plus the amount produced in one batch of pyrometallurgical treatment. A design factor of 30% was used for sizing of both the kettle and the silos. The resulting volume was 0.4 m^3 for the kettle, 2 m^3 for the silo holding the germanium-indium dross and 1 m^3 for the silo holding the indium dross.

The heating duty of the rotary furnace was estimated to equal the thermal enthalpy difference of one tin smelting batch, formed in half an hour. This resulted in

a 0.2 MW duty. For the estimation of the screen area, a base screen capacity for a 0.32 mm screen, was corrected for the density of the dross and the fraction of oversize particles, as described by Fuerstenau and Han (2003). With this screen capacity, the screen area was calculated as the area needed for screening of the indium dross produced in one batch, in one and a half hours, resulting in a screen area of 0.5 m^2. The bag filter and the fan were estimated to work with a gas flow of 1,000 Nm^3/h.

5.8.2 Equipment for hydrometallurgical treatment

The hydrometallurgical equipment, illustrated in Figure 22, includes one leaching tank (BA-201), one thickener (CD-201), one filter press (CC-201), one heat exchanger (EA-201), one silo (FA-201) and four pumps (DA-201, DA-202, DA-203, DA-204). All stages of the hydrometallurgical treatment involve the leaching tank, from which the suspension is pumped to the thickener. The thickened suspension is filtered with a filter press, but first directed to the heat exchanger if cooling is required. Depending on the stage of the process, the overflow from the thickener and the filtrate from the filter press is directed either back to the leaching tank or to wastewater treatment. The filtered precipitate is either sent back to the leaching tank for pulping, or collected in the silo, from which it is packed to a bag before the next filtration.

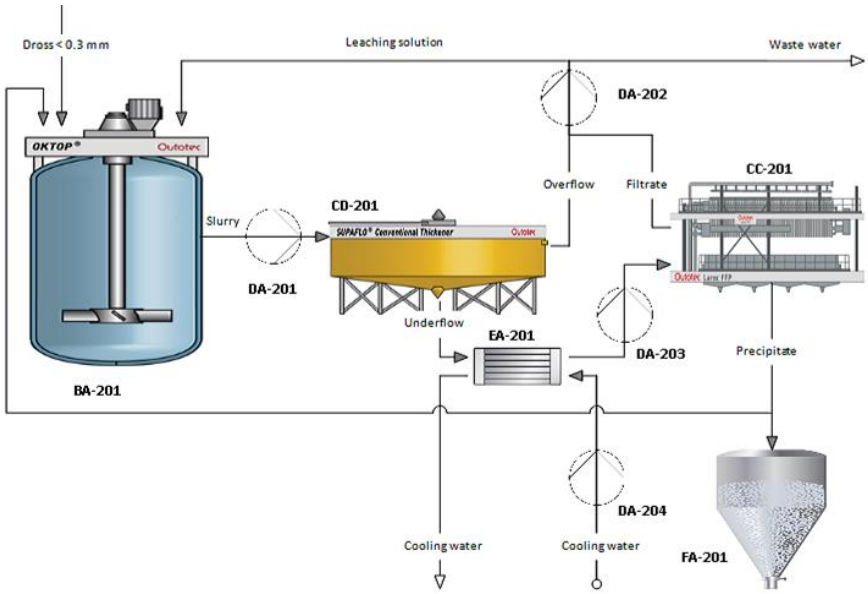

Figure 22. Major equipment for the hydrometallurgical treatment of indium and germanium-indium dross.

The leaching and neutralization stage of the hydrometallurgical treatment of the indium dross was assumed to be conducted in one day, and the pulping stage was assumed to be conducted the following day, regardless of the treatment of which dross is on the schedule. The hydrometallurgical treatment of the germanium-indium dross was assumed to be conducted in three days. Leaching and tin precipitation was considered to be performed in one day, and germanium precipitation and indium precipitation were considered to be performed in one day each. Pulping of the germanium concentrate could be conducted the same day as indium precipitation and pulping of the indium concentrate could be conducted the day following indium precipitation, regardless of the scheduled dross treatment.

The batch size was estimated by considering the stages of hydrometallurgical treatment where the volume is the highest. The volume was calculated by addition of the precipitate volume, which was calculated using bulk densities, to the output volume of the liquid phase, obtained from the simulation. This resulted in a batch volume of 8.2 m^3. The volume of the silo was estimated using the germanium concentrate volume of one batch. For the sizing of the leaching tank, the thickener and the silo, a design factor of 30% was used. This resulted in a volume of 11 m^3 for the leaching tank and thickener, and a volume of 4 m^3 for the silo.

The volumetric flow of the pump emptying the leaching tank was calculated for an emptying time of 20 minutes, resulting in a volumetric flow rate of 7 l/s. A volumetric flow of about half of this was assumed for the other pumps, and a heat transfer area of 5 m^2 was assumed for the heat exchanger. For the filter press, a thickness of 30 mm, typical for filtration of urban sludge, was assumed (Deltreil, 2003). Since the volume of one batch of germanium concentrate is multiple times higher than the volume of the other precipitates, the filter press was dimensioned to filter the germanium concentrate in three cycles, resulting in a filter area of 40 m^2. With this filter area, filtering of the other precipitates can be conducted in one cycle.

5.8.3 Results

The key dimensions of the major equipment required for processing of 250 t/a PbSnIn alloy and 30 t/a PbSnCuInGe alloy are compiled in Table 22. Carbon steel was chosen as the default material for the process. For the equipment which handles strong acids, fiber-reinforced plastic was chosen.

Table 21. Key dimensions of the major equipment required for the process.

UNIT	DESCRIPTION	SIZE	MATERIAL
AA-101	Kettle furnace[a]	0.4 m^3	CS
AB-101	Rotary furnace	0.2 MW	CS
BA-201	Leaching tank[a]	11 m^3	FRP
CA-101	Screen	0.5 m^2	CS
CB-101	Bag filter	1,000 Nm^3/h	CS
CC-201	Filter press	60 m^2	CS, PVC
CD-201	Thickener[a]	11 m^3	FRP
DA-201	Pump	7 l/s	FRP
DA-202	Pump	4 l/s	FRP
DA-203	Pump	4 l/s	FRP
DA-204	Water pump	4 l/s	CS
DB-101	Fan	1,000 Nm^3/h	CS
EA-201	Heat exchanger	5 m^2	FRP
FA-101	Silo[a]	1.5 m^3	CS
FA-102	Silo[a]	2 m^3	CS
FA-201	Silo[a]	4 m^3	CS
[a] Design factor = 30%			

6. Economic feasibility

For the economic feasibility assessment, the operational and capital expenses of the process are estimated, the net present value is calculated and a sensitivity analysis is performed.

6.1 Methodology

Economic assessment was conducted based on the operational expenses and capital investment. The components of fixed operational investment were estimated as ratios of the capital costs, as suggested by Towler and Sinnott (2013). The variable operational expenses were calculated based on the previously presented technical assessment and mass and energy balances of the process.

The capital investment is based on the main process units sized in the pevious chapter. The total capital expenses are estimated based on the costs of main process units as suggested by Towler and Sinnott (2013). The material costs are considered using material-specific factors. In addition, inflation is considered by applying cost indices such as CEPCI. All prices are given in EUR for 2018.

6.2 Operational expenses

Operational expenses consist of variable and fixed costs. The fixed operational costs include costs for labor, maintenance, insurance, land rental, property taxes and administrative costs. The labor costs were calculated for four employees working two shifts with an average salary of 3,000 EUR/month and one supervisor with a salary of 4,000 EUR/month. The other fixed costs were estimated as percentages of the capital costs, as suggested by Towler and Sinnott (2013). The fixed operational costs are presented in Table 23 and total 450,000 EUR/a.

Table 22. Fixed operational costs.

FIXED COSTS	BASIS	COST (EUR/a)
Maintenance	4% of ISBL	65,000
Labor	3000–4000 EUR/month[a]	192,000
Administrative	65% of labor	125,000
Insurance	1% of ISBL+OSBL	23,000
Land rental & property taxes	2% of ISBL+OSBL	45,000
Total		**450,000**

[a] four employees working with an average salary of 3,000 EUR/month and one supervisor with a salary of 4,000 EUR/month

The variable costs include the cost of chemicals, utilities, energy and waste treatment or disposal. The total amount of chemicals, process water and cooling water used in the process, as well as wastewater generated in the process, were obtained from the process simulation. Wastewater is the only stream considered as waste in the cost estimation. Either redirection to the process or processing to byproducts has been proposed for all the other side streams. This is assumed to be implemented with no addition to capital costs and zero net effect on the cash flow, and is thereby excluded from the cost estimations.

All stages of pyrometallurgical treatment and tin recovery were assumed to be heated with natural gas. Heat losses equaling the reaction heat generated for each stage was assumed to occur, resulting in the required natural gas amount equaling the thermal enthalpy difference for the units. Heat losses were not considered for the hydrometallurgical stages and consequently the steam amount could be calculated directly from the heat balances obtained in the simulation. The price applies to an over-the-fence supply of steam and therefore no investment for production of steam should be considered in the estimation of the capital costs. The electricity amount was calculated using the average electricity requirements of various lead processes (European IPPC Bureau, 2017).

The variable operational costs were calculated for processing of 250 t/a PbSnIn alloy and 30 t/a PbSnCuInGe alloy. They are presented in Table 24 and total 175,000 EUR/a. The prices are converted using an exchange rate of 1 USD equaling 0.86 EUR and adjusted to current value using the producer price index for all commodities in August 2018 (U.S. Bureau of Labor Statistics, 2018).

6.3 Capital expenses

The capital investment consists of fixed capital costs and working capital. The capital tied up in inventories is, together with cash on hand, termed the working capital of the plant. The fixed capital costs include inside battery limits (ISBL) investment, outside battery limits (OSBL) investment, engineering costs and contingency charges. The ISBL investment is the cost of the plant itself. It includes the cost of structures and buildings, the cost of electrical and civil works and the installed cost of all process equipment. The OSBL investment is the cost of added infrastructure to the site, such as boilers, water pipes, a wastewater treatment plant, offices and site security. The engineering costs consist of detailed design and other engineering services. On top of this, contingency charges are added to allow for variation from the cost estimate.

The fixed capital investment was estimated based on the purchase cost of the major equipment required for the process. The purchase cost of major equipment is presented in Table 25. A material cost factor of 1.5 was used for conversion of the cost of equipment in carbon steel (CS) to fiber-reinforced plastic (FRP). The purchase costs were adjusted to current value using the annual Chemical Engineering Plant Cost Index for 2017 and converted to EUR using an exchange rate of 1 USD equaling 0.86 EUR.

Table 23. Variable operational costs, calculated using an exchange rate of 1 USD equaling 0.86 EUR and adjusted to current value using the producer price index for all commodities in August 2018.

VARIABLE COSTS	AMOUNT	PRICE	REFERENCE	COST
Chemicals	(t/a)	(EUR/t)		(EUR/a)
NaOH	49.8	390	(Eggeman, 2011)	19,000
$NaNO_3$	4.0	360	(CEIC, 2018)	1,000
HCl	52	270	(ICIS, 2006)	14,000
H_2SO_4	27	70	(Muller, 2006)	2,000
H_2O_2	0.4	370	(ICIS, 2006)	1,000[a]
Tannic acid	24.6	5,000	Own estimate	123,000
Flocculant	0.0054	N/A	N/A	0
Sulfur	0.3	50	(Apodaca, 2018)	1,000[a]
Coke	2.0	288	(Steelonthenet.com, 2018)	1,000[a]
Utilities	(t/a)	(EUR/t)		(EUR/a)
Process water	940	0.1	(Kangas, Kaijaluoto and Määttänen, 2014)	0
Cooling water	400	0.05	(Kangas, Kaijaluoto and Määttänen, 2014)	0
Energy	(MWh/a)	(EUR/MWh)		(EUR/a)
Electricity	40	75	(IEA, 2018)	3,000
Natural gas	40	24	(IEA, 2018)	1,000
Steam	119	61[b]	(Intratec, 2010)	7,000
Waste	(t/a)	(EUR/t)		(EUR/a)
Wastewater	1,200	1.3	(Towler and Sinnott, 2013)	2,000
Total				**175,000**

[a] The cost is rounded up to 1,000 EUR/a, as the required amount of the chemical is small.
[b] Medium pressure steam

Table 24. Cost estimates for major equipment.

UNIT	DESCRIP-TION	SIZE	MATE-RIAL	COST (€)	REFERENCE
AA-101	Kettle furnace[a]	0.4 m^3	CS	34,000	(Matches, 2014)
AB-101	Rotary furnace	0.2 MW	CS	101,000	(Towler and Sinnott, 2013)
BA-201	Leaching tank[a]	11 m^3	FRP	43,000	Own estimation
CA-101	Screen	0.5 m^2	CS	11,000	(Peters, Timmerhaus and West, 2004)
CB-101	Bag filter	1,000 Nm^3/h	CS	27,000	(Matches, 2014)
CC-201	Filter press	60 m^2	CS, PVC	147,000	(Matches, 2014)
CD-201	Thickener[a]	11 m^3	FRP	109,000	Own estimation
DA-201	Pump	7 l/s	FRP	13,000	(Towler and Sinnott, 2013)
DA-202	Pump	4 l/s	FRP	12,000	(Towler and Sinnott, 2013)
DA-203	Pump	4 l/s	FRP	12,000	(Towler and Sinnott, 2013)
DA-204	Water pump	4 l/s	CS	8,000	(Towler and Sinnott, 2013)
DB-101	Fan	1,000 Nm^3/h	CS	3,000	(Matches, 2014)
EA-201	Heat exchanger	5 m^2	FRP	3,000	(Towler and Sinnott, 2013)
FA-101	Silo[a]	1.5 m^3	CS	4,000	(Matches, 2014)
FA-102	Silo[a]	2 m^3	CS	4,000	(Matches, 2014)
FA-201	Silo[a]	4 m^3	CS	6,000	(Matches, 2014)
	Total			**537,000**	

Prices are adjusted to current value using the annual Chemical Engineering Plant Cost Index for 2017.
1 USD = 0.86 EUR.
[a] Design factor = 30%

The total capital expenses, estimated as suggested by Towler and Sinnott (2013), are presented in Table 26. The piping costs were calculated using the total purchase cost of the equipment, while other ISBL costs were calculated using the purchase costs of the equipment in carbon steel. The OSBL costs were estimated as 40% of the ISBL costs and the engineering and contingency costs were estimated as percentages of the combined ISBL and OSBL investment. The spare parts

inventory was estimated as 1% of the combined ISBL and OSBL investment. Other working capital was estimated based on the operational costs. The raw material inventory was estimated as the cost of chemicals for four weeks of production, the product inventory as four weeks' operational costs and cash on hand as one week's operational costs.

Table 25. Total capital expenses, estimated as suggested by Towler and Sinnott (2013).

ISBL COSTS	BASIS	COST (€)
Purchase cost of major equipment	Table 26	537,000
Piping	60% of equipment cost	322,000
Equipment erection	50% of equipment cost in CS	237,000
Instrumentation and control	30% of equipment cost in CS	142,000
Electrical	20% of equipment cost in CS	95,000
Civil	30% of equipment cost in CS	142,000
Structures and buildings	20% of equipment cost in CS	95,000
Lagging and paint	10% of equipment cost in CS	47,000
Total		**1,617,000**
WORKING CAPITAL		
Raw material inventory	4 weeks' cost of raw materials	13,000
Product inventory	4 weeks' cost of production	50,000
Cash on hand	1 week's cost of production	13,000
Spare parts inventory	1% of ISBL+OSBL	23,000
Total		**99,000**
OSBL COSTS	40% of ISBL	**647,000**
ENGINEERING	25% of ISBL+OSBL	**566,000**
CONTINGENCY	10% of ISBL+OSBL	**226,000**
TOTAL CAPITAL COSTS		**3,155,000**

6.4 Net present value

The net present value (NPV) for the investment was calculated with the following formula, where C_t is the net cash flow for the period t and r is the discount rate.

$$NPV = \sum_{t=0}^{T} \frac{C_t}{(1+r)^t} \quad (26)$$

The NPV was calculated for a time period of 20 years, using a discount rate of 10%. A capacity of 250 t/a PbSnIn alloy and 30 t/a PbSnCuInGe was considered. The plant was assumed to be constructed in one year, and the capacity of the plant was assumed to be at 75% the first year of production. Accordingly, C_0 equals the capital investment, C_1 is zero and C_2 is 75% of the revenue minus 75% of the variable operational costs and 100% of the fixed operational costs. The cash flow for the remaining years is the revenue minus the total operational costs. The calculations were conducted on an Earnings Before Interest, Taxes, Depreciation and Amortization (EBITDA) basis. The cumulative net present value was calculated for five scenarios, with a revenue equaling of 50–90% of the pure metal value for the main component in each product.

The results are presented in Figure 23. For the case of 70% of pure metal value, the payback time is seven years and the NPV for 20 years is about 3.5 million EUR. For 90% of pure metal value, the NPV for 20 years is 6.7 million EUR and for 50% of pure metal value it is 0.2 million EUR.

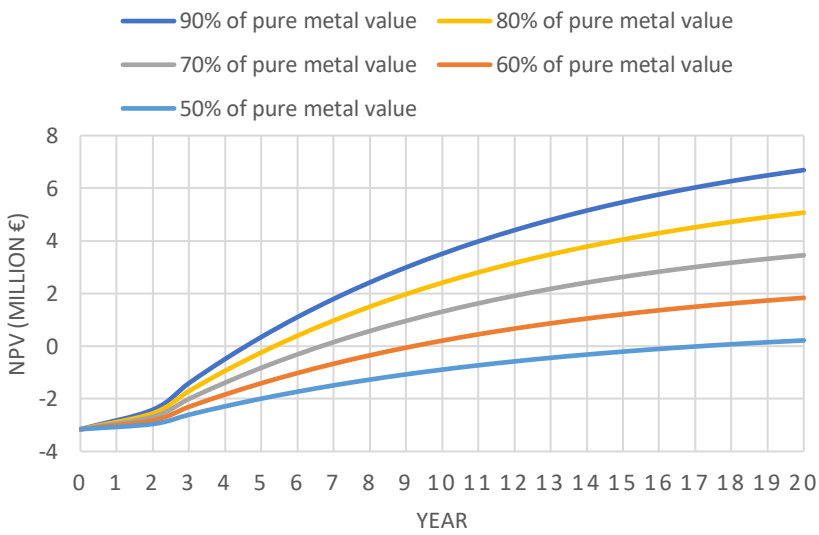

Figure 23. Cumulative net present value of the investment for a concentrate value of 50–90% of pure metal value. Calculations are conducted with a 10% discount rate and a capacity of 250 t/a PbSnIn and 30 t/a PbSnCuInGe, assuming a construction time of one year and a capacity of 75% in the first year of production.

6.5 Sensitivity analysis

The sensitivity of the net present value for 70% of pure metal value to a variation of key economic factors with ±25% was investigated. The results are presented in Figure 24.

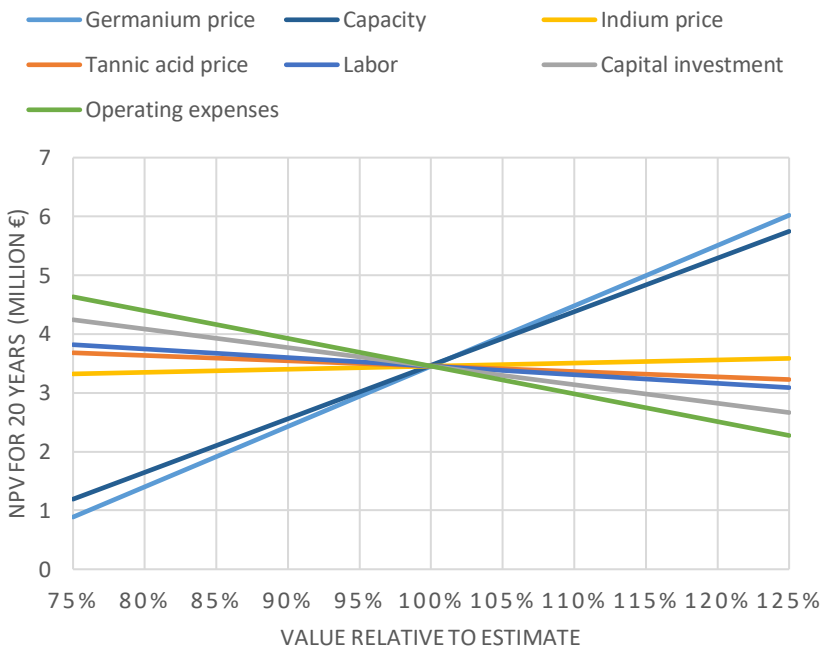

Figure 24. Sensitivity analysis for selected process parameters.

The net present value is the most sensitive for the germanium price. With a 25% increase in the market price of germanium, the net present value is almost 7 million EUR, while it with a 25% decrease in the market price of germanium is only one million EUR. The same applies to a ±25% variation in the germanium yield, i.e. a variation of the yield between 60% and 100%. A 25% increase or decrease in indium or tin prices results in only a 4% change in the net present value.

The variation in capacity applies to a 25% variation in revenue and a 25% variation the key dimension of each major equipment, which also affects the remaining capital costs. A 25% increase in the capacity of the plant results in a net present value of 5.7 million EUR, and a 25% decrease in capacity results in a net present value of 1.2 million EUR.

A change in the price of tannic acid, the cost of which constitutes 76% of the total chemical costs, results in a 7% change in the net present value. A variation in the total chemical costs has a similar effect on the net present value as a change in

cost for labor, which is only slightly higher than the effect of tannic acid price variation. A ±25% variation of the total operating expenses results in a change in the net present value of about 1.3 million EUR and a ±25% variation of the capital investment results in a change in the net present value of about 0.9 million EUR.

7. Discussion & conclusion

The aim of this study was to assess the techno-economic feasibility of a process for recovery of indium, germanium and tin from two alloys, obtained as byproducts in zinc production. The results of the techno-economic assessment give no definite answer regarding the feasibility of the process at the capacity which was studied, but can serve as a basis for further investigation of the feasibility of implementation of the process at a given plant site. Other considerable uncertainties in the results include the value of the products, the effect of recirculation of byproducts on yield, the OSBL costs and equipment cost.

The value of the germanium concentrate produced in the process is the most crucial factor for the determination of economic feasibility. The germanium concentrate value is also subject to high uncertainty, due to the uncertain ratio of the concentrate value to pure metal value and the uncertain development of the market price of pure germanium in the future. The increase in demand that is expected in the fiber optics sector indicates an increasing germanium market price, but the price development in the long term is unpredictable.

The value of the indium concentrate and tin-lead alloy are not as crucial to the economic feasibility as the value of the germanium concentrate, but they are of equal uncertainty. The value of all the products and the intermediates are relevant for optimization of the extent to which the concentrates are refined. Most notably, it should be investigated whether the difference in the value of the tin-lead alloy and the tin dross is sufficient to justify an investment in a rotary furnace.

In the sensitivity analysis, it was concluded that the net present value was the second most sensitive to capacity changes. This indicates that recirculation of the lead concentrate and the lead-tin-copper concentrate back to the process, as proposed but not included in the simulation, would significantly increase the net present value. Since recirculation does not necessarily imply an equal increase in both the revenue and in the size of the major equipment, this is uncertain and further studies are needed.

For the concept-level techno-economic assessment, the cost of the major equipment is uncertain, mostly due to the small size of especially the pyrometallurgical equipment. Since most of the capital costs are estimated as a ratio of the major equipment, this affects the precision of the entire capital cost estimation. The total equipment cost would be lower and the profitability of an investment higher in situations where a plant site contains major equipment, such as a kettle or rotary furnace, with a sufficient amount of free capacity to process the material for this process.

The reason behind the uncertainty of the OSBL costs is that the location of the plant was not set. The OSBL costs depend on what kind of infrastructure is available at the site and whether modifications have to be made to increase capacity. For a given plant site with known condition of the infrastructure, estimation of the OSBL costs with higher precision is possible. Underused capacity of infrastructure at the plant site lowers the OSBL cost and improves economic feasibility.

In addition to the OSBL costs, also the operational costs can be estimated more precisely for a known site location, as especially the labor costs and energy costs vary depending on the country. Additionally, it enables the consideration of interest, taxes, depreciation and amortization in economic feasibility calculations.

For a revenue equaling 70% of the pure metal value of the products and a capacity of 280 t alloy per year, the net present value of the investment is 3.5 million EUR and the payback time is seven years. Although a definite conclusion cannot be drawn regarding the feasibility of the process in general, the results show that an investment in the process, especially for a plant with a somewhat higher capacity, has potential to be profitable. The estimated contribution to the European indium and germanium supply via production of the metals, on the scale studied in this thesis, would have limited significance and the contribution to tin production would be insignificant.

References

Alfantazi, A. M. and Moskalyk, R. R. (2003) 'Processing of indium: a review', *Minerals Engineering*. Pergamon, 16(8), pp. 687–694. doi: 10.1016/S0892-6875(03)00168-7.

Anderson, C. S. (2016) 'Mineral Commodity Summaries 2016: Tin', *U.S. Geological Survey*. Available at: https://minerals.usgs.gov/minerals/pubs/commodity/tin/mcs-2016-tin.pdf.

Anderson, C. S. (2017a) '2015 Minerals Yearbook: Tin', *U.S. Geological Survey*. Available at: https://minerals.usgs.gov/minerals/pubs/commodity/tin/myb1-2015-tin.pdf.

Anderson, C. S. (2017b) 'Conflict Minerals from the Democratic Republic of the Congo — Global Tantalum Processing Plants, a Critical Part of the Tantalum Supply Chain', *U.S. Geological Survey*. doi: 10.3133/fs20153022.

Anderson, C. S. (2018a) 'Mineral Commodity Summaries 2018: Indium', *U.S. Geological Survey*, pp. 78–79. doi: 10.3133/70194932.

Anderson, C. S. (2018b) 'Mineral Commodity Summaries 2018: Tin', *U.S. Geolocial Survey*, pp. 172–173. Available at: https://minerals.usgs.gov/minerals/pubs/commodity/tin/mcs-2018-tin.pdf.

Anderson, C. S. (2018c) 'Mineral Industry Surveys: Tin in April 2018', *U.S. Geological Survey*. Available at: https://minerals.usgs.gov/minerals/pubs/commodity/tin/mis-201804-tin.pdf.

Angerer, G. et al. (2009) *Rohstoffe für Zukunftstechnologien*. The Society for Mining, Metallurgy, and Exploration, Inc. Available at: https://www.isi.fraunhofer.de/content/dam/isi/dokumente/ccn/2009/Schlussbericht_lang_20090515.pdf.

Apodaca, L. E. (2018) 'Mineral Commodity Summaries: Sulfur', *U.S. Geological Survey*, (703), pp. 2017–2018.

Barthelmy, D. (2012) 'Mineral Species sorted by the element Ge (Germanium)', p. Webmineral Mineralogy Database. Available at: http://webmineral.com/chem/Chem-Ge.shtml (Accessed: 20 June 2018).

Britton, S. C. (2013) 'Tin and Tin Alloys', in *Corrosion: Third Edition*. Hoboken, NJ, USA: John Wiley & Sons, Inc., p. 4:157-4:167. doi: 10.1016/B978-0-08-052351-4.50048-0.

Brown, R. D. J. (1996) '1996 Minerals Yearbook: Indium', *U.S. Geological Survey*, pp. 1–4. Available at: https://minerals.usgs.gov/minerals/pubs/commodity/indium/490496.pdf.

Brown, R. D. J. (2001) ‘Mineral Commodity Summaries 2001: Germanium’, *U.S. Geological Survey*, pp. 68–69.

Brown, T. J. et al. (2018) *World mineral production 2012-2016.* British Geological Survey, Keyworth, Nottingham.

Brunot, A. et al. (2013) ‘Raw material profiles’, *CRM Innonet*.

Butterman, W. C. and Jorgenson, J. D. (2005) ‘Mineral Commodity profiles: Germanium’, *U.S. Geological Survey*.

Callaghan, R. M. and Carlin, J. F. (2007) ‘2005 Minerals Yearbook: Indium’, *U.S. Geological Survey*.

Cambrios (2018) *ClearOhm® Silver Nanowire Coating Material*. Available at: https://www.cambrios.com/products (Accessed: 4 May 2018).

Carlin, J. F. (2002) ‘2000 Minerals Yearbook: Tin’, *U.S. Geological Survey*. Available at: https://minerals.usgs.gov/minerals/pubs/commodity/tin/660400.pdf.

Carlin, J. F. (2003) ‘Mineral Commodity Summaries 2003: Tin’, *U.S. Geological Survey*. Available at: https://minerals.usgs.gov/minerals/pubs/commodity/tin/660303.pdf.

Carlin, J. F. (2005) ‘Mineral Commodity Summaries 2005: Tin’, *U.S. Geological Survey*. Available at: https://minerals.usgs.gov/minerals/pubs/commodity/tin/tin__mcs05.pdf.

Carlin, J. F. (2006) ‘Mineral Commodity Summaries 2006: Indium’, *U.S. Geological Survey*. Available at: https://minerals.usgs.gov/minerals/pubs/commodity/indium/indiumcs06.pdf.

Carlin, J. F. (2007) ‘2005 Minerals Yearbook: Tin’, *U.S. Geological Survey*. Available at: https://minerals.usgs.gov/minerals/pubs/commodity/tin/tinmyb05.pdf.

Carlin, J. F. (2008) ‘Mineral Commodity Summaries 2008: Tin’, *U.S. Geological Survey*. Available at: https://minerals.usgs.gov/minerals/pubs/commodity/tin/mcs-2008-tin.pdf.

Carlin, J. F. (2010) ‘Mineral Commodity Summaries 2010: Tin’, *U.S. Geological Survey*. Available at: https://minerals.usgs.gov/minerals/pubs/commodity/tin/mcs-2010-tin.pdf.

Carlin, J. F. (2012a) ‘2010 Minerals Yearbook: Tin’, *U.S. Geological Survey*. Available at: https://minerals.usgs.gov/minerals/pubs/commodity/tin/tinmyb05.pdf.

Carlin, J. F. (2012b) ‘Mineral Commodity Summaries 2012: Tin’, *U.S. Geological Survey*.

CEIC (2018) *China | CN: Market Price: Monthly Avg: Inorganic Chemical Material: Sodium Nitrate*. Available at: https://www.ceicdata.com/en/china/china-petroleum--chemical-industry-association-petrochemical-price-inorganic-chemical-material/cn-market-price-monthly-avg-inorganic-chemical-material-sodium-nitrate (Accessed: 18 September 2018).

Chagnon, M. J. (2010) *Indium and indium compounds*, *Kirk-Othmer Encyclopedia of Chemical Technology*. Hoboken, NJ, USA: John Wiley & Sons, Inc. doi: 10.1002/0471238961.0914040919120120.a01.pub3.

Chu, S. (2011) 'Critical Materials Strategy 2011', *Energy*, p. 191. doi: DOE/PI-0009.

Ciacci, L. et al. (2018) 'Backlighting the European Indium Recycling Potentials', *Journal of Industrial Ecology*. Wiley/Blackwell (10.1111). doi: 10.1111/jiec.12744.

Cook, N. J. et al. (2012) 'Determination of the oxidation state of Cu in substituted Cu-In-Fe-bearing sphalerite via -XANES spectroscopy', *American Mineralogist*. GeoScienceWorld, 97(2–3), pp. 476–479. doi: 10.2138/am.2012.4042.

Corning (2016) *Frequently Asked Questions on Fiber Reliability*. Available at: https://www.corning.com/media/worldwide/coc/documents/Fiber/RC- White Papers/WP5082 3-31-2016.pdf.

Creedy, S. et al. (2013) 'Outotec Ausmelt Technology for Treating Zinc Residues', *World of Metallurgy - ERZMETALL*, 66(4), pp. 230–235.

Das, D. K. and Sahoo, S. (2016) 'Graphene in the Core of Optical Fibers', *2016 International Conference on Computing for Sustainable Global Development (INDIACom)*, pp. 358–361.

Deltreil, J. P. (2003) 'Mechanical Dewatering Using Filter Presses Technology', pp. 1–30. Available at: https://sswm.info/sites/default/files/reference_attachments/DELTREIL 2003 Mechanical Dewatering Using Filter Presses Technology.pdf.

Drzazga, M. (2018) 'Production technologies of CRM from primary resources: germanium', pp. 75–82.

Du, G. et al. (2009) 'Ge distribution in the Wulantuga high-germanium coal deposit in the Shengli coalfield, Inner Mongolia, northeastern China', *International Journal of Coal Geology*. Elsevier, 78(1), pp. 16–26. doi: 10.1016/J.COAL.2008.10.004.

East, A. J. (2006) 'Polyesters, Thermoplastic', in *Kirk-Othmer Encyclopedia of Chemical Technology*. Hoboken, NJ, USA: John Wiley & Sons, Inc. doi: 10.1002/0471238961.1615122505011920.a01.pub2.

Eggeman, T. (2011) 'Sodium Hydroxide', in *Kirk-Othmer Encyclopedia of Chemical Technology*. Hoboken, NJ, USA: John Wiley & Sons, Inc., pp. 1–16. doi: 10.1002/0471238961.1915040905070705.a01.pub2.

European Commission (2014a) ‘EU critical raw materials profiles’. doi: Ref. Ares(2015)1819595 - 29/04/2015.

European Commission (2014b) ‘Report on Critical Raw Materials for the EU - Report of the Ad hoc Working Group on defining critical raw materials’.

European Commission (2017) *Study on the review of the list of critical raw materials - Critical Raw Materials Factsheets*, *European Commission*. doi: 10.2873/876644.

European IPPC Bureau (2017) *Reference Document on Best Available Techniques for the Non-Ferrous Metals Industries*. doi: 10.2760/8224.

Eurostat (2017) *Waste statistics - electrical and electronic equipment*. Available at: http://ec.europa.eu/eurostat/statistics-explained/index.php/Waste_statistics_-_electrical_and_electronic_equipment#Further_Eurostat_information (Accessed: 18 May 2018).

Fraunhofer Institute for Solar Energy Systems (2018) *Photovoltaics report*. Available at: https://www.ise.fraunhofer.de/content/dam/ise/de/documents/publications/studies/Photovoltaics-Report.pdf.

Frenzel, M. et al. (2017) ‘Quantifying the relative availability of high-tech by-product metals – The cases of gallium, germanium and indium’, *Resources Policy*. Pergamon, 52, pp. 327–335. doi: 10.1016/j.resourpol.2017.04.008.

Frenzel, M., Ketris, M. P. and Gutzmer, J. (2014) ‘On the geological availability of germanium’, *Mineralium Deposita*. Springer Berlin Heidelberg, 49(4), pp. 471–486. doi: 10.1007/s00126-013-0506-z.

Frenzel, M., Tolosana-Delgado, R. and Gutzmer, J. (2015) ‘Assessing the supply potential of high-tech metals – A general method’, *Resources Policy*. Pergamon, 46, pp. 45–58. doi: 10.1016/J.RESOURPOL.2015.08.002.

Fu, X., Polli, A. and Olivetti, E. (2018) ‘High-Resolution Insight into Materials Criticality: Quantifying Risk for By-Product Metals from Primary Production’, *Journal of Industrial Ecology*. Wiley/Blackwell (10.1111). doi: 10.1111/jiec.12757.

Fuerstenau, M. C. and Han, K. N. (2003) *Principles of Mineral Processing*.

Gabby, P. N. (2006) *Mineral Commodity Summaries 2006: Germanium*. Available at: https://minerals.usgs.gov/minerals/pubs/commodity/germanium/germamcs06.pdf.

George, M. W. (2005a) ‘Mineral Commodity Summaries 2005: Germanium’, *U.S. Geological Survey*, pp. 70–71.

George, M. W. (2005b) ‘Mineral Commodity Summaries 2005: Indium’, *U.S. Geological Survey*.

Graedel, T. E. et al. (2013) ‘On the materials basis of modern society.’, *Proceedings of the National Academy of Sciences of the United States of America*. National Academy of Sciences, 112(20), pp. 6295–300. doi: 10.1073/pnas.1312752110.

Guberman, D. E. (2009) ‘Mineral Commodity Summaries 2009: Germanium’, *U.S. Geological Survey*, pp. 66–67.

Guberman, D. E. (2010) *Mineral Commodity Summaries 2010: Germanium*. Available at: https://minerals.usgs.gov/minerals/pubs/commodity/germanium/mcs-2010-germa.pdf.

Guberman, D. E. (2011) *Mineral Commodity Summaries 2011: Germanium*. Available at: https://minerals.usgs.gov/minerals/pubs/commodity/germanium/mcs-2011-germa.pdf.

Guberman, D. E. (2012) *Mineral Commodity Summaries 2012: Germanium*. Available at: https://minerals.usgs.gov/minerals/pubs/commodity/germanium/mcs-2012-germa.pdf.

Guberman, D. E. (2013) ‘Mineral Commodity Summaries 2013: Germanium’, *U.S. Geological Survey*, pp. 64–65. Available at: http://minerals.usgs.gov.

Guberman, D. E. (2015) *Mineral Commodity Summaries 2015: Germanium*. Available at: https://minerals.usgs.gov/minerals/pubs/commodity/germanium/mcs-2015-germa.pdf.

Guberman, D. E. (2016a) ‘2014 Minerals Yearbook: Germanium’, *U.S. Geological Survey*.

Guberman, D. E. (2016b) *Mineral Commodity Summaries 2016: Germanium*. Available at: https://minerals.usgs.gov/minerals/pubs/commodity/germanium/mcs-2016-germa.pdf.

Guberman, D. E. (2017) ‘Mineral Commodity Summaries 2017: Germanium’, *U.S. Geological Survey*, pp. 70–71. Available at: https://minerals.usgs.gov/minerals/pubs/commodity/germanium/mcs-2017-germa.pdf.

Guberman, D. E. and Thomas, C. L. (2017) ‘2015 Minerals Yearbook: Germanium’, *U.S. Geological Survey*, pp. 1–8.

Guo, X. et al. (2015) ‘Recovery of metal values from waste printed circuit boards using an alkali fusion-leaching-separation process’, *Hydrometallurgy*. Elsevier B.V., 156, pp. 199–205. doi: 10.1016/j.hydromet.2015.06.011.

Harper, E. M. et al. (2015) ‘Criticality of the Geological Zinc, Tin, and Lead Family’, *Journal of Industrial Ecology*. Wiley/Blackwell (10.1111), 19(4), pp. 628–644. doi: 10.1111/jiec.12213.

Hoch, M. (2001) ‘Organotin compounds in the environment — an overview’, *Applied Geochemistry*. Pergamon, 16(7–8), pp. 719–743. doi: 10.1016/S0883-2927(00)00067-6.

Hoshino, Y., Utsunomiya, T. and Abe, O. (1981) ‘Thermal Decomposition of Sodium Nitrate and the Effects of Several Oxides on the Decomposition.’, *Bulletin of the Chemical Society of Japan*, pp. 1385–1391. doi: 10.1246/bcsj.54.1385.

Howard, S. M. (2006) ‘Ellingham Diagrams’, *South Dakota School of Mines and Technology*, p. 31. doi: 10.1017/CBO9781107415324.004.

Howe, P., Wood, M. and Watts, P. (2005) ‘Concise international chemical assessment document 65: Tin and inorganic tin compounds’, *World Health Organization*, (65), p. v. doi: publication no. 2005/06OSH. ISBN 90-5549-568-9.

Hu, Z. and Gao, S. (2008) ‘Upper crustal abundances of trace elements: A revision and update’, *Chemical Geology*. Elsevier, 253(3–4), pp. 205–221. doi: 10.1016/J.CHEMGEO.2008.05.010.

ICIS (2006) *Chemicals A-Z*. Available at: https://www.icis.com/chemicals/channel-info-chemicals-a-z/ (Accessed: 17 September 2018).

IEA (2018) ‘The International Energy Agency: Key World Energy Statistics’, p. 82. Available at: https://webstore.iea.org/key-world-energy-statistics-2018.

IMN (2018) ‘Unpublished results of pilot-scale experiments’.

Intratec (2010) *Steam Price History & Forecast: Medium Pressure Steam*. Available at: https://www.intratec.us/chemical-markets/steam-prices.

ITRI (2016) ‘2016 Report on Global Tin Resources & Reserves’, p. 20. Available at: https://www.internationaltin.org/wp-content/uploads/2018/01/ITRI-2016-Report-on-Global-Tin-Resources-and-Reserves.pdf.

Jackson, W. (Indium C. (2012) *The future of indium supply and ITO*. Available at: http://www.aimcal.org/uploads/4/6/6/9/46695933/jackson_pres.pdf.

Jorgenson, B. J. D. (2003) ‘2002 Minerals Yearbook: Germanium’, *U.S. Geological Survey*, pp. 1–5. Available at: https://minerals.usgs.gov/minerals/pubs/commodity/germanium/germmyb02.pdf.

Jorgenson, J. D. (2004) *Mineral Commodity Summaries 2004: Germanium*. Available at: https://minerals.usgs.gov/minerals/pubs/commodity/germanium/germamcs04.pdf.

Jorgenson, J. D. (2006) ‘Germanium Recycling in the United States in 2000’, *U.S. Geological Survey*, p. 15. Available at: https://pubs.usgs.gov/circ/c1196v/c1196v.pdf.

Kamili, R. J., Kimball, B. E. and Carlin, J. F. J. (2017) ‘Tin, chap. S’, in *Critical*

Mineral Resources of the United States—Economic and Environmental Geology and Prospects for Future Supply: U.S. Geological Survey Professional Paper 1802, pp. S1–S53. doi: 10.3133/pp1802S.

Kangas, P. et al. (2017) 'The Jarogain Process for Metals Recovery from Jarosite and Electric Arc Furnace Dust - Process Design and Economics', *VTT Technology*, 317. Available at: https://cris.vtt.fi/en/publications/the-jarogain-process-for-metals-recovery-from-jarosite-and-electr.

Kangas, P., Kaijaluoto, S. and Määttänen, M. (2014) 'Evaluation of future pulp mill concepts - Reference model of a modern Nordic kraft pulp mill', *Nordic Pulp and Paper Research Journal*, 29(4), pp. 620–634. doi: 10.3183/NPPRJ-2014-29-04-p620-634.

Ketris, M. P. and Yudovich, Y. E. (2009) 'Estimations of Clarkes for Carbonaceous biolithes: World averages for trace element contents in black shales and coals', *International Journal of Coal Geology*. Elsevier, 78(2), pp. 135–148. doi: 10.1016/J.COAL.2009.01.002.

Licht, C., Peiró, L. T. and Villalba, G. (2015a) 'Global Substance Flow Analysis of Gallium, Germanium, and Indium: Quantification of Extraction, Uses, and Dissipative Losses within their Anthropogenic Cycles', *Journal of Industrial Ecology*. Wiley/Blackwell (10.1111), 19(5), pp. 890–903. doi: 10.1111/jiec.12287.

Licht, C., Peiró, L. T. and Villalba, G. (2015b) 'Supporting information for: Global Substance flow analysis for gallium, germanium, and indium: Quantification of extraction, uses, and dissipative losses within their anthropogenic cycles', *Journal of Industrial Ecology*, 19(5), pp. 890–903.

Liu, B. et al. (2016) 'Phase Evolution of Tin Oxides Roasted Under CO–CO2Atmospheres in the Presence of Na2CO3', *Mineral Processing and Extractive Metallurgy Review*. Taylor & Francis, 37(4), pp. 264–273. doi: 10.1080/08827508.2016.1190355.

Lokanc, M. et al. (2015) 'The Availability of Indium: The Present, Medium Term, and Long Term', *National Renewable Energy Laboratory*.

Matches (2014) *Matches' 275 Equipment Cost Estimates.* Available at: http://matche.com/equipcost/Default.html (Accessed: 2 October 2018).

Melcher, F. and Buchholz, P. (2012) 'Current and future Germanium availability from primary sources', *Deutche Rohstoffagentur*, p. 31.

Melcher, F., Oberthür, T. and Rammlmair, D. (2006) 'Geochemical and mineralogical distribution of germanium in the Khusib Springs Cu–Zn–Pb–Ag sulfide deposit, Otavi Mountain Land, Namibia', *Ore Geology Reviews*. Elsevier, 28(1), pp. 32–56. doi: 10.1016/J.OREGEOREV.2005.04.006.

Messina, C. J. (1975) *The effect of tin on the mechanical and physical properties of gray cast iron*. Leigh University. Available at:

https://preserve.lehigh.edu/cgi/viewcontent.cgi?article=2795&context=etd.

Metal Packaging Europe (2018) *Key facts*. Available at: http://www.metalpackagingeurope.org/pa/key-facts (Accessed: 1 August 2018).

Moskalyk, R. R. (2004) 'Review of germanium processing worldwide', *Minerals Engineering*. Pergamon, 17(3), pp. 393–402. doi: 10.1016/J.MINENG.2003.11.014.

Muller, T. L. (2006) 'Sulfuric Acid and Sulfur Trioxide', in *Kirk-Othmer Encyclopedia of Chemical Technology*. Hoboken, NJ, USA: John Wiley & Sons, Inc. doi: 10.1002/0471238961.1921120613211212.a01.pub2.

National Enviromental Research Council (2015) 'Risk List 2015 - An update to the supply risk index for elements or element groups that are of economic value', *British Geological Survey*, 1, p. 11. doi: 10.1017/CBO9781107415324.004.

Nyrstar (2018) *Annual Report*. Available at: https://www.virginatlantic.com/content/dam/vaa/documents/footer/mediacentre/VAL_FY16_Annual_Report.pdf.

O'Neill, B. (2010) 'Indium market forces, a commercial perspective', *Conference Record of the IEEE Photovoltaic Specialists Conference*, pp. 556–559. doi: 10.1109/PVSC.2010.5616842.

Outotec (2018) *HSC Chemistry*. Available at: https://www.outotec.com/products/digital-solutions/hsc-chemistry/ (Accessed: 5 November 2018).

Paschotta, R. (2008) *Encyclopedia of Laser Physics and Technology - Fiber core*. Available at: https://www.rp-photonics.com/fiber_core.html (Accessed: 19 June 2018).

Pavel, C. C. et al. (2016) 'Critical raw materials in lighting applications: Substitution opportunities and implication on their demand', *Physica Status Solidi (A) Applications and Materials Science*, 213(11), pp. 2937–2946. doi: 10.1002/pssa.201600594.

Peters, M. S., Timmerhaus, K. D. and West, R. E. (2004) *Plant Design and Economics for Chemical Engineers*. 5th edn.

Phipps, G., Mikolajczak, C. and Guckes, T. (2008) 'Indium and Gallium: long-term supply', *Renewable Energy Focus*. Elsevier, 9(4), pp. 56–59. doi: 10.1016/S1471-0846(08)70140-9.

Pickerel, K. (2017) 'NREL licenses inverted metamorphic multi-junction solar cell technology', *Solar Power World*, 24 October. Available at: https://www.solarpowerworldonline.com/2017/10/nrel-licenses-inverted-metamorphic-multi-junction-solar-cell-technology/ (Accessed: 18 June 2018).

Pleşa, C. et al. (2015) ‘Investigations on infrared chalcogenide glasses used in night vision devices’, *Chalcogenide Letters*, 12(11), pp. 633–638. doi: 10.13140/RG.2.1.3984.9040.

Reck, B. K. and Graedel, T. E. (2012) ‘Challenges in metal recycling’, *Science*, 337(6095), pp. 690–695. doi: 10.1126/science.1217501.

Roskill (2015) ‘Marketing sheet for: Roskill Market Outlook Reports - Tin 2015 9 th edition’. Available at: http://www.mncttf.gov.mn/chamber/index.php/2015-06-09-07-49-12/2015-06-11-01-57-33/item/download/219_c971197c032c88e53e38756f827438f2.

Sancaktar, E. and Bai, L. (2011) ‘Electrically Conductive Epoxy Adhesives’, *Polymers*. Molecular Diversity Preservation International, 3(1), pp. 427–466. doi: 10.3390/polym3010427.

Schwarz-Schampera, U. (2014) ‘Indium’, in *Critical Metals Handbook*, pp. 204–229. doi: 10.1002/9781118755341.ch9.

Shanks, W. C. P. I. et al. (2017) *Germanium and indium*, *Professional Paper*. doi: 10.3133/pp1802i.

Smith, G. R. (2008) *Mineral Commodity Summaries 2008: Germanium*. Available at: https://minerals.usgs.gov/minerals/pubs/commodity/germanium/mcs-2008-germa.pdf.

Sprecher, B. et al. (2017) ‘How “black swan” disruptions impact minor metals’, *Resources Policy*. Pergamon, 54, pp. 88–96. doi: 10.1016/J.RESOURPOL.2017.08.008.

Steelonthenet.com (2018) *Met Coke Prices - Europe 2014-2018*. Available at: https://www.steelonthenet.com/files/blast-furnace-coke.html (Accessed: 5 September 2018).

Swedish Chemicals Agency (2008) *European Union Risk Assessment Report - Diantimony trioxide*. Available at: https://echa.europa.eu/documents/10162/553c71a9-5b5c-488b-9666-adc3af5cdf5f.

Tadjfar, N. (2017) ‘Assessing the criticality of germanium as a by-product’. Massachusetts Institute of Technology. Available at: https://dspace.mit.edu/handle/1721.1/111354#files-area (Accessed: 31 May 2018).

Tercero, L. (2018) ‘Critical Raw Material Substitution Profiles’, (730227).

The Pewter Society (2014) *What is pewter?* Available at: http://www.pewtersociety.org/pewter/what-is-pewter (Accessed: 27 July 2018).

Thomas, C. L. (2018a) ‘2016 Minerals Yearbook: Germanium’, *U.S. Geological*

Survey. Available at: https://minerals.usgs.gov/minerals/pubs/commodity/germanium/myb1-2016-germa.pdf.

Thomas, C. L. (2018b) 'Mineral Commodity Summaries 2018: Germanium', *U.S. Geological Survey*, pp. 68–69. Available at: https://minerals.usgs.gov/minerals/pubs/commodity/germanium/mcs-2018-germa.pdf.

Thomas, D. W., Mahmood, T. and Lindhal, C. B. (2011) 'Germanium and Germanium Compounds', in *Kirk-Othmer Encyclopedia of Chemical Technology*. Hoboken, NJ, USA: John Wiley & Sons, Inc., pp. 1–17. doi: 10.1002/0471238961.0705181301040113.a01.pub4.

Tolcin, A. C. (2008) 'Mineral Commodity Summaries 2008: Indium', *U.S. Geological Survey*. Available at: https://minerals.usgs.gov/minerals/pubs/commodity/indium/mcs-2008-indiu.pdf.

Tolcin, A. C. (2010) 'Mineral Commodity Summaries 2010: Indium', *U.S. Geological Survey*.

Tolcin, A. C. (2011) 'Mineral Commodity Summaries 2011: Indium', *U.S. Geological Survey*. Available at: https://minerals.usgs.gov/minerals/pubs/commodity/indium/mcs-2011-indiu.pdf.

Tolcin, A. C. (2012) '2010 Minerals Yearbook: Indium', *U.S. Geological Survey*, (September), p. 7. doi: 10.1016/j.ecolecon.2008.01.027.

Tolcin, A. C. (2016) 'Mineral Commodity Summaries 2016: Indium', *U.S. Geological Survey*, pp. 80–81. doi: dx.doi.org/10.3133/70140094.

Tolcin, A. C. (2017a) '2015 Minerals Yearbook: Indium', *U.S. Geological Survey*. Available at: https://minerals.usgs.gov/minerals/pubs/commodity/lithium/myb1-2015-lithi.pdf.

Tolcin, A. C. (2017b) 'Mineral Commodity Summaries 2017: Indium', *U.S. Geological Survey*, pp. 80–81. Available at: https://minerals.usgs.gov/minerals/pubs/commodity/indium/mcs-2017-indiu.pdf.

Towler, G. and Sinnott, R. (2013) *Chemical engineering design: principles, practice, and economics of plant and process design*. 2nd edn.

U.S. Bureau of Labor Statistics (2018) *Producer Price Index for All Commodities [PPIACO], retrieved from FRED, Federal Reserve Bank of St. Louis*. Available at: https://fred.stlouisfed.org/series/PPIACO (Accessed: 18 September 2018).

U.S. Geological Survey (2015a) *Germanium statistics, in Kelly, T. D., and Matos G.R., comps., Historical Statistics for Mineral Commodities in the United States: U.S. Geological Survey Data Series 140*. Available at: https://minerals.usgs.gov/minerals/pubs/historical-statistics/ (Accessed: 10 July

2018).

U.S. Geological Survey (2015b) *Tin statistics in Kelly, T.D., and Matos, G.R., comps., Historical statistics for mineral and material commodities in the United States (2016 version): U.S. Geological Survey Data Series 140*. Available at: https://minerals.usgs.gov/minerals/pubs/historical-statistics/ (Accessed: 31 July 2018).

Umicore (2018a) *Umicore - Materials*. Available at: http://eom.umicore.com/en/infrared-optics/products/materials/ (Accessed: 19 June 2018).

Umicore (2018b) *Umicore - Special metals*. Available at: http://pmr.umicore.com/en/metals-products/special-metals (Accessed: 15 May 2018).

UNEP (2011) *Recycling rates of metals - A Status Report, A Report of the Working Group on the Global Metal Flows to the international Resource Panel*. Graedel, T. E., Allwood, J.,Birat, J.-P. Reck, B. K., Sibley, S. F., Sonnemann, G., Buchert, M., Hagelüken, C. doi: ISBN 978-92-807-3161-3.

Velis, C. A. and Brunner, P. H. (2013) 'Recycling and resource efficiency: it is time for a change from quantity to quality', *Waste Management & Research*. SAGE PublicationsSage UK: London, England, 31(6), pp. 539–540. doi: 10.1177/0734242X13489782.

Velte, D. (2015) 'Final Roadmap Report', (319024).

Vulcan, T. (2013) 'Indium At Your Fingertips; The Go-To Minor Metal For Flat-Panel Displays', *ETF.com*, 10 June. Available at: http://www.etf.com/sections/features-and-news/4864-indium-at-your-fingertips-the-go-to-minor-metal-for-flat-panel-displays?nopaging=1 (Accessed: 12 July 2018).

Werner, T. T. et al. (2018) 'Looking Down Under for a Circular Economy of Indium', *Environmental Science & Technology*. American Chemical Society, 52(4), pp. 2055–2062. doi: 10.1021/acs.est.7b05022.

Werner, T. T., Mudd, G. M. and Jowitt, S. M. (2017) 'The world's by-product and critical metal resources part III: A global assessment of indium', *Ore Geology Reviews*. Elsevier, 86, pp. 939–956. doi: 10.1016/j.oregeorev.2017.01.015.

Wiesenfarth, M. et al. (2017) 'Current Status of Concentrator Photovoltaic (CPV) Technology', *National Renewable Energy Laboratory*, pp. 1–27. Available at: http://www.ise.fraunhofer.de/en/publications/veroeffentlichungen-pdf-dateien-en/studien-und-konzeptpapiere/current-status-of-concentrator-photovoltaic-cpv-technology.pdf.

Yang, C. et al. (2017) 'Recycling Tin from Electronic Waste: A Problem That Needs More Attention', *ACS Sustainable Chemistry & Engineering*. American Chemical Society, 5(11), pp. 9586–9598. doi: 10.1021/acssuschemeng.7b02903.

Ylä-Mella, J. and Pongrácz, E. (2016) ‘Drivers and Constraints of Critical Materials Recycling: The Case of Indium’, *Resources*. Multidisciplinary Digital Publishing Institute, 5(4), p. 34. doi: 10.3390/resources5040034.

ZincOx Resources plc (2002) *ZincOx Adds Significant Resource to its International Portfolio*. Available at: https://www.investegate.co.uk/articlePrint.aspx?id=200201070700185340P (Accessed: 18 July 2018).

Series title and number

VTT Technology 345

Title	**Techno-economic assessment of the process for recovery of indium, germanium and tin from alloys obtained as byproducts of zinc production**
Author(s)	Iris Winberg
Abstract	A techno-economic assessment for a process for recovery of indium, germanium and tin was conducted. The proposed process involves the use of both pyro- and hydrometallurgical methods to recover the metals from two lead-bearing alloys, which are obtained as byproducts in zinc production. Lead-tin alloy, germanium concentrate and two different indium concentrates are obtained as main products in the process. Additionally, a literature review of the indium, germanium and tin markets was conducted, with the main purpose to provide a background for the metals which market prices the profitability of an investment in the process relies on. The proposed concept was simulated to provide mass and energy balances for the process. The mass distribution of elements, obtained from pilot-scale experiments performed by the research institute IMN, was used as input data in the process simulation. Using the mass balances obtained from the simulation, the main equipment required for the process was dimensioned. The capital cost, the operational costs and the revenue for the process were estimated and using these, the net present value of the investment was calculated for a time period of 20 years. A sensitivity analysis was conducted by varying the estimation of metal prices and selected costs and studying its impact on the net present value. For a revenue equaling 70% of the pure metal value of the products and a capacity of 280 t alloy per year, the net present value of the investment is 3.5 million EUR and the payback time is seven years. The net present value is the most sensitive for variation of the germanium price and for variation of the capacity. A higher capacity would increase the net present value substantially.
ISBN, ISSN, URN	ISBN 978-951-38-8678-3 (Soft back ed.) ISBN 978-951-38-8677-6 (URL: http://www.vttresearch.com/impact/publications) ISSN-L 2242-1211 ISSN 2242-1211 (Print) ISSN 2242-122X (Online) http://urn.fi/URN:ISBN:978-951-38-8677-6 https://doi.org/
Date	November 2018
Language	English
Pages	97 p.
Name of the project	RIGAT - Technology for recovery of indium, germanium and tin from lead bearing alloys generated in zinc refinement for direct implementation in industrial practice
Commissioned by	
Keywords	indium, germanium, tin, zinc, lead, residue, techno-economic assessment
Publisher	VTT Technical Research Centre of Finland Ltd P.O. Box 1000, FI-02044 VTT, Finland, Tel. 020 722 111

Techno-economic assessment of the process for recovery of indium, germanium and tin from alloys obtained as byproducts of zinc production

Indium and germanium are important elements for modern information and communication technology. These elements are required for manufacturing of LCD panels and optical fiber cables. Both of them are listed as critical elements by the European Commission, due to their importance to the economy and their supply risk.

Both indium and germanium are commonly produced as byproducts from zinc production. This report presents a new process concept where these metals are recovered from lead-bearing alloys obtained as side streams in the imperial smelting zinc process. The proposed process consists of pyro- and hydrometallurgical treatment steps. Concept-level process design, mass and energy balances and economic feasibility of the process are presented in this report. The new concept is a promising option for recovery of indium and germanium from side streams of zinc smelting.

ISBN 978-951-38-8678-3 (Soft back ed.)
ISBN 978-951-38-8677-6 (URL: http://www.vttresearch.com/impact/publications)
ISSN-L 2242-1211
ISSN 2242-1211 (Print)
ISSN 2242-122X (Online)
http://urn.fi/URN:ISBN:978-951-38-8677-6
https://doi.org/

VTT beyond the obvious